THE UNIVERSITY OF MICHIGAN

INDUSTRY PROGRAM OF THE COLLEGE OF ENGINEERING

CRYSTALLIZATION KINETICS AND MORPHOLOGY OF ISOTACTIC POLYSTYRENE BLENDS

Steven L. Lambert

A dissertation submitted in partial fulfillment
of the requirements for the degree of
Doctor of Philosophy
(Chemical Engineering)
in The University of Michigan

November, 1970

IP-835

ACKNOWLEDGMENTS

The author wishes to express his appreciation to many people who made this study possible:

To Associate Professor Gregory S. Y. Yeh, chairman of the doctoral committee, who contributed unselfishly of his time, advice, and assistance during the course of this work.

To Professor G. B. Williams whose wise counsel, patient advice, and encouragement during the critical stages of this study greatly contributed to its successful conclusion.

To the members of the doctoral committee: Professors W. C. Bigelow and L. O. Brockway, and Associate Professor Orville F. Kimball, who have offered helpful criticisms, suggestions, and advice throughout this study.

To the National Science Foundation, Rackham Graduate School, the Dow Chemical Company, the Whirlpool Corporation, and the Department of Chemical and Metallurgical Engineering for financial assistance.

To Dan Luch for the many hours of helpful and interesting discussions and suggestions during the years of our graduate studies.

To Jens and Leah Pedersen for many years of common joy and mutual suffering as neighbors and fellow graduate students.

To the folks in Warsaw for care packages and for caring.

To my parents for their quiet encouragement, high standards, patient love, and unselfish support.

To my family, Bamse, Tinker, and Mano who provided many a joyous and fun-loving moment during the past several years and above all to my wife, Jackie, who with her constant love, patience, and confidence has made the truly great sacrifices necessary for the successful completion of this dissertation.

TABLE OF CONTENTS

LIST OF TABLES

LIST OF FIGURES

FIGURE PAGE

LIST OF SYMBOLS USED IN THIS STUDY

b_o = thickness of monomolecular layer

Ci = interfacial concentration of rejected impurity

$C_\infty(T)$ = concentration of the crystallizable polymer far removed from the crystallization front

C_1 = WLF constant, C_1 = 4120 cal./mole

C_2 = WFL constant, C_2 = 75°K (Boon and Azcue); C_2 = 30.7°K (Suzuki and Kovacs)

ΔC_p = change in heat capacity

E_D = free energy of activation for transport across the liquid-nucleus interface

ΔF = Gibbs free energy difference per unit volume between the supercooled phase and the crystalline phase

ΔF^* = free energy required to form a nucleus of critical size

Δf_u = free energy of fusion per molecule

G = spherulitic growth rate, μ/minute

G(undil) = spherulitic growth rate for homopolymer systems

G(dil) = spherulitic growth rate for diluted polymer systems

G_o = constant which is independent of temperature

G_T = threshold spherulitic growth rate

ΔH = Heat of fusion

k = Boltzmans Constant

M_n = number average molecular weight

M_w = weight average molecular weight

R = gas constant, 1.98 cal./mole-°K

T_g = glass transition temperature

T_{max} = temperature for maximum spherulitic growth rate

T_m = melting temperature

T_m° = melting temperature of homopolymer

T_T = threshold crystallization temperature

T_x = crystallization temperature

V_1 = molar volume per repeat unit of diluent

V_u = molar volume per repeat unit of crystallizable polymer

υ_2 = volume fraction of crystallizable polymer

X_1 = polymer-diluent interaction free energy

y = exponential variable

η = melt viscosity

ρ = cross sectional area of nucleus

ξ = length of molecular segment in nucleus

σ_e = end interfacial energy per molecule

σ_u = lateral interfacial free energy per molecule

$I = -2080/(C_2+T-Tg)$

$II = -279T_m/T(T_m-T)$

$III = 0.2T_m \ell n \upsilon_2/(T_m-T)$

CHAPTER I

GENERAL INTRODUCTION

Polymeric materials are of commercial importance primarily because their long chain molecular structure generates a unique set of physical properties not found in comparable monomeric materials. The behavior of this long chain structure is greatly influenced by the chemical arrangement of the monomeric units along the chain backbone and the physical conformation of the molecules or morphology. Previous studies [17, 21] on polymer morphology and related crystallization phenomena have generally concentrated on homopolymer or undiluted pure polymer systems. However, commercial polymers are often diluted with either impurities or by plasticizers which have been purposely added, and these diluents are known to influence both the crystallization kinetics and the resulting morphology of diluted polymer systems [30].

Previous studies on mixtures of isotactic/atactic polystyrene [30] and isotactic polystyrene/benzophenone [5] have indicated that the concentration and molecular weight of the added diluent strongly affects the morphology and crystallization kinetics of isotactic polystyrene. However, the mechanism of the polymer-diluent interaction is not clearly understood, since only a limited range of diluent

molecular weights and plasticizers were considered. It was therefore decided to make a more detailed study of this polymer-diluent interaction phenomenon by considering a wider range of atactic polystyrene molecular weights and several different types of low molecular weight commercial plasticizers. In this study we used optical and electron microscopy, wide angle x-ray and optical melting temperature measurements to analyze the morphology and crystallization kinetics of isotactic/atactic polystyrene, as well as isotactic polystyrene/di-methyl or di-decyl phthalate over a wide range of concentrations and crystallization temperatures.

Another mode of polymer crystallization which is of great importance is that of crystallization under strain. Melt extrusion, fiber spinning, and injection molding are perhaps the most common fabrication techniques used for polymer processing, and each of these produces a strain field in the polymer melt prior to crystallization. As a result, most studies have generally concentrated on strain induced crystallization from the melt, and studies of this type are currently being carried on in our laboratory and in others [1, 34]. However, there are few comparable studies of strain induced crystallization from the glassy amorphous or rubbery states of a pure or diluted polymer system. Since the basic mechanism of strain induced crystallization still remains a subject of major speculation, we decided to examine in detail strain induced crystallization behavior of isotactic polystyrene and isotactic polystyrene/benzophenone systems under a variety of conditions from the glassy amorphous and rubbery

states. In this study we used bright and dark field electron microscopy and electron diffraction to examine the morphology of thin films stretched to various elongations and annealed at several different temperatures.

Finally, recent studies [12, 62] have indicated that the microstructure of amorphous polymers might play an important role in the mechanism of crystallization from the glassy amorphous state. Since the mechanism and mode of crystallization are of primary importance as far as crystalline morphology is concerned, the morphology of amorphous thin films of isotactic and atactic polystyrene was also examined.

The combined study of crystallization kinetics and morphology of isotactic polystyrene blends is organized into five major chapters. Chapter II contains a listing of the common materials and primary techniques used in Chapters III, IV, V, and VI. These chapters deal respectively with: the crystallization of mixtures of isotactic/atactic polystyrene; the crystallization of mixtures of isotactic polystyrene/plasticizer; strain induced crystallization; and miscellaneous studies dealing with the morphology of amorphous polystyrene and related topics. Each of these chapters (III, IV, V, VI) has a technical review section, as well as sections dealing with experimental procedures, results, discussion, and conclusions. General conclusions and major findings are indicated in Chapter VII.

CHAPTER II

MATERIALS, EQUIPMENT, AND ELECTRON MICROSCOPY TECHNIQUES

The purpose of this chapter is to combine together a common listing of the materials, equipment, and some of the electron microscopy techniques used in the kinetic and morphology sections of this work. Other preparation techniques having to do with optical microscopy and thin film preparation for electron microscopy will be considered under the experimental heading of the appropriate chapter in which the experimental techniques are discussed.

A. Materials

All the materials used for the following study are characterized in Table I with regard to molecular weight, structure, and source.

B. Equipment

A JEM-6A electron microscope was used to examine thin films of crystalline and amorphous polystyrene indicated in Chapters IV, V, and VI. The electron microscope was operated for this study at 80 killivolts accelerating potential with magnifications ranging from 5,000 to 40,000X. These magnifications were carefully calibrated and periodically rechecked

Table I

Materials Used for Crystallization Study

Material	M. W.	Structure	Source
isotactic polystyrene*	550,000 (viscosity)	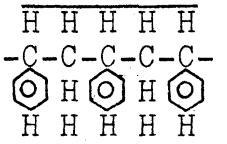	Dow Chemical Company
Isotactic polystyrene**	1,200,000 (viscosity)	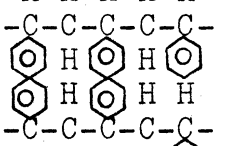	Dow Chemical Company
atactic polystyrene***	900 (light scat.)	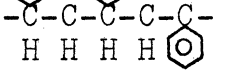	Pressure Chemical Company
	2,300 (light scat.)		
	4,800 (light scat.)		
	10,000 (light scat.)		
	19,800 (light scat.)		
	51,000 (light scat.)		
	411,000 (light scat.)		
	1,800,000 (light scat.)		
atactic polystyrene (commercial)	----------	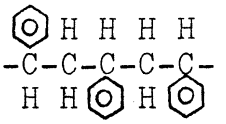	Shell Chemical Company
benzophenone	182	$(C_6H_5)_2CO$	Eastman Chemical Company
di-methyl phthalate	194	$C_6H_4(COOCH_3)_2$	Aldrich Chemical Company
di-decyl phthalate	446	$C_6H_4(COOC_{10}H_{21})_2$	Eastman Chemical Company
benzene	78	C_6H_6	Baker Chemical Company
chloroform	118	$CHCl_3$	Baker Chemical Company
dichloro-benzene	146	$C_6H_4Cl_2$	Baker Chemical Company
cyclohexanone	98	$C_6H_{10}O$	Baker Chemical Company

*According to x-ray analysis, the relative crystallinity of this material as received is 28%, and it contains 15% atactic polymer which was removable by extraction in boiling methyl ethyl ketone. The crystalline melting point was measured to be 235°C by Dr. F.L. Saunders, Dow Chemical Company.

**This material also contained 15% atactic polymer which was removed by extraction in boiling methyl ethyl ketone.

***The ratio of the weight average (light scattering) molecular weight to the number average molecular weight is 1.06.

using a 54,864 line per inch grating replica supplied by William Ladd Inc. A Phillips EM300 electron microscope was also employed for a portion of this study.

The transmission x-ray scatter from bulk samples of crystalline isotactic polystyrene (Chapter III) was measured by a Norelco vertical diffractometer using nickel filtered Cu Kα radiation at 35 killivolts and 15 milliamperes. Samples of crystallized polystyrene were scanned through 2θ angles ranging from 2.0° to 18.0° at a rate of 0.5° per minute and strip chart recorded at a speed of one inch per minute. 1° disperse and scatter slits and .006" receiving slits were used.

C. Electron Microscopy Techniques

Thin films prepared for examination in the electron microscope were usually shadowed with platinum or decorated with gold in order to enhance the contrast or to bring out surface features. Fine platinum shadowing on the specimen surface was produced by positioning the specimen grids at an angle of 30° and twelve centimeters away from a platinum wire-carbon rod assembly in a vacuum chamber. The assembly consists of 4 millimeters of 0.008 inch diameter platinum wire wrapped around a thin carbon rod connected to two electrodes. Upon reaching a vacuum of approximately 10^{-5} torr, the voltage across the carbon rod was slowly increased until the platinum wire melted and formed a bead. The vacuum chamber was opened and the carbon rod rotated until the bead was directed at the specimen grids. Upon re-establishing

the vacuum and slowly increasing the voltage, a point was reached where the platinum bead vaporized, thereby shadowing the surface features or surface contours of the thin films mounted on the specimen grids.

Gold decoration was applied to the specimen surface by placing the grids thirteen centimeters directly beneath a V-shaped thin tungsten wire filament with three millimeters of 0.008 inch diameter gold wire wrapped around the bottom of the V. After evacuating the chamber to approximately 10^{-5} torr, voltage was slowly increased across the filament until the gold wire melted and formed a bead. By further increasing the voltage, a point was reached where the gold bead uniformly wet the tungsten wire and vaporized, thereby decorating the surface of the thin films mounted on the specimen grids. Although the exact mechanism of gold decoration is not understood, it is known [55] that gold decoration provides a surface mapping which is sensitive to crystalline fibers of polymers.

CHAPTER III

CRYSTALLIZATION OF ISOTACTIC/ATACTIC POLYSTYRENE BLENDS

A. Introduction

Spherulitic crystallization from mixtures of isotactic/atactic polystyrene is strongly influenced by the nature of the noncrystallizable impurity---atactic polystyrene. Published results [30] indicate that the morphology and crystallization kinetics are related to both the concentration and molecular weight of the impurity, as well as the conditions of crystallization. However, the "interaction" of polymer-diluent molecules is not clearly understood since only a very limited range of diluent molecular weights were considered by Keith and Padden [30,31]. In addition, there is an apparent discrepancy between the data of Keith and Padden [31] and Boon and Azcue [5]. We therefore decided to make a more detailed examination using a wider range of atactic polystyrene molecular weights (900 to 1,800,000). In this study we used optical microscopy to measure the crystallization kinetics of various blends and optical and electron microscopy as well as wide angle x-ray diffraction and melting temperature measurements to examine the morphology of crystallized mixtures. In particular, x-ray line broadening and melting temperature depression were used to detect possible lattice defects caused by atactic polystyrene impurity.

1. Technical Review

Previous studies by Hay [21], Keith and Padden [30], and Boon, Challa, and Krevelen [7] have established that at a fixed temperature, the radius of a growing spherulite of pure isotactic polystyrene increases linearly with time over a wide range of crystallization temperatures. As the concentration of available amorphous material is depleted, the diffusion of polymer segments to the interface between the crystal and the melt becomes rate controlling, and the radius of a growing crystal correspondingly becomes proportional to the square root of time, retarding the crystallization process [41]. According to the data of Boon, Challa, and Krevelen [7] and Keith and Padden [31], the linear growth rate of pure isotactic polystyrene reaches a maximum at 175°C and 178.5°C respectively, and is uniformly depressed at both higher and lower temperatures, forming a generally symmetrical gaussian curve over a wide range of crystallization temperatures.

Keith and Padden [31] reported that at a given temperature, dilution of isotactic polystyrene with non-crystallizable atactic polystyrene depresses the spherulitic growth rate in proportion to the amount of diluent added. Under these conditions the growth rate is also influenced by the molecular weight of the diluent in that higher molecular weight atactic polystyrene, 247,000, depresses the growth rate more than lower molecular weight atactic diluent, 41,700, at similar concentrations. They also reported that the position of the maximas in the growth rate curves tends to shift toward 190°C for high concentrations of atactic diluent molecular weight 247,000. Finally, Keith and Padden

observed that the optical melting temperature of pure isotactic polystyrene is only slightly depressed--2°C to 3°C--by the addition of up to 75% atactic polystyrene, molecular weight 41,700 or 247,000. These results are in qualitative agreement with those subsequently reported by Boon and Azcue [5], who also noted that the spherulitic growth rate of isotactic polystyrene is depressed by the addition of atactic polystyrene, while the melting temperature is essentially unaffected. Boon and Azcue, however, observed that at the optimum growth rate, the amount of depression is approximately proportional to the concentration of isotactic polystyrene to the 2.58 power, rather than to the first power, as reported by Keith and Padden [31].

Keith and Padden [30] also investigated the effect of impurity segregation on the morphology of spherulitic crystallization of isotactic/atactic polystyrene. Their results show that impurities are rejected preferentially by the growing crystals and that impurity diffusion plays an important role in governing the overall crystalline morphology. In particular, the openness of the texture of the resulting spherulites is a direct function of the amount of slowly diffusing impurity entraped within the growing crystal. Based on these results, they proposed a phenomenological theory of spherulitic crystallization which states that the polycrystalline character of this type of crystallization arises principally because the entrapment or accumulation of impurities rejected at the growing crystal front causes the radically growing fibers of the spherulite to branch

noncrystallographically.

Keith [29] also observed this type of noncrystallographic branching in small hexagonal hedrite nuclei generated at high temperatures in thin films (2-20μ) of mixtures of isotactic/atactic polystyrene. Upon reaching a critical diameter, the hexagonal edges of these hedrite nuclei become unstable and develop multibranched radial fibrous structures characteristic of spherulitic crystallization. Keith interprets this behavior in terms of the phenomenological theory mentioned earlier.

Based on all of these results, Keith and Padden [31] proposed an approach to absolute theory of spherulitic growth kinetics which takes into account the interfacial concentration of the crystallizable constituent, Ci. According to their model, the interfacial concentration, Ci, is a general function of the spherulitic growth rate, G, the molecular diffusivity, D, and the concentration of the crystallizable polymer at a distance far removed from the crystallization front, $C_\infty(T)$, i.e. $Ci = f[G,D,C_\infty(T)]$. The resulting growth rate G does not appear as an explicit function of known parameters of the system, since it is also dependent on the interfacial concentration, Ci. Therefore, according to their model, the overall growth rate cannot be directly calculated when the effect of rejected impurity on the interfacial concentration is considered. In addition, Keith and Padden reported that a parameter of major significance is $\delta = D/G$, where D is the diffusivity of the impurity in the melt and G is the spherulitic growth rate. They suggest

that δ should be the equilibrium width of the crystalline fibers and that noncrystallographic branching occurs when the fibers reach this width.

In a related study, Magill [36] found that, in addition to other factors, the spherulitic growth rate G is dependent on the molecular weight of the crystallizable material, P-Silphenylene Siloxane (TMPS), crystallized from the amorphous melt of a homopolymer system. In this case he was working with a one component system rather than the two component system studied by Keith and Padden. Results show that the growth rate $G \propto (1/Mn)^y$ where Mn is the number average molecular weight and y is a factor which usually varies from 0 to 1.0. In the high molecular weight range y=0, but as the molecular weight decreases below to the critical molecular weight for chain entanglements, y suddenly assumes values approaching 1.0.

Fox and Flory [15] also observed significant changes over the range of the critical molecular weight for the melt viscosity and glass transition temperature of atactic polystyrene. In the case of the melt viscosity, they interpret these changes in terms of the molecular chain entanglements which occur above the critical molecular weight, Mc=36,000.

2. Kinetic Theory

As mentioned earlier, numerous studies show that at a fixed temperature, the radius of a growing spherulite increases linearly with time over a wide range of crystallization temperatures. An analysis of the temperature

coefficients, as well as the rate of formation and growth of spherulitic centers suggests that nucleation theory may be applied to the crystallization process.

Utilizing transition state theory, Turnbull and Fisher [58] have developed an expression for the rate of nucleation in condensed systems. The solid state nucleation rate per unit volume is given by:

$$N=N_o \exp\left(\frac{-E_D-\Delta F^*}{RT}\right) \qquad (1)$$

where E_D is the free energy of activation for transport across the liquid-nucleus interface, ΔF^* is the free energy required to form a nucleus of critical size, and N_o is related to the number of molecules per unit volume in the liquid.

For homopolymers the rate of secondary nucleation or the radial growth rate G of spherulites follows a relation of the form:

$$G=G_o \exp \frac{-E_D-\Delta F^*}{RT} \qquad (2)$$

where G_o is thought to be a constant independent of temperature, although some experimental results suggest that G_o is dependent upon molecular weight [23]. Other investigators [56] have found that the value of G_o is also dependent upon the type of analysis used to evaluate the empirical constants found in the E_D and ΔF^* terms. As a means of evaluating the term E_D describing the segmental jump rate across the liquid-nucleus interface, Hoffman and Weeks [23] suggested the following approximation based on the empirical expression

of Williams, Landel, and Ferry [60]:

$$E_D=C_1T/(C_2+T-Tg)= 4.12X10^3T/(C_2+T-Tg) \qquad (3)$$

where Tg is the glass transition temperature and C_1 and C_2 are empirical constants usually taking values of C_1 = 4.12 Kcal/mole and C_2 = 51.6°K for most polymers. This expression describes the segmental jump rate required for the initiation of viscous flow in the bulk. Substitution of equation 3 into 2 yields:

$$G=G_o\exp[-4.12X10^3/R(C_2+T-Tg)]\ \exp[\Delta F^*/RT] \qquad (4)$$

The expression of the free energy required to form a nucleus of critical size, ΔF^*, is presented by several authors. For example Mandelkern [41] uses the following expression:

$$\Delta F=2\sigma_e\rho b_o+2\sigma_u\xi b_o-\rho\xi b_o\Delta f_u \qquad (5)$$

where Δf_u is the free energy of fusion per molecule, b_o the thickness of one molecule, σ_u the lateral interfacial free energy per molecule, and σ_e the end interfacial free energy per molecule. The further development of this expression is identical to the development to be used for the diluted system, and therefore will not be discussed here. The final form of equation 4 is as follows:

$$G(undil)=G_o\exp[-4.12x10^3/R(C_2+T-Tg)]\ \exp\left[\frac{-4b_o\sigma_u\sigma_e Tm}{R\Delta HT\ (Tm-T)}\right] \qquad (6)$$

This equation describes the theoretical spherulitic growth rate for homopolymers and is based on a development using monomeric nucleation theory and an empirical approximation for the interfacial jump rate term. In addition, it is assumed that the heat (ΔH) and entropy (ΔS) of fusion are independent of temperature.

The addition of noncrystallizable diluent to a crystallizable polymer affects the spherulitic growth rate by diluting the concentration of crystallizable molecules. According to the analysis of Gornick and Mandelkern [19], the dilution effect is accounted for by altering the free energy of formation for a critical size nucleus, ΔF^*, as well as the pre-exponential term.

The free energy of formation for a two-dimensional nucleus from a polymer-diluent mixture is given by [19]:

$$\Delta F=2\sigma_e\rho b_o+2\sigma_u\xi b_o-\rho\xi b_o\Delta f_u-RT(\rho/b_o)\ell n\upsilon_2 \qquad (7)$$

Except for the last term, equation (7) is identical to the free energy expression used for the homopolymer system, equation (5). The term $RT(\rho/b_o)\ell n\upsilon_2$ is an entropic contribution to the free energy because $R\ell n\upsilon_2$ represents the probability of selecting a number of ρ/b_o crystalline sequences of length ξ from the mixture [5]. The free energy surface represented by equation (7) contains a saddle point. The coordinates of the saddle point are obtained by setting $(\partial\Delta F/\partial\xi)_\rho$ and $(\partial\Delta F/\partial\rho)_\xi$ equal to zero. It is then found that:

$$\rho^* = 2\sigma_u/\Delta f_u$$

$$\xi^* = (2\sigma_e/\Delta f_u) - (RT\ell n\upsilon_2/b_o^2\Delta f_u)$$

At the saddle point:

$$\Delta F=\Delta F^*=4b_o\sigma_u\sigma_e/\Delta f_u - 2\sigma_u RT\ell n\upsilon_2/b_o\Delta f_u \qquad (8)$$

The free energy of fusion, Δf_u, can be approximated by:

$$\Delta f_u = \Delta H(Tm-T) \qquad (9)$$

where ΔH is the heat of fusion and Tm is the equilibrium melting temperature. This approximation implicitely assumes that the heat (ΔH) and entropy (ΔS) of fusion are independent of temperature and equal to ΔH_f and ΔS_f at Tm respectively. Other approximations [56] for Δf_u considering ΔCp=constant or $d(\Delta Cp)/dT$=constant, result in lower values of Δf_u than found with the first approximation, particularly for temperatures close to Tg. However, Suzuki and Kovacs [56] indicate that the first approximation (equation 9), although being of simplest form, provides a best fit with the experimentally measured spherulitic growth rates of pure isotactic polystyrene over crystallization temperatures ranging from near Tg to Tm. Substitution of equations (8) and (9) into (4) gives:

$$G(dil)=\upsilon_2 G_o \exp\left[\frac{-4.12X10^3}{R(C_2+T-Tg)}\right] \exp\left[\frac{-4b_o\sigma_u\sigma_e Tm}{RT\Delta H(Tm-T)} + \frac{2\sigma_u Tm\ell n\upsilon_2}{b_o\Delta H(Tm-T)}\right] \qquad (10)$$

where the pre-exponential term G_o is multiplied by the concentration υ_2 of the crystallizable constituent because the rate of nucleation is directly proportional to the

concentration of crystallizable units [19]. This equation describes the theoretical spherulitic growth rate for polymer-diluent mixtures based on the assumptions inherent in the development of equation 6 and the dilution analysis by Gornick and Mandelkern [19].

The relationship between the spherulitic growth rate G(dil) of a polymer-diluent mixture and the spherulitic growth rate G(undil) of the pure homopolymer can be derived by combining equations 6 and 10, assuming that the melting temperature Tm, the glass transition temperature Tg and the pre-exponential constant G_o are the same for the pure and diluted systems.

$$G(dil) = \upsilon_2 \exp\left[\frac{2\sigma_u Tm \ \ell n \ \upsilon_2}{b_o \Delta H (Tm-T)}\right] G(undil) \qquad (11)$$

The assumption of constant glass transition temperature Tg for polystyrene of molecular weights greater than 30,000 is verified by the experimental data of Fox and Flory [15]. The assumption of constant melting temperature for both the pure and diluted isotactic/atactic polystyrene systems, however, is valid only over certain concentration ranges and molecular weights of the atactic diluent, according to the experimental results to be presented in Chapter III. In estimating the term $2\sigma_u/b_o\Delta H$, Boon and Azcue [5] used the empirical relation $\sigma_u = \alpha b_o \Delta H$ with $\alpha=0.1$ for the lateral surface of a chain type crystal. This gives $2\sigma_u/b_o\Delta H = 0.2$. Substitution of this value into equation 11 gives:

$$G(dil) = \upsilon_2 \exp\left[\frac{0.2Tm \ \ell n \ \upsilon_2}{(Tm-T)}\right] G(undil) \qquad (12)$$

which is the equation used to compare theoretical predictions to the experimentally determined spherulitic growth rates for the isotactic/atactic polystyrene system.

B. Experimental

1. Preparation

Solutions containing 0.4% polystyrene in benzene were made by completely dissolving a weighed amount of either isotactic or atactic polystyrene in a measured volume of boiling benzene. Upon cooling to room temperature, predetermined ratios of clear 0.4% atactic and 0.4% isotactic solutions were pipetted together to make up a clear 0.4% mixed solution of isotactic/atactic polystyrene in benzene. We have also mixed hot solutions, but there is no difference. Transparent thin films approximately 60 microns thick, as determined by density calculations based on a polystyrene density of 1.0 gram/cm^3 [5], were prepared by casting from the 0.4% mixed solution onto thin cover glasses placed on a hot plate set at 50°C. These thin films were then dried under vacuum at 50°C for 24 hours to insure removal of any residual solvent.

Samples suitable for x-ray analysis were prepared by mixing the proper ratio of finely ground powders of isotactic and atactic polystyrene. The mixed powders were melted on a hot plate at 260°C for one half hour in a 1/8 inch thick aluminum mold, sandwiched between cover glass in order to protect the melted polymer from oxidative degradation. After complete melting, the mold was quickly transferred to a

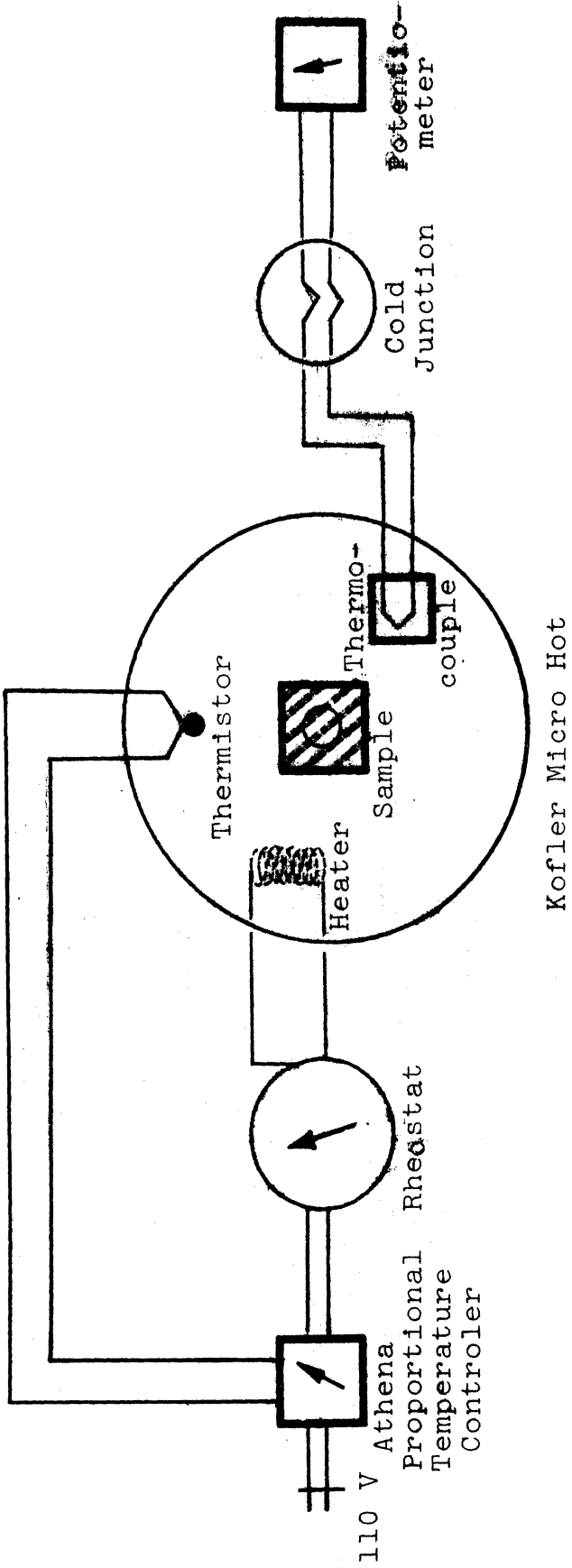

CIRCUIT DIAGRAM FOR THE HOT STAGE OF THE OPTICAL MICROSCOPE

Figure 1

silicone oil temperature control bath set at 180°C for subsequent isothermal crystallization.

2. Optical Microscopy

The radial increase in size of the growing spherulitic crystals of isotactic polystyrene were measured through a 400 power Unitron optical polarizing microscope equipped with a Kofler micro hot stage and a filar micrometer eyepiece which was calibrated with a Unitron precision etched slide with markings at 0.01 millimeters. The Kofler micro hot stage was controlled by an Athena model 51T proportional temperature controller equipped with a 0.04 inch diameter glass bead Fenwal thermistor (GA52J16). The controller is capable of full scale response at temperature fluctuations on the order of ± .15°C. The accompanying diagram, figure 1, illustrates the hot stage circuitry. Because of the high temperature environment, the glass bead thermistor was connected to the controller lead wires by high melting point solder. The thermistor was positioned under a set screw and in direct contact with the heated surface. The surface temperature of the Kofler hot stage was intermittently measured by a 22 gauge chromel-alumel thermocouple sandwiched between two cover glasses and sealed with epoxy resin. This thermocouple sandwich was placed directly on the surface of the hot stage and maintained in a flat position by a small ring weight. Lead wires from the thermocouple and thermistor, sheathed in ceramic insulation, extended out from the hot stage through a small grove in the ring spacer placed

on top of the stage. Additional temperature control was afforded by placing a ground glass lid over the ring spacer on the top of the hot stage assembly. The thermocouple response was measured on a Leeds and Northrup potentiometer capable of accurately measuring temperatures to within ± .5°C, and it was calibrated against three mercury thermometers at 97°C, 175°C, 210°C, and 220°C in a controlled temperature silicone oil bath. Overall temperature control on the Kofler hot stage was better than ± .5°C, since the thermocouple could not detect any temperature fluctuations once the isothermal crystallization temperature had been reached. In similar studies, Keith and Padden [31] claimed a Kofler hot stage temperature control of ± .2°C, although no specific details were advanced as to how they achieved this.

3. Measurement of Growth Rate

Thin films of well blended isotactic and atactic polystyrene, sandwiched between two cover glasses, were heated on the microscope hot stage to 250°C (10°C above the melting point of isotactic polystyrene) for five minutes, then cooled at a rate of about 20°C per minute for isothermal crystallizing at temperatures ranging from 100°C to 210°C. According to growth rate measurements extrapolated back to zero time, most spherulitic crystals generally did not start to nucleate and grow until some time after the hot stage had cooled down to the isothermal crystallization temperature. This result indicates that many of the nuclei were destroyed by the thermal treatment at 250°C.

The spherulites within a given field of view were very uniform in size, suggesting that they were all generated at the same time. The spherulitic growth rate at a given temperature was determined by measuring the size of a number of spherulites within a field as a function of time, by means of the filar eyepiece micrometer. Spherulitic growth rates were measured for thin films having various concentrations of atactic polystyrene, molecular weights ranging from 900 to 1,800,000, added to isotactic polystyrene of molecular weight 550,000. Thus, the growth rate, G, is the dependent variable effected by the concentration and molecular weight of the atactic impurity, as well as the temperature of crystallization. Data scatter from duplicate measurements indicates that the growth rate is reproducible for identical conditions to within ±5%. The crystals were also photographed by a 35 millimeter Exacta single lens reflex camera directly mounted on the optical microscope.

4. Melting Temperature Determination

Spherulitic crystals of isotactic polystyrene are birefringent under crossed polarizers in the optical microscope, and the temperature at which this birefringence totally disappears is designated as the optical melting point. Consequently, the optical melting point represents the temperature at which the onset of crystalline disorganization is observed. Melting points measured by careful dilatometry yield results 3-5°C higher than those measured optically [22]. However, optical measurements are a relatively

convenient means of establishing the dependence of the crystalline melting temperature on the concentration and molecular weight of the impurity diluent. Care was taken when making such measurements, since the crystalline melting point is affected by the heating rate [31]. Thin films of isotactic/atactic polystyrene samples crystallized at 180°C were individually heated on the Kofler hot stage at rates ranging from 0.5°C to 1.0°C per minute until the birefringence totally disappeared. These films were then cooled to 180°C and recrystallized, a process which generally occurred within ten to twenty minutes.

The morphology of recrystallized spherulites was quite different from the fibrous morphology of the original spherulites. Within the former boundaries of the original spherulites, the recrystallized structure appears to consist of tiny birefrigent beads closely impinging upon one another. However, unrestricted growth from these same beads out into the melt caused small spherulitic structures to develop along the original boundaries, figure 2 (page 24). Banks, Gordon, and Sharples [2] noted similar structural changes in partially melted spherulites of polyethylene and attributed it to residual seed nuclei which act as centers for further growth on subsequent cooling.

The optical melting points of these spherulites were measured a second time to insure that the measured melting point was not a function of the heating rate. In general, it was observed that heating rates less than 0.7°C per minute do not influence the ultimate optical melting point. This

rate is similar to the heating rate of 0.5°C per minute used by Keith and Padden [30] for their determinations of spherulitic melting point. The accuracy of the melting temperature values is judged to be within ± 1.5°C, as indicated by the data scatter (see Figure 11).

5. X-ray Studies

X-ray studies were also carried out on spherulites of isotactic polystyrene isothermally crystallized from mixtures with a high concentration (80%) of noncrystallizable atactic polystyrene impurity. The x-ray scatter was measured by a Norelco diffractometer as described in Chapter II. The range of 2θ angles scanned includes the (110), (220), and (211) crystalline peaks of isotactic polystyrene, but background scatter from noncrystallizable amorphous material tended to obscure all of these peaks except the (110) d_{110}=11.02Å between 2θ of 4.5° and 6.5°. Accordingly, the (110) peak was scanned between four and six times for each specimen, and the resulting values of the peak half-width were averaged.

C. Results

1. Morphology

Electron microscopy examination of typical crystallized thin films of pure isotactic polystyrene shows that spherulitic aggregates are made of radiating bundles of fine ribbon fibers, approximately 150Å thick, as illustrated in Figure 3. Since these fibers grow at a uniform rate in the

Figure 3: Electron micrograph of isotactic polystyrene crystallized from the glassy amorphous state at 140°C. Platinum shadowed at 30°.

radial direction, the spherulite crystals are usually symmetrically round in shape. Under crossed polarizers in the optical microscope, the crystals have a positive birefringence with the normal maltese cross. At these crystallization temperatures there is no evidence of the ring type or zig-zag extinction contours observed in polyethylene and polyamide spherulites [38].

The spherulites in thin films (approximately 60μ thick) develop from either 1 to 2μ fibrous nuclei or from hexagonal hedrite nuclei. Generation of fibrous nuclei is favored by high molecular weight noncrystalline impurity (above 51,000) and crystallization temperatures below 180°C, while hexagonal nuclei appear for low molecular weight impurity (below 19,800) and crystallization temperatures above 180°C. Both of these results are in qualitative agreement with Keith [29] who noted such hexagonal aggregates in mixtures of low molecular weight atactic (4,500) in isotactic polystyrene, particularly at temperatures above 200°C in thin films ranging from 2 to 20μ thick. He found that after reaching a certain diameter, the edges of the hexagonal hedrite nuclei became serrated and started to develop a radial fibrous conformation which later developed in the normal spherulitic mode. Examination of Figure 4, however, will show that for the present system, the spherulitic mode tends to initiate at the center of the hexagonal hedrites, rather than at the edge, as indicated by Keith. Subsequent growth follows a normal fibrous morphology and hexagonal nuclei become overgrown with radial spherulitic fibers. The

reason for the difference between our observations and Keith's probably is related to film thickness. Keith worked with very thin films (2-20μ) which tended to inhibit the initiation of spherulitic growth on the lateral surface, whereas the present work was based on films approximately 60μ thick.

Qualitatively, high concentrations of impurity cause the fibrous texture of the resulting spherulites to be more "open", (note the edges of the spherulites, Figure 4), than spherulites grown from pure isotactic polystyrene, Figure 5. This characteristic was also noted by Keith and Padden [30], who observed a direct correlation between the "openness" of the fibrous texture and the concentration of atactic polypropylene in the isotactic/atactic polypropylene system.

2. Effect of Temperature

The spherulitic growth rate of pure isotactic polystyrene is linear with respect to time over a wide range of temperatures, as shown in Figure 6. In addition, the growth rate reaches a clear maximum at approximately 178°C (± 2°C) and is depressed at higher and lower crystallization temperatures, Figure 7. These results are in good agreement with previous studies by Keith and Padden [31] and Boon, Challa, and Krevelen [7], who noted the growth rate maxima for pure isotactic polystyrene at 178.5°C and 175.0°C respectively. In general, the growth rate becomes nonlinear only under the conditions in which the diffusion of the crystallizing species becomes rate controlling because of the exhaustion

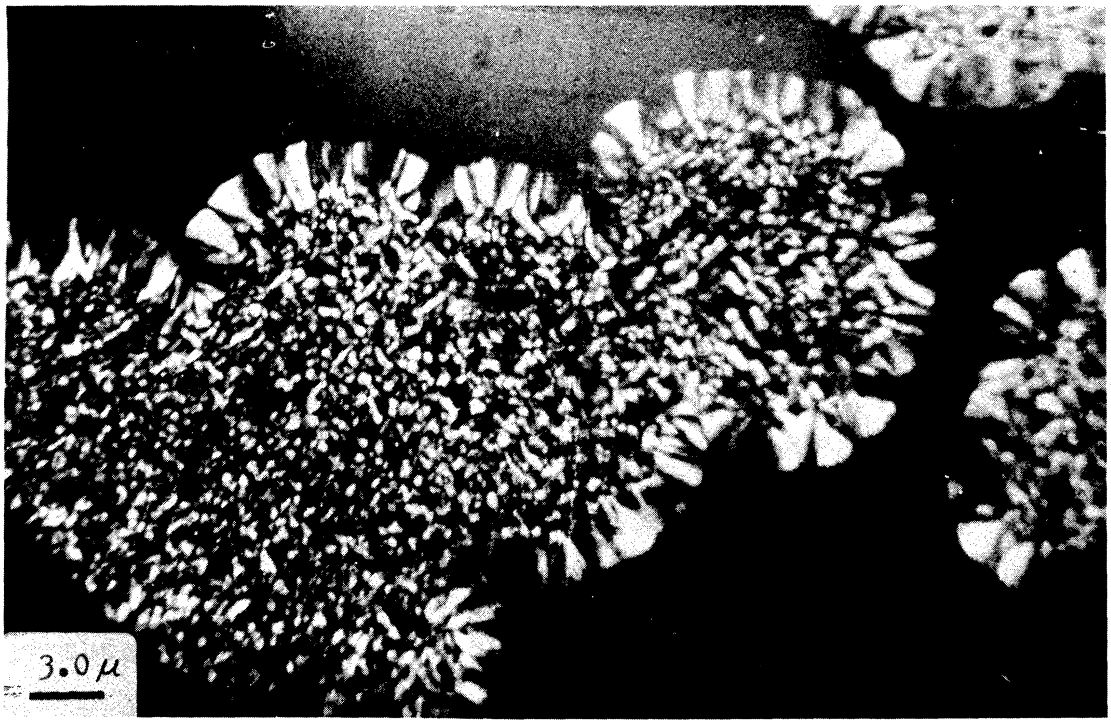

Figure 2: Light micrograph (through crossed polarizers) of isotactic polystyrene partially melted and recrystallized at 180°C.

Figure 4: Light micrograph (through crossed polarizers) of isotactic/atactic polystyrene 40/60 (APS M_w=19,800) crystallized from the melt at 180°C. Arrows indicate serrated edge of spherulite.

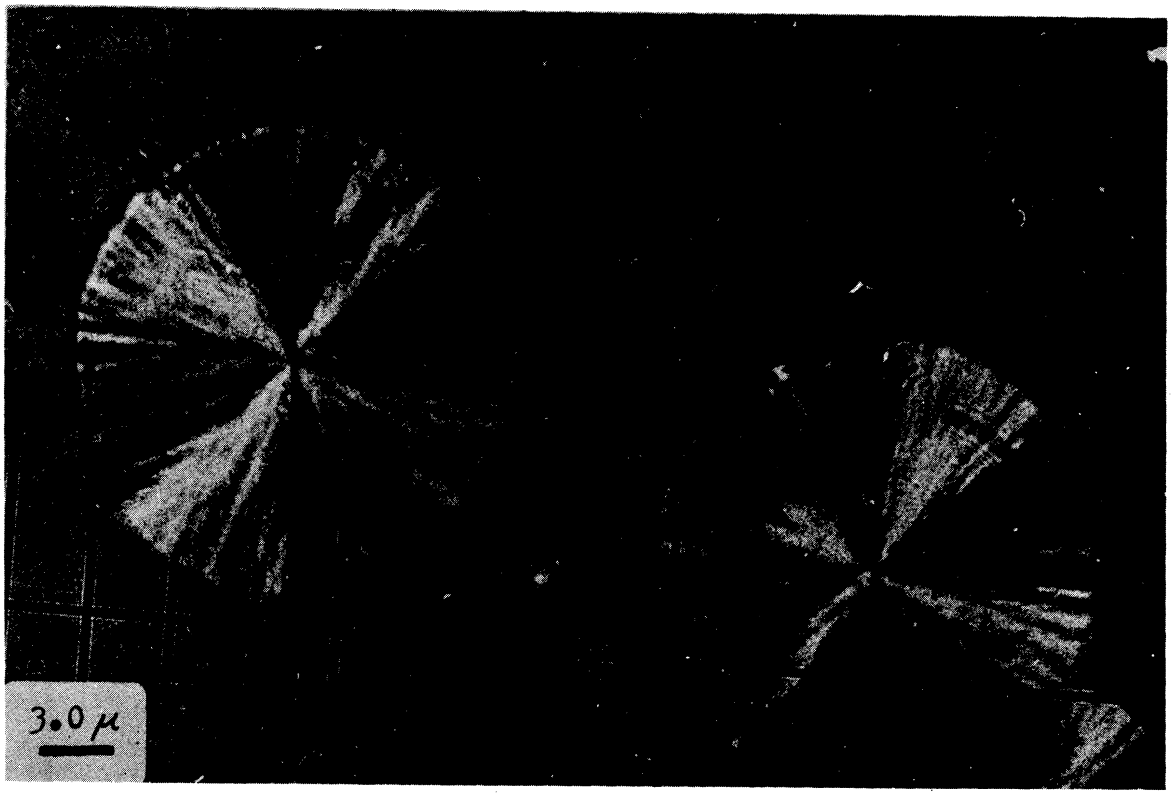

Figure 5: Light micrograph (through crossed polarizers) of isotactic polystyrene crystallized from the melt at 180°C. Arrows indicate smooth edge of spherulite.

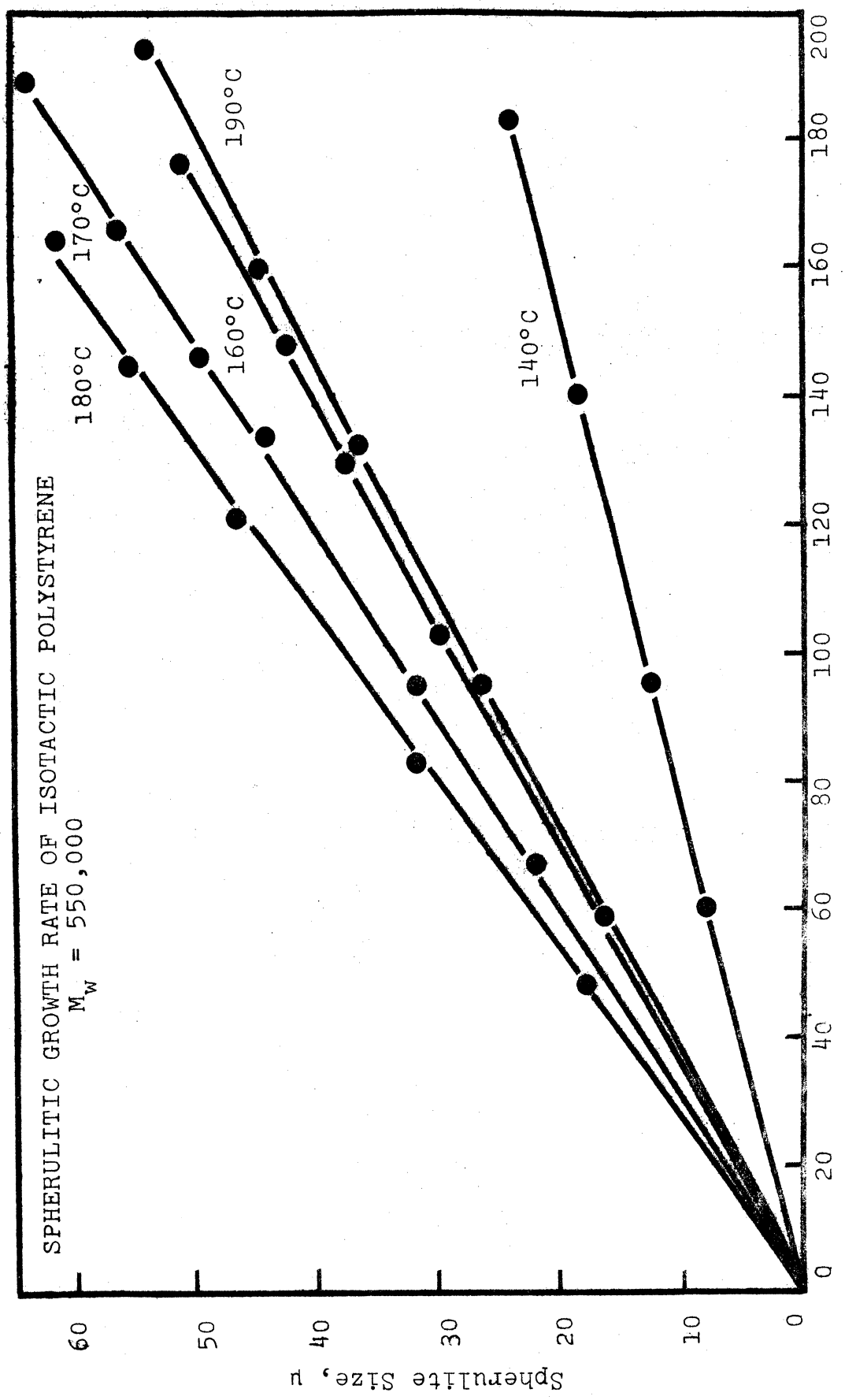
SPHERULITIC GROWTH RATE OF ISOTACTIC POLYSTYRENE
M_w = 550,000
180°C
170°C
160°C
190°C
140°C
Spherulite Size, μ
Time, minutes
0
10
20
30
40
50
60
0
20
40
60
80
100
120
140
160
180
200

Figure 6

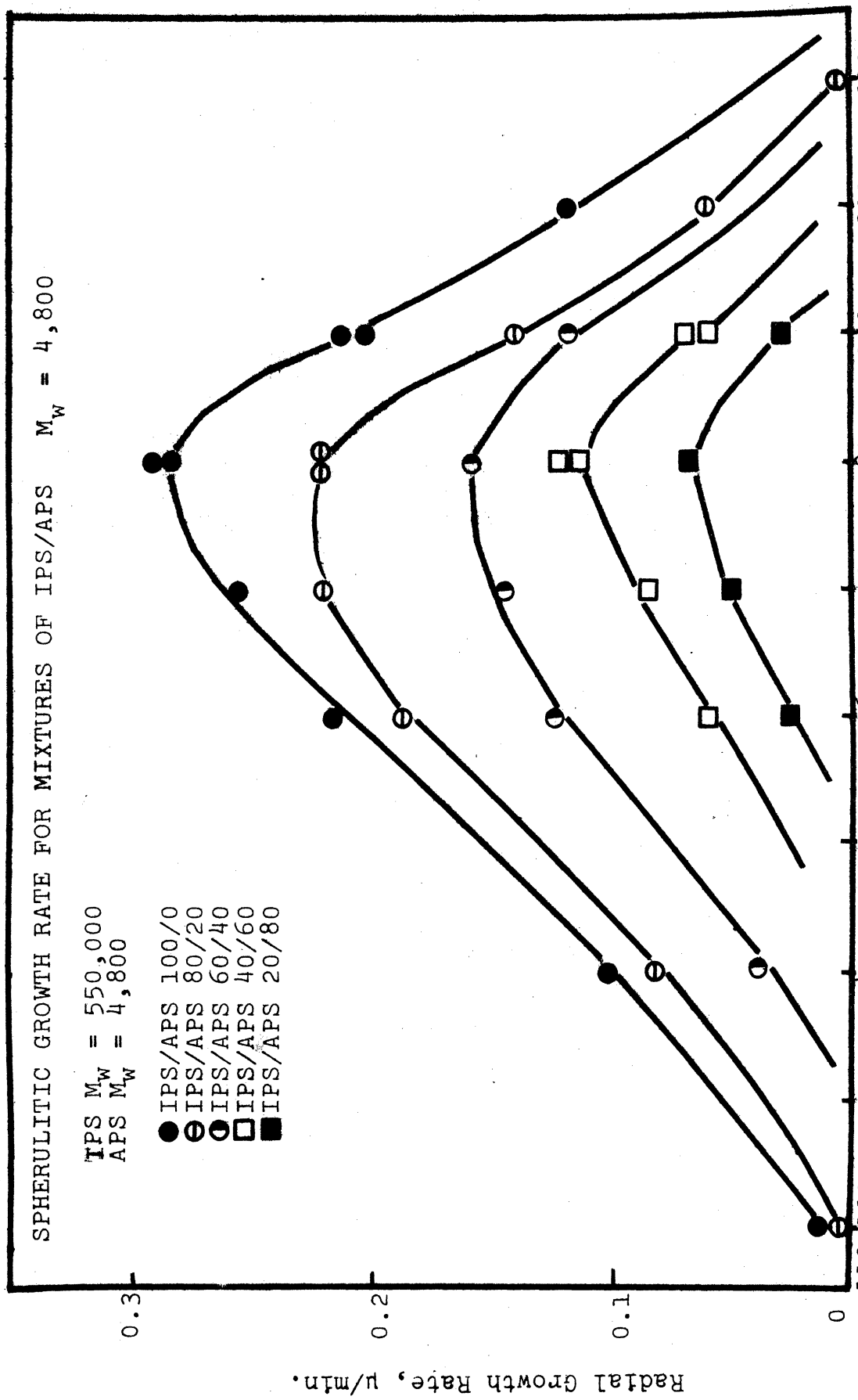
SPHERULITIC GROWTH RATE FOR MIXTURES OF IPS/APS M_w = 4,800
IPS M_w = 550,000
APS M_w = 4,800
IPS/APS 100/0
IPS/APS 80/20
IPS/APS 60/40
IPS/APS 40/60
IPS/APS 20/80
Radial Growth Rate, μ/min.
0
0.1
0.2
0.3
110
120
130
140
150
160
170
180
190
200
210
Temperature, °C

Figure 7

or depletion of the crystallizable constituent or when spherulites impinge upon one another.

3. Effect of Diluent Concentration

Figure 7 shows that dilution with noncrystallizable atactic polystyrene, molecular weight 4,800, causes a general depression of the spherulitic growth rate, with the maximas still occurring in about the same temperature range (178°C ± 2°C), as for undiluted isotactic polystyrene. Dilution with the highest molecular weight atactic polystyrene (1,800,000) does not cause the temperature range for the maximum growth rate to shift to higher temperatures, while similar dilution with very low molecular weight atactic polystyrene, 900 and 2,030, only causes a shift to lower temperatures for the 900 molecular diluent, Table IX. In this case, the maximum growth rate temperature range shifts to about 175°C (± 2°C). Therefore, for the system being studied, the maximum growth rate occurs at about 178°C (± 2°C) for diluent molecular weights ranging from 2,030 to 1,800,000. In the system studied by Keith and Padden [31] high dilutions with atactic polystyrene, molecular weight 247,000, caused the growth maximas of isotactic polystyrene, molecular weight 60,000, to shift to higher temperatures (190°C). There is no clear explanation as to why the shift should definitely occur in one case but not appear to in the other, although the difference in molecular weight of the isotactic component, 550,000 vs. 60,000, most likely has an important effect.

Figure 8 presents the growth rate data at 180°C for atactic diluents of different concentrations and molecular weights. This temperature was chosen because the maximum growth rates for pure and diluted isotactic polystyrene all occur at about 180°C. In addition, the change in growth rate as a function of temperature, $\Delta G/\Delta T$, is minimized at this temperature, thus reducing the effect of temperature fluctuations on the accuracy of the growth rate measurement. At this temperature (180°C), dilution with atactic impurity results in a more or less linear depression of the growth rate, in proportion to the amount of diluent added. This result is in general agreement with data by Keith and Padden [31] for two different molecular weight atactic polystyrene diluents at 178.5°C, but disagrees with the scattered data taken by Boon and Azcue [5] for mixtures of isotactic (M_w 185,000) and atactic (M_w 260,000) polystyrene, as shown in Figure 9. There is a clear discrepancy between the results of Keith and Padden and those of Boon and Azcue which cannot be accounted for by the slight difference in crystallization temperature [5].

4. Effect of Diluent Molecular Weight

Figure 10 shows a cross plot of Figure 8 using diluent concentration as the parameter. Data for atactic polystyrene, molecular weight 900, with a maximum crystallization temperature at about 175°C (± 2°C), is also included. Both the uncertainty of the exact maximum growth rate temperature (± 2°C), as well as the reproducibility of the data in

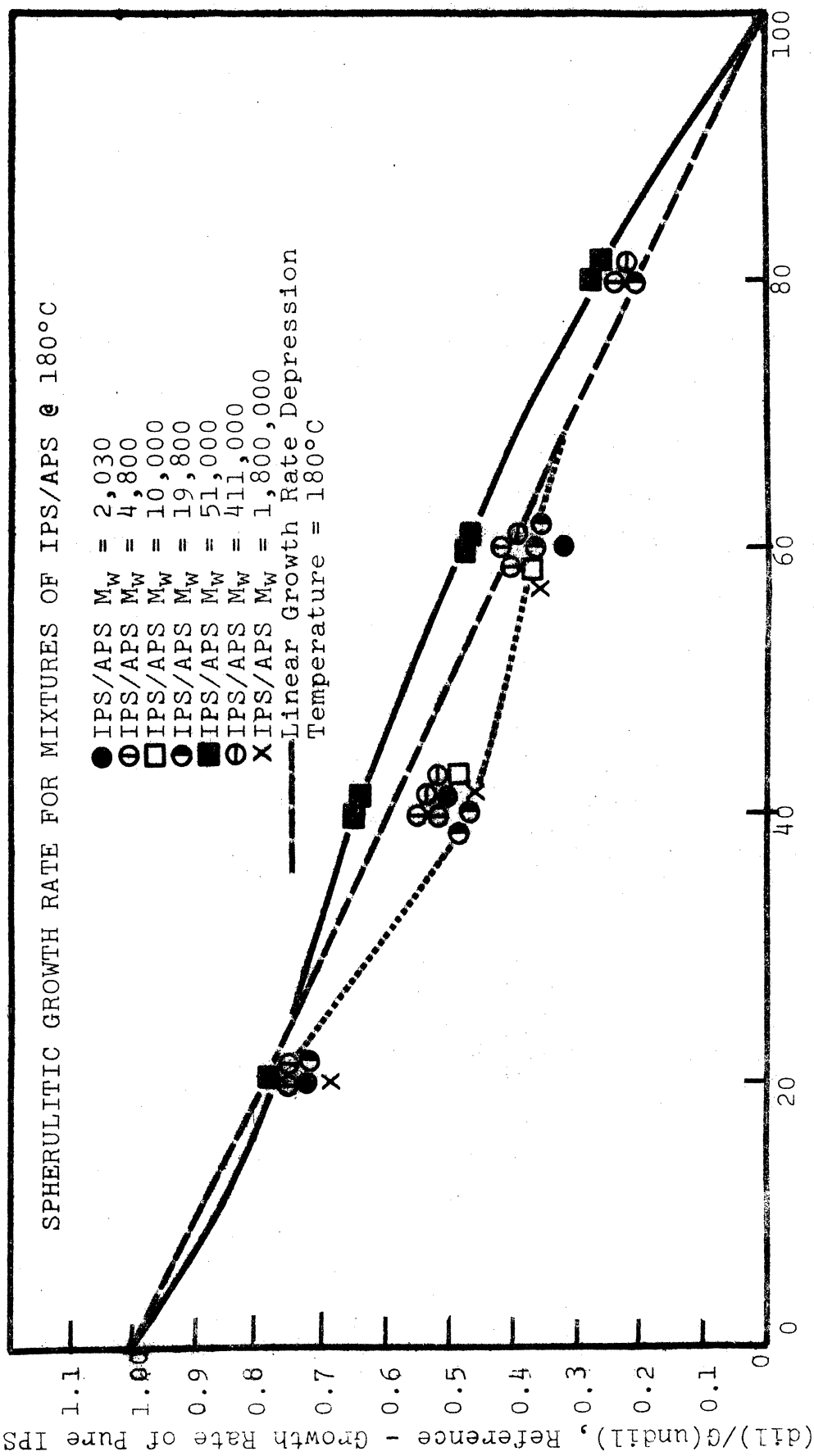
SPHERULITIC GROWTH RATE FOR MIXTURES OF IPS/APS @ 180°C
IPS/APS M_w = 2,030
IPS/APS M_w = 4,800
IPS/APS M_w = 10,000
IPS/APS M_w = 19,800
IPS/APS M_w = 51,000
IPS/APS M_w = 411,000
IPS/APS M_w = 1,800,000
Linear Growth Rate Depression
Temperature = 180°C
G(dil)/G(undil), Reference - Growth Rate of Pure IPS
% Atactic Polystyrene (APS)
0
0.1
0.2
0.3
0.4
0.5
0.6
0.7
0.8
0.9
1.00
1.1
0
20
40
60
80
100

Figure 8

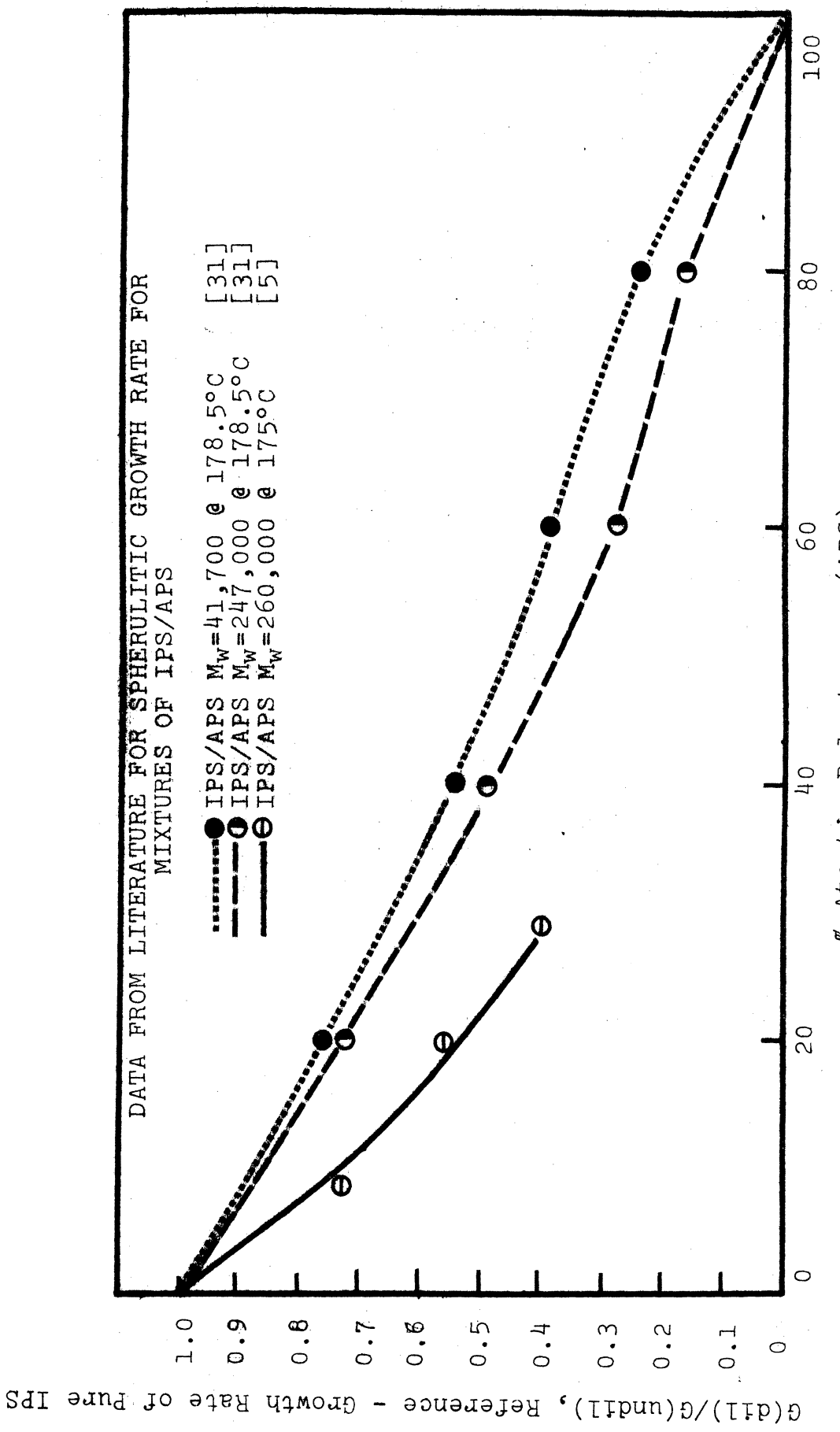
DATA FROM LITERATURE FOR SPHERULITIC GROWTH RATE FOR MIXTURES OF IPS/APS
IPS/APS Mw=41,700 @ 178.5°C [31]
IPS/APS Mw=247,000 @ 178.5°C [31]
IPS/APS Mw=260,000 @ 175°C [5]
G(dil)/G(undil), Reference - Growth Rate of Pure IPS
% Atactic Polystyrene (APS)
0
0.1
0.2
0.3
0.4
0.5
0.6
0.7
0.8
0.9
1.0
0
20
40
60
80
100

Figure 9

Figures 7 and 8, suggests that the confidence limit on the data points in Figure 10 ought to be about ± 5%. The results show that the spherulitic growth rate for low dilutions (20%) of noncrystallizable impurity is nearly independent of the impurity molecular weight, except for very high molecular weight diluent. This finding suggests that in this concentration range (20%) the diffusional characteristics of the impurity play only a very minor role in the determination of the overall growth kinetics. Apparently, low concentrations of rejected impurity can be efficiently accommodated between the fibrils of the growing crystal and prevented from diffusing radially. This is in agreement with the morphological observations by Keith and Padden [30] who noted that significant amounts of rejected impurity are entrapped within the growing spherulite and do not diffuse away from the growing crystal front.

At intermediate diluent concentrations (40% and 60%), quite noticible effects are observed over the entire molecular weight range. Of particular importance is the sudden 30% increase in the radial growth rate as the diluent molecular weight is increased from 19,800 to 51,000. This is surprising because one would normally expect the growth rate kinetics to be more or less uniformly depressed with increasing diluent molecular weight, similar to the trends noted by Keith and Padden [30] (Figure 9) and by Magill [36]. This result cannot be explained by macroscopic ($\gtrsim$ 2000 Å) phase separation since the films were quite transparent for all mixtures prior to crystallization. In regions from 4,800

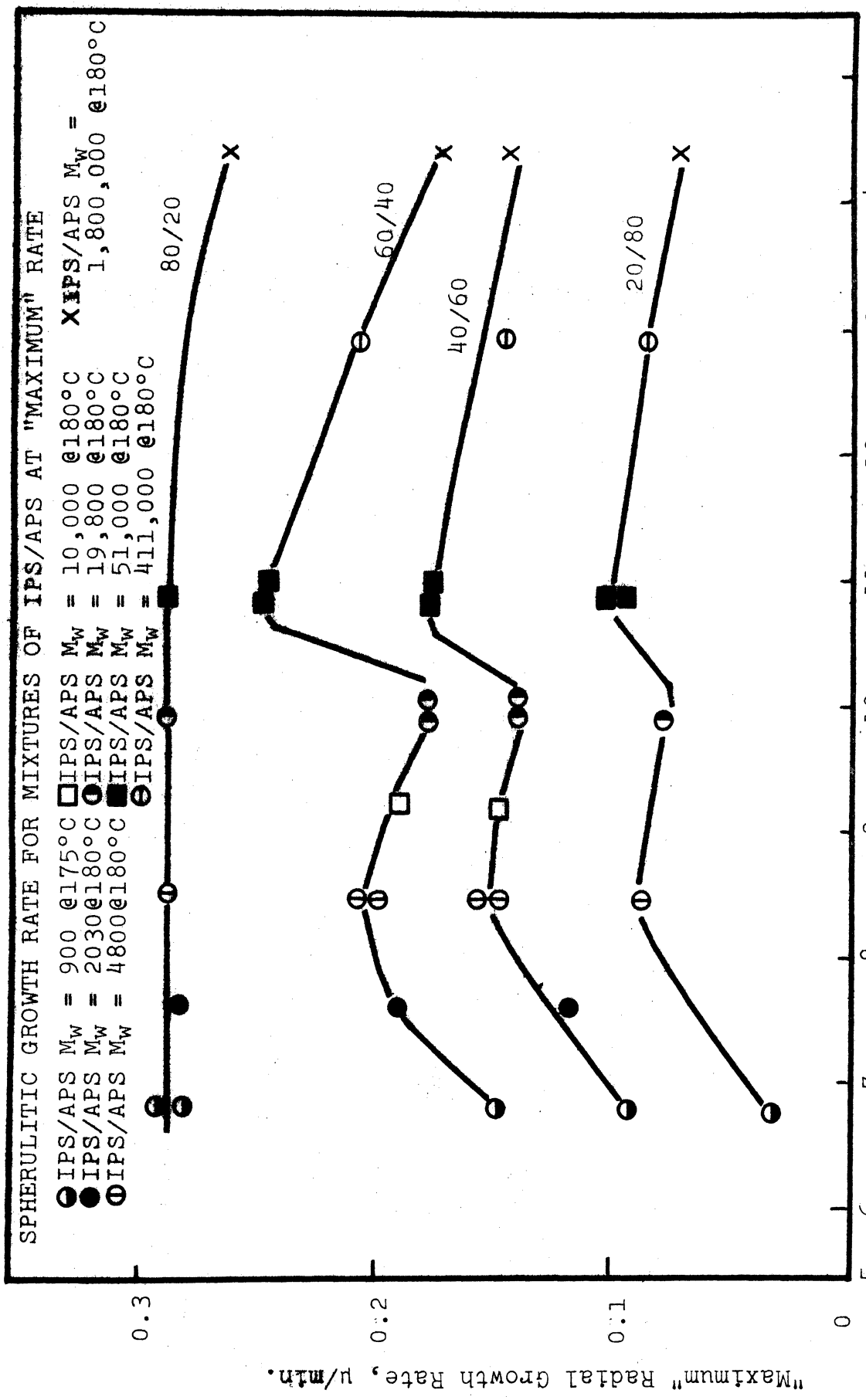
SPHERULITIC GROWTH RATE FOR MIXTURES OF IPS/APS AT "MAXIMUM" RATE
IPS/APS Mw = 900 @175°C
IPS/APS Mw = 2030@180°C
IPS/APS Mw = 4800@180°C
IPS/APS Mw = 10,000 @180°C
IPS/APS Mw = 19,800 @180°C
IPS/APS Mw = 51,000 @180°C
IPS/APS Mw = 411,000 @180°C
IPS/APS/APS Mw = 1,800,000 @180°C
80/20
60/40
40/60
20/80
"Maximum" Radial Growth Rate, μ/min.
0
0.1
0.2
0.3
5
6
7
8
9
10
11
12
13
14
15
Ln Molecular Weight APS

Figure 10

to 19,800 and above 51,000 molecular weight, the curves for intermediate concentrations (40% and 60%) have a similar negative slope, although being displaced. However, in the region for very low molecular weight diluents (4,800 to 900), the growth rate shows a maximum at 4,800 and is depressed with decreasing molecular weight. This growth rate trend for lower molecular weights was also observed by Keith and Padden [31] for a 40% concentration of atactic (molecular weights 540; 2,600) in isotactic polypropylene at 125°C and 130°C. These effects will be discussed in more detail in a later section.

At high diluent concentrations (80%), the effect of impurity molecular weight is essentially damped out over the range of particular interest: 19,800 to 51,000. There were no observable changes in spherulitic morphology which could be associated with the effects noted in Figure 10. However, gradual changes in general morphology for spherulites grown from these mixtures are discussed on page 26.

5. Optical Melting Temperatures

Figure 11 shows the relationship between optical melting temperature and the concentration and molecular weight of atactic polystyrene diluent in thin films crystallized at 180°C. In general, the melting temperature is depressed with increasing concentration and decreasing molecular weight (below 19,800) of the added atactic impurity. Neither Keith and Padden [30] nor Boon and Azcue [5] observed any significant melting point depression, probably because

they used only two atactic polystyrene diluents and both were high molecular weight fractions, 178,000 and 247,000, respectively. In somewhat similar studies, Mandelkern [41] noted that low molecular weight diluents, particularly α-chloronaphthalene, significantly depressed the melting temperature of linear polyethylene. He concluded that the melting point of linear polyethylene was depressed by increasing the solubility and the concentration of the diluent. However, in cases where very poor solvents were used as diluents, he observed that the melting temperature was relatively uneffected. He was able to correlate this result with the appearance of macroscopic (> 2000Å) phase separation in the melt, thus suggesting that according to the Gibbs phase rule, the melting temperature should remain invariant. The melting point-composition relation is, in effect, an expression of the temperature limit of the solubility of the crystalline polymer in the given solvent. Figure 12 shows a cross plot of Figure 11 with the diluent concentration being the parameter. The crystalline melting temperature is relatively constant above molecular weight 51,000, but is considerably depressed for lower molecular weight diluents. This depression is particularly noticable for atactic diluent molecular weight 900, the effect being most severe for the highest diluent concentration. This result indicates that 900 molecular weight diluent is a much better solvent for crystalline isotactic polystyrene than is higher molecular weight atactic diluent. The data scatter, particularly for diluent molecular weight 411,000, can be directly related

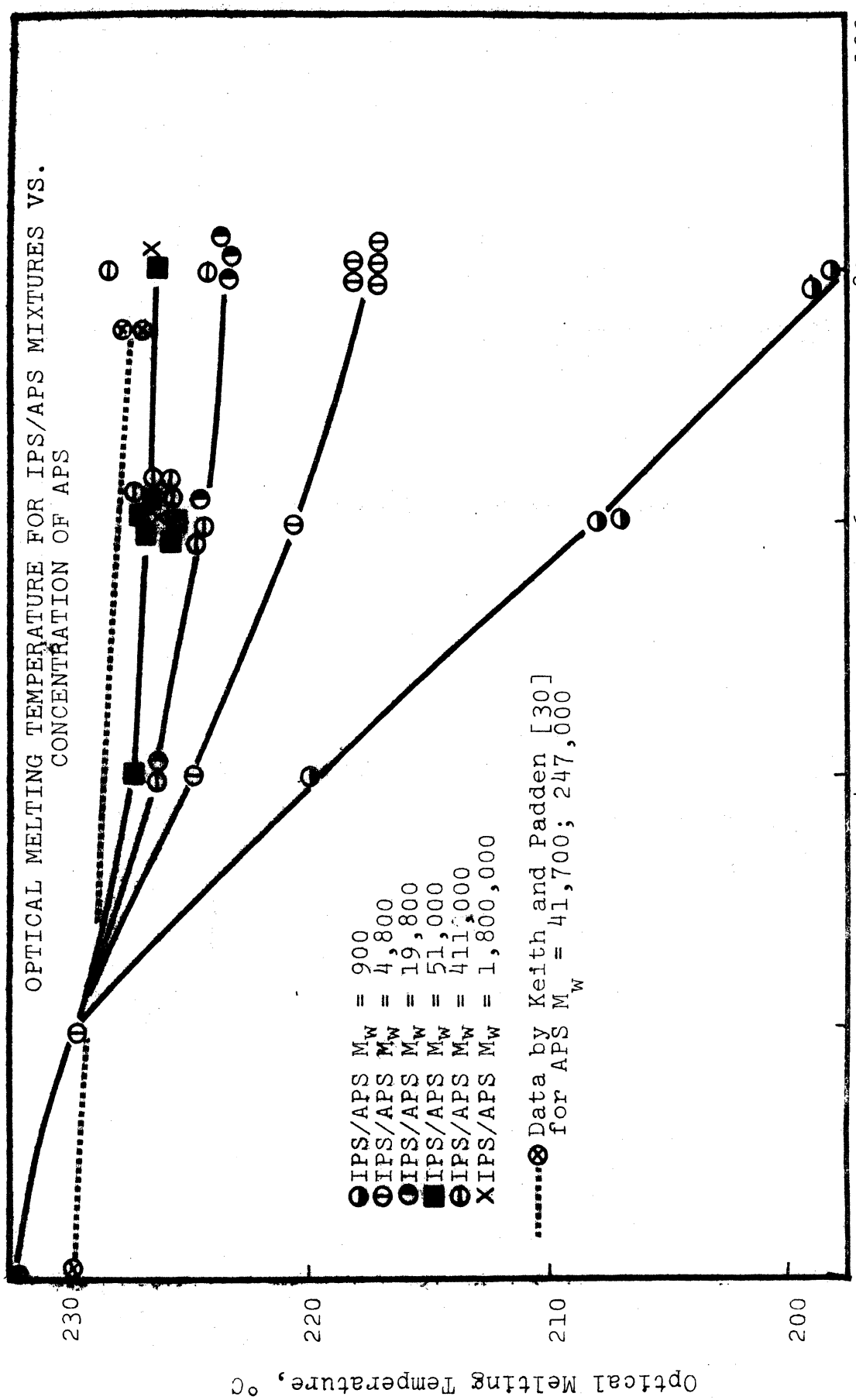
OPTICAL MELTING TEMPERATURE FOR IPS/APS MIXTURES VS.
CONCENTRATION OF APS
IPS/APS Mw = 900
IPS/APS Mw = 4,800
IPS/APS Mw = 19,800
IPS/APS Mw = 51,000
IPS/APS Mw = 411,000
IPS/APS Mw = 1,800,000
Data by Keith and Padden [30]
for APS Mw = 41,700; 247,000
Optical Melting Temperature, °C
230
220
210
200
0
20
40
60
80
100
% Atactic Polystyrene (APS)

Figure 11

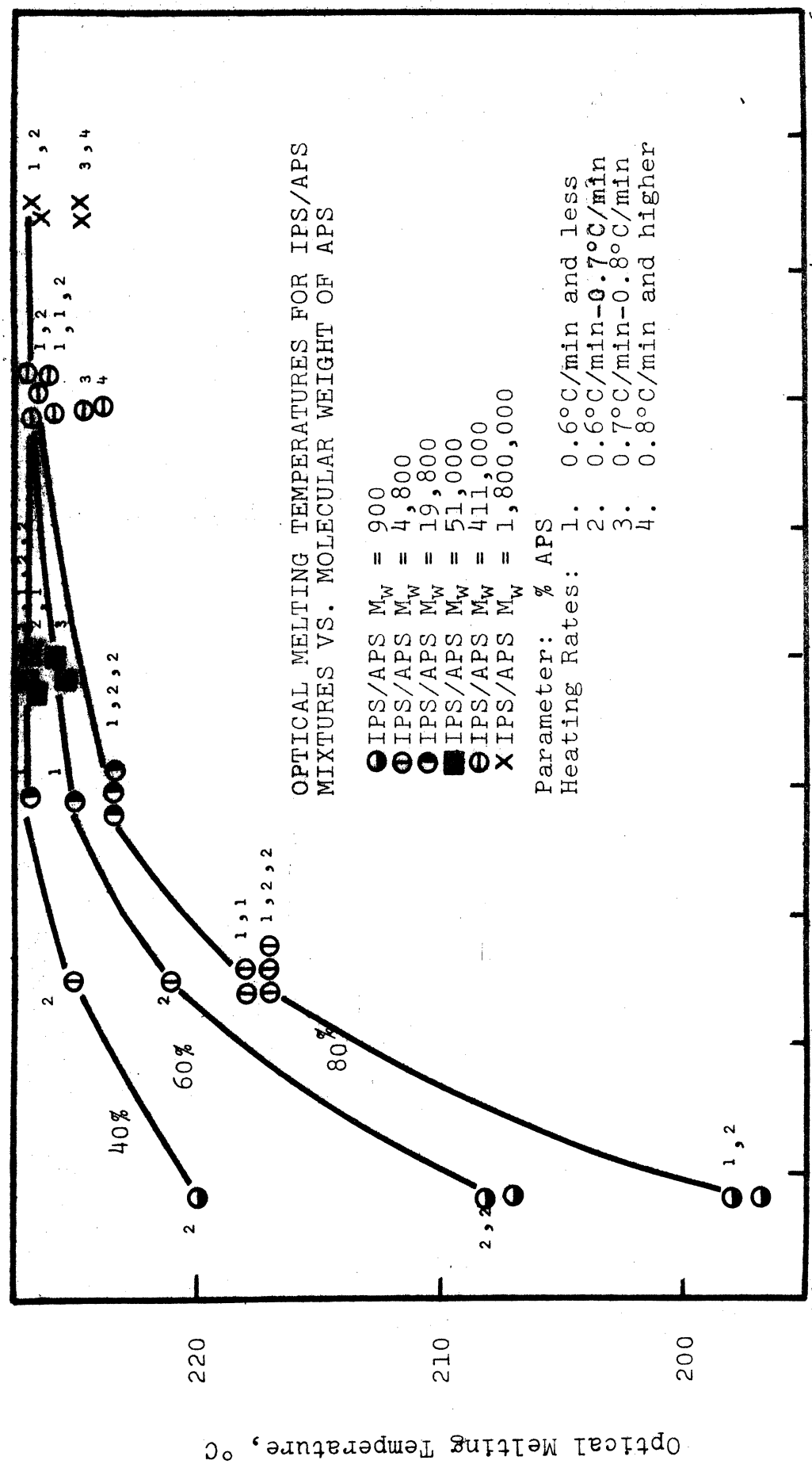
OPTICAL MELTING TEMPERATURES FOR IPS/APS
MIXTURES VS. MOLECULAR WEIGHT OF APS
IPS/APS Mw = 900
IPS/APS Mw = 4,800
IPS/APS Mw = 19,800
IPS/APS Mw = 51,000
IPS/APS Mw = 411,000
IPS/APS Mw = 1,800,000
Parameter: % APS
Heating Rates:
1. 0.6°C/min and less
2. 0.6°C/min-0.7°C/min
3. 0.7°C/min-0.8°C/min
4. 0.8°C/min and higher
40%
60%
80%
Optical Melting Temperature, °C
220
210
200
Ln Molecular Weight APS
6
7
8
9
10
11
12
13
14
15
16

Figure 12

to the faster heating rate used. Various heating rates were used to check the effect of rate on the resulting value of the melting temperature.

6. X-ray Examination of Lattice Parameters and Defects

In order to determine whether or not melting point depression is caused by incorporation of noncrystalline impurity in the crystalline lattice of isotactic polystyrene, x-ray line broadening measurements were made on bulk samples of isotactic/atactic polystyrene. The average values of the (110) peak half width and 2θ Bragg angles for specimens of isotactic/atactic polystyrene are recorded in Table II. The average of the standard deviation for all specimens measured was 0.11°, which exceeds the maximum variation in the average values recorded for each sample. In another line broadening study, Buchanan and Miller [9] noted a 100% increase in the x-ray half width for the (110) peak upon stretching a bulk specimen of isotactic polystyrene at 105°C some 400% prior to isothermal crystallization at 165°C. Buchanan and Miller [9] used line broadening analysis of the (102) reflection to calculate a crystallite size of 85-100Å in the direction parallel to stretch.

Table II

Half Width of the (110) X-ray Peak for Mixtures of IPS/APS

Concentration	Crystallization Temperature	2θ	Half Width (110)**
IPS	180°C	4.5-6.5	1.67°
IPS/APS M_w=4800***	180°C	4.5-6.5	1.65°
IPS/APS M_w=411,000***	180°C	4.5-6.5	1.65°
IPS/APS M_w=900***	175°C	4.5-6.5	1.72°
IPS/APS M_w=4800***	180°C	4.5-6.5	1.75°
IPS/APS M_w=411,000***	180°C	4.5-6.5	1.71°
IPS/APS M_w=900***	175°C	4.5-6.5	1.69°

*Specimen partially melted and recrystallized for 24 hours.

**The estimated experimental error based on a scanning rate of 0.5° per minute and a chart speed of 1 inch per minute (10 boxes) per minute is approximately ± .05° (± 1 box).

***IPS/APS 20/80.

D. Discussion

1. Kinetics of Spherulitic Growth Rate

The experimental data for the spherulitic growth rate of the diluted isotactic/atactic polystyrene system can be used to evaluate the theoretical kinetics equation for diluted systems as developed by Gornick and Mandelkern [19] and Boon and Azcue [5]. A relationship between the growth rate, G(dil), of the diluted isotactic/atactic polystyrene mixtures, and the growth rate, G(undil), of the pure isotactic polystyrene system was developed in the introduction following the analysis of Boon and Azcue [5]:

$$G(dil)=\upsilon_2 \exp\left[0.2 \frac{Tm}{(Tm-T)} \ln \upsilon_2\right] G(undil) \qquad (13)$$

where υ_2 is the volumetric fraction of isotactic polystyrene and Tm is the melting temperature of the diluted mixture. The assumptions upon which equation 13 is based are that the glass transition temperature, Tg, the melting temperature, Tm, and the pre-exponential constant, Go, are the same for both the diluted and undiluted systems. The experimental data was taken at the maximum crystallization temperature, Tx, of 180°C, and this temperature will be used in the evaluation of equation 13. Since it is known that the melting temperatures determined by optical microscopy are 3° to 5°C below the values found by dilatometry, a value of 513°K, as determined by Dedeurwaerder and Oth [14] using dilatometric techniques will be used as the melting temperature of pure isotactic polystyrene. Substitution of these two temperatures into equation 13 gives:

$$G(dil)=\upsilon_2^{2.71} G(undil) \quad @180°C \qquad (14)$$

If we had used the melting temperature as determined by optical microscopy, the exponent of the υ_2 term in equation 14 would equal 2.935, a decidedly poorer value, as will be shortly indicated. Figure 13 shows a graphical comparison between the experimental data and equation 14. The experimental results clearly do not agree with the theoretical equation. Refinement of the melting temperature approximation to account for the maximum difference of the melting temperature between pure and diluted isotactic polystyrene (16°C) results in the following form of equation (14):

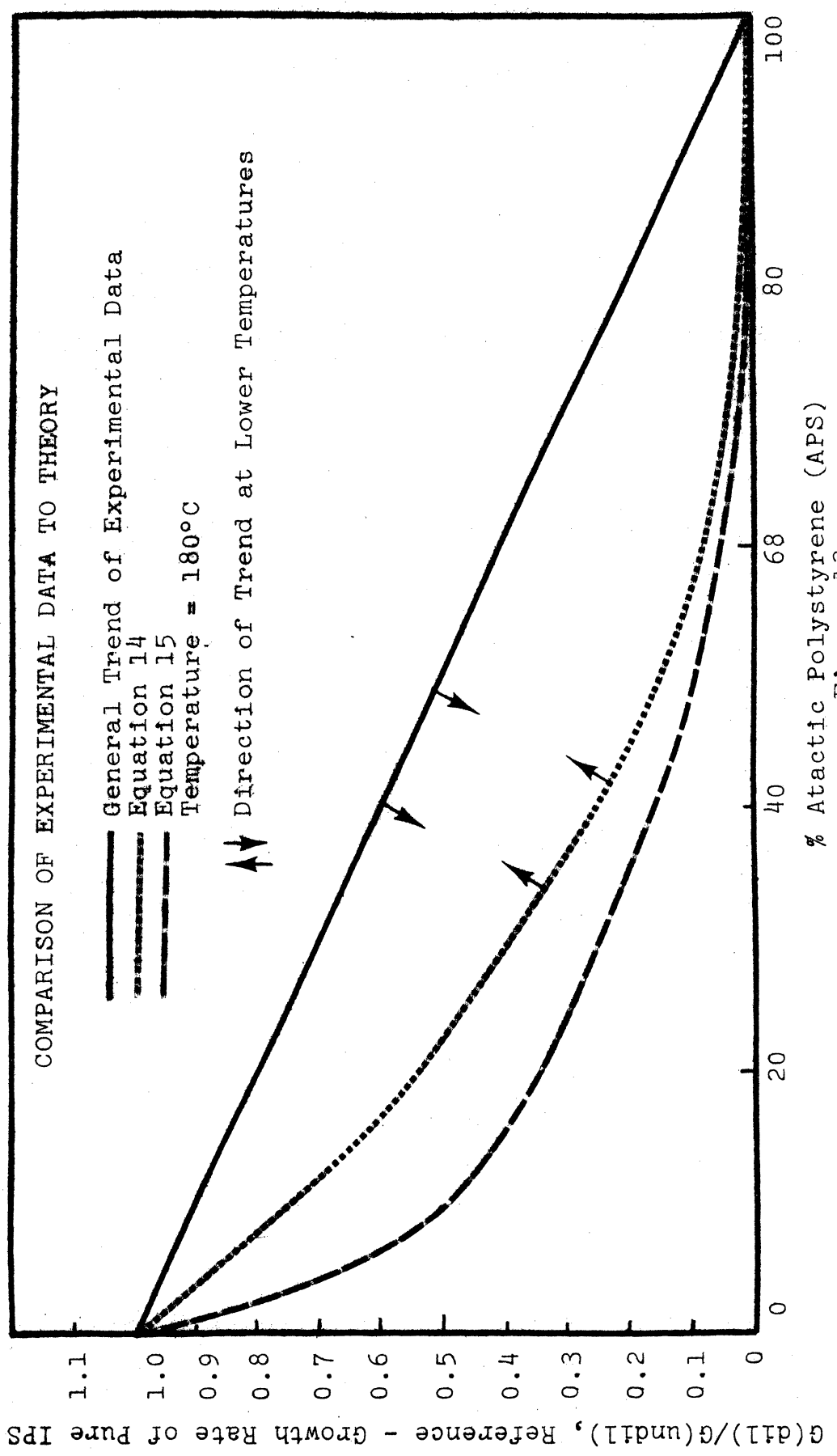
COMPARISON OF EXPERIMENTAL DATA TO THEORY
General Trend of Experimental Data
Equation 14
Equation 15
Temperature = 180°C
Direction of Trend at Lower Temperatures
G(dil)/G(undil), Reference - Growth Rate of Pure IPS
1.1
1.0
0.9
0.8
0.7
0.6
0.5
0.4
0.3
0.2
0.1
0
0
20
40
68
80
100
% Atactic Polystyrene (APS)

Figure 13

$$G(dil)=0.645\ \upsilon_2^{2.71}\ G(undil) \qquad (15)$$

The factor 0.645 arises from separate evaluation of equations 6 and 10 by substituting Tm = 513°K and Tm = 497°K respectively for pure and diluted polystyrene with 80% atactic diluent molecular weight 4,800. As Figure 13 clearly shows, such a melting temperature refinement makes a correction in the wrong direction. At crystallization temperatures lower than 180°C, equation 13 and the experimental data of Keith and Padden [31] have opposite temperature coefficients, as indicated by the arrows in Figure 13. These results clearly demonstrate that the theoretical kinetics equation developed for diluted systems does not agree with the experimental data obtained for the isotactic/atactic polystyrene system over a wide range of diluent concentrations and molecular weights. Although Boon and Azcue [5] pointed out the effect of opposite temperature coefficients, they did not have sufficient data to conclude that the theoretical equation does not agree with experimental results. Data from the present study, as well as that from the work of Keith and Padden [31], clearly show the discrepancy between predictions and experimental data.

2. Growth Rate Phenomena

The dependence of spherulitic growth rate on the average viscosity or molecular weight of the polymer system has taken the following form, according to Keith and Padden [31], and Hoffman and Weeks: $G\propto(1/M_n)^y$ where M_n is the average number average molecular weight with y normally

assuming values $0<y<1$. If the behavior of the present system can be adequately described on the basis of normal viscosity or diffusional effects, then the appropriate values of y are 0.16 and 0.70 for 40/60 and 60/40 mixtures between atactic polystyrene, molecular weights 4,800 and 19,800, Figure 10. At the critical molecular weight for chain entanglements in polystyrene, 36,000 [15], y should become increasingly positive in proportion to the increase noted for the melt viscosity over the same molecular weight range, since $\eta \propto M_w^{y}$. However, we find that in the region of the critical molecular weight (between 19,800 and 51,000), y suddenly becomes negative: $y = -3.0$. This surprising growth rate behavior cannot be explained in terms of normal viscosity or diffusional effects.

The increase in growth rate over this molecular weight range (19,800 to 51,000), nevertheless, can be explained by a model based on the phenomenological theory of Keith and Padden [30]. Morphological evidence [30] supporting this theory suggests that significant amounts of noncrystallizable rejected impurity are entrapped within the growing spherulites, as indicated by the increased "openness" of the texture of high impurity concentrations. The means by which entrapment occurs is not considered, although slow radial diffusion is the implied basis for impurity entrapment. At molecular weights above the critical molecular weight, chain entanglements are known to influence the viscous transport properties of a polymer melt. Thus, it would be reasonable to suspect that such entanglements might effectively tend to entrap rejected impurity molecules and inhibit radial diffusion

away from the growing crystal front. Such entrapment of rejected impurity might also cause crystalline lattice defects, although x-ray line broadening (Table II) and melting temperature depression (Figure 12), do not indicate such defects. Alternately, impurity entrapment might primarily involve self-entanglement rather than entanglement with crystallizing molecules. In either case, as the molecular weight of the rejected impurity is increased above the critical molecular weight, chain entanglements, according to the proposed model, would start to entrap impurity molecules and inhibit radial diffusion. As a result of this entrapment, the effective interfacial concentration of the crystallizable molecules would tend to increase, because the diffusion barrier generated by interfacial accumulation of rejected impurity would be reduced correspondingly by impurity entrapment within the growing spherulites. Since the growth rate is directly proportional to the interfacial concentration of the crystallizable constituent (equation 12), the growth rate would therefore be expected to increase over the range of the critical molecular weight (19,800 to 51,000).

In the molecular weight range above 51,000 (Figure 10), the growth rates for the 60/40 and 40/60 mixtures are more or less uniformly depressed with increasing molecular weight. The slopes of the growth rate curves over this region are strikingly similar to the slopes of the same curves between molecular weights 4,800 and 19,800. This similarity suggests that in these two regions (4,800 to 19,800 and 51,000 to 1,800,000), the decreasing growth rate might be explained

in terms of the viscosity or diffusional effects of increasing diluent molecular weights, although the exact growth mechanism is not clearly understood.

Depression of the growth rate for very low molecular weight diluents (Figure 10) is clearly not the result of increased molecular viscosity. Similar depression of the melting temperature, Tm, over the same molecular weight range (Figure 12), however, suggests that there might be a correlation between these two phenomena. At the maximum crystallization temperature, T_{max}, a reduced temperature difference, T_m-T_{max}, directly corresponds to a reduced rate of nucleation, and as a result, a reduced growth rate (equation 12). Since a reduced temperature difference, T_m-T_{max}, occurs for 60/40 and 40/60 mixtures of atactic polystyrene diluent, molecular weight 900 (Figures 10, 12), one would also normally expect the growth rate to be reduced.

In general, significant melting temperature depression can be caused by introduction of crystalline lattice defects, increased concentration of chain ends, or decreased polymer-diluent interaction free energy (increased solubility). X-ray analysis suggests that the addition of noncrystalline atactic polystyrene diluent affects neither the amount of line broadening nor the crystalline lattice spacings within the spherulitic structures. Apparently, the noncrystalline impurity is substantially rejected from the growing crystal lattice, since no lattice defects resulting from the incorporation of such impurity molecules can be experimentally detected by relative line broadening. This

result suggests that impurity entrapment occurs primarily by self-entanglement of impurity molecules and/or by entrapment in such a manner that the impurities do not affect the ordering of the chains in the crystal lattice.

Melting temperature depression caused by the concentration of chain ends would suggest that there is a linear relationship between the inverse of molecular weight (concentration of chain ends), and the amount of melting temperature depression. Figure 14 shows quite clearly that there is no linear relationship between these two parameters.

Flory and Huggins [41] proposed the following equation, derived from basic thermodynamics, for the melting temperature depression caused by the dilution of a polymer:

$$\frac{1}{T_m} - \frac{1}{T_m^o} = \frac{RV_u}{\Delta H_u V_1} [(1-\upsilon_2) - X_1(1-\upsilon_2)^2] \qquad (16)$$

where υ_2 is the volume fraction of isotactic polystyrene, V_u and V_1 are the molar volumes of the repeat unit for isotactic and atactic polystyrene respectively; ΔHu is the heat of fusion per mole of repeat unit, and X_1 is the isotactic-atactic polystyrene interaction free energy. Other quantities being equal, a larger depression of the melting temperature should be noted with a good solvent (small X_1) than with a poor one. The depression should also be greater for diluents of smaller molar volume. In the case of isotactic/atactic polystyrene mixtures, parameters R, Vu, V_1, and ΔHu would all have constant values. Therefore, the amount of melting temperature depression would be dependent upon values of υ_2 and X_1. Since similar concentrations of atactic

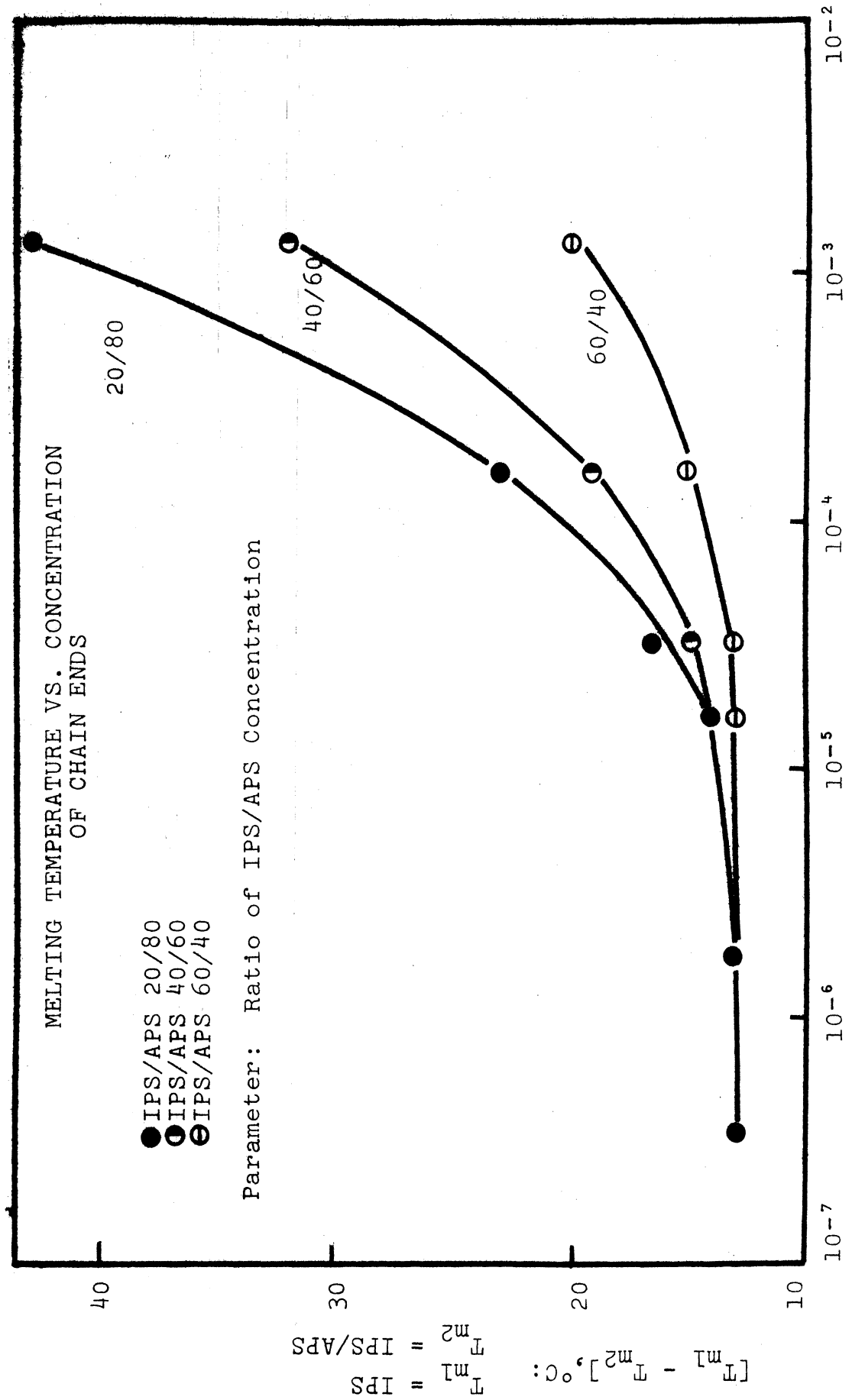
MELTING TEMPERATURE VS. CONCENTRATION
OF CHAIN ENDS
Parameter: Ratio of IPS/APS Concentration
●IPS/APS 20/80
◑IPS/APS 40/60
⊖IPS/APS 60/40
20/80
40/60
60/40
[Tm1 - Tm2],°C:
Tm1 = IPS
Tm2 = IPS/APS
40
30
20
10
10-7
10-6
10-5
10-4
10-3
10-2
1/MW (MW = Molecular Weight of APS)

Figure 14

polystyrene have widely different temperature depressions (Figure 12), values of X_1 must be dependent upon the molecular weight of atactic polystyrene diluent. Values of the optical melting point are not sufficiently accurate to give meaningful values of the X_1 parameter, but they are accurate enough to indicate that the interaction free energy is considerably lower for atactic polystyrene molecular weight 900, than for higher molecular weight diluents. This result indicates that very low molecular weight atactic polystyrene diluents are better solvents than higher molecular weight atactic polystyrene. Thus, the observed melting point depression appears to be related to the solubility of isotactic molecules in atactic polystyrene diluent.

E. Conclusions

1. For the isotactic/atactic polystyrene system, the dependence of growth rate on temperature is very similar to that for the undiluted polymer.
2. Dilution of isotactic polystyrene (molecular weight 550,000) with noncrystallizable atactic polystyrene (for particular molecular weights ranging from 2,030 to 1,800,000) causes a uniform depression of the resulting spherulitic growth rate with the optimum growth rates occurring in about the same temperature range as for undiluted isotactic polystyrene (178° ± 2°C).
3. For a 20% dilution with atactic polystyrene, the growth rate is independent of impurity molecular weights up to 411,000.

4. For 40% and 60% dilutions, the dependence of the growth rate on diluent molecular weight can be described by normal viscosity effects for impurity molecular weights ranging from 4,800 to 19,800 and from 51,000 to 1,800,000. In between these two ranges, anomalous growth rate behavior suggests that molecular chain entanglements play an important role in determining the interfacial concentration of rejected impurity. For very low molecular weight diluents (900; 2,030), the growth rate is depressed by the corresponding depression of the crystalline melting temperature over the same molecular weight range.

5. The optical melting temperature range for mixtures of isotactic and atactic polystyrene is unaffected by high concentrations of impurity having molecular weights greater than 19,800. However, the melting temperature is rapidly depressed for high concentrations of very low molecular weight atactic diluent.

6. The measured x-ray line broadening for the (110) peak of crystalline isotactic polystyrene is not affected by the addition of high concentrations of various molecular weight atactic polystyrene diluents.

7. The theoretical growth rate equation derived for diluted systems does not describe the experimental data for the isotactic/atactic polystyrene system at 180°C.

CHAPTER IV

CRYSTALLIZATION OF ISOTACTIC POLYSTYRENE/PLASTICIZER BLENDS

A. Introduction

Spherulitic crystallization from mixtures of crystallizable polymer and low molecular weight plasticizer has received very limited attention, compared to the numerous studies on spherulitic crystallization of homopolymers. Mixtures of polymer and low molecular weight plasticizer are often commercially important systems because the mechanical properties of some polymers can be favorably altered by the addition of plasticizer [45]. Therefore, it was decided to examine the influence of di-methyl and di-decyl phthalate, as well as benzophenone on the spherulitic crystallization kinetics of isotactic polystyrene and to compare these results to those obtained in Chapter III. We also determined the threshold crystallization temperatures for mixtures of isotactic/atactic polystyrene as well as isotactic polystyrene/benzophenone. The threshold crystallization temperature (T_T) is the lowest temperature at which the onset of crystallization can be detected. This temperature gives us a relative measure of the magnitude of the viscous transport term in the theoretical growth rate equation.

Boon and Azcue [5] recently reported that at a fixed temperature, the spherulitic growth rate from mixtures of isotactic polystyrene and benzophenone is linear over a wide range of crystallization temperatures. The overall linear growth rate reaches a maximum at a crystallization temperature which is dependent on the benzophenone concentration, and is uniformly depressed at temperatures above and below the optimum crystallization temperature. The resulting growth rate curves are generally gaussian in shape and similar to the growth rate curve found for the undiluted homopolymer system. The growth rate maximas for each concentration ratio shift to lower crystallization temperatures, the amount of shift being proportional to the amount of benzophenone added to the mixture. Furthermore, the maximas of the growth rate curve first increase with the increasing benzophenone content up to about 20% dilution and are gradually depressed at higher dilutions. Boon and Azcue [5] established that there is a qualitative agreement between the experimentally measured growth rate and the theoretical rates predicted by equation 12 in the introduction of Chapter III particularly for benzophenone concentrations less than 20%. The agreement is increasingly poorer for higher concentrations of benzophenone.

The shift of the crystallization range of isotactic polystyrene/benzophenone mixtures to lower temperatures is primarily the consequence of the depression of the melting temperature T_m and the glass transition temperature T_g with increasing benzophenone concentration. Boon and Azcue [5]

correlate this shift along the temperature axis with a reduced temperature parameter θ which is defined as: $\theta = (T-Tg)/(Tm-Tg)$. The growth rate maximas for all concentrations of benzophenone occur at about $\theta = 0.57$.

Mandelkern [42] studied the crystallization kinetics of mixtures of linear polyethylene and α-chloronaphthlene over a wide range of concentrations near the melting temperature by means of dilatometric techniques. As the pure polymer is diluted, the shapes of the isotherms change and are no longer superimposable over the complete transformation range. In the range of very dilute concentrations of polyethylene, 1% to 0.01%, the shapes of the isotherms no longer change, indicating a constant free energy for the formation of a critical size nucleus over the range. However, over the same concentration range, 1% to 0.01%, the crystallization rate is still dependent on concentration, since it continues to be depressed with decreasing polymer concentration.

Other studies on the crystallization kinetics of polymer diluent mixtures were reported by Lunak and Bohdanecký [35] and Holland and Lindenmeyer [24]. These studies will not be reviewed in detail because they considered different systems than the one of present interest.

Mandelkern [41] also studied the effect of low molecular weight plasticizer on the melting temperature depression of diluted linear polyethylene. Melting temperature depression can be quantitatively described by the Flory-Huggins equation (equation 16), which is based on the thermodynamics

of ideal solution behavior using a correlation factor X_1 called the polymer-diluent interaction parameter. Other quantities being equal, a larger depression of the melting temperature, Tm, should be observed with a good solvent (smaller values of X_1), than with a poor one. The size of the diluent molecule should also affect Tm, the depression being predicted to be greater for diluents of smaller molar volume.. Experimental results for the melting temperature depression of linear polyethylene with n-butyl phthalate, O-nitrotoluene, α-chloronaphthalene, and tetralin show good agreement with the predictions of the Flory-Huggins equation. Poorer solvents such as n-butyl phthalate and O-nitrotoluene depress Tm much less than similar concentrations of better solvents, α-chloronaphthalene and tetralin.

Other important properties of polymer-diluent systems were examined by Taeger and Suvorova [57], who studied the effect of di-methyl and di-decyl phthalate on the viscosity, glass transition temperature, and phase separation temperature of plasticized polystyrene mixtures. The phase separation temperatures and solution viscosity are uniformly higher for mixtures of polystyrene and di-decyl phthalate than for similar mixtures using di-methyl phthalate, because di-decyl phthalate is both a poorer solvent and has a higher molar volume (molecular size) than does di-methyl phthalate. This behavior is consistent with the results usually found when comparing similar diluents having widely different molecular weights. Polystyrene mixtures with di-decyl phthalate, however, have a surprisingly lower glass transition temperature

than comparable mixtures with di-methyl phthalate. Taeger and Suvorova [57] explain this behavioral contradiction in terms of a proposed model based on the existence of a super-molecular structure in the polystyrene phase. According to their explanation, a rather poor high molecular weight solvent such as di-decyl phthalate, which cannot successfully penetrate and dissolve these structures, absorbs onto the surface and lubricates the movement of one structure with respect to its neighbors. Good solvents such as di-methyl phthalate, however, penetrate and partially dissolve the polystyrene structure, thereby inhibiting the translational movement of these structures and causing a higher glass transition temperature. In viscosity studies, these structures are apparently destroyed by concentrated shear stresses, and the molecular volume of the diluent, rather than the diluent solubility, has the predominate influence on the resulting properties.

B. Experimental

1. Preparation

The characteristics of all materials used in this study are discussed in Chapter II. Dilute 0.4% solutions of both isotactic polystyrene and low molecular weight plasticizer in chloroform were made by completely dissolving a weighed amount of polymer or plasticizer in a measured volume of boiling chloroform. After cooling to room temperature, predetermined ratios of clear 0.4% isotactic and 0.4% plasticizer solutions were pipetted together to make

up a clear 0.4% mixed solution of isotactic polystyrene/plasticizer in chloroform. Thin films approximately 60μ thick, as determined by density calculations based on a polystyrene/plasticizer density of ~1.0 gram/cm^3, were prepared by casting from the 0.4% mixed solution onto thin cover glasses at room temperature under a cool air fan. These films were then exposed to the ambient atmosphere at room temperature for 12 hours to allow complete removal of residual chloroform solvent. Prolonged exposure for several days under these conditions would result in significant evaporation of volatil benzophenone and di-methyl phthalate plasticizers.

Samples suitable for a threshold crystallization study in the electron microscope were prepared by casting thin films (~ 500Å thick) from 0.2% benzene solutions of isotactic polystyrene/benzophenone (ranging from 100/0 to 50/50) onto surfaces of freshly cleaved mica. Similar thin films of isotactic/atactic polystyrene molecular weight 4,800 were prepared in exactly the same way. The pieces of mica were then sealed in pyrex glass tubes and annealed at various temperatures in silicone oil temperature control baths (± .5°C) for 24 hours. After thermal treatment, the mica pieces were removed from the pyrex tubes and the crystallized thin films were floated off the mica onto a water surface and picked up on 200 mesh copper grids for subsequent study in the electron microscope.

2. Measurement of Growth Rate

The optical microscope assembly used in this study is

the same as described in Chapter III. Thin films of isotactic polystyrene/plasticizer, sandwiched between two cover glasses, were heated on the microscope hot stage to 250°C for five minutes before cooling at the desired isothermal crystallization temperature, ranging from 103°C to 185°C. Spherulitic crystals generally started to nucleate and grow before the hot stage had finished cooling to the isothermal crystallization temperature, cooling at a rate of 20°C per minute. Accordingly, it was particularly important to view just one field of growing spherulites in order to measure the growth rate of crystals, most of which are generated at about the same time. Within this given field of view, the crystals were very uniform in size and the resulting growth rate was determined by measuring the size of a number of spherulites as a function of time. Data scatter caused by variations in concentration due to excessive loss of volatile plasticizer were minimized by using fresh films for each growth rate measurement. Spherulitic growth rates were measured in thin films having various concentrations of di-methyl phthalate or di-decyl phthalate added to isotactic polystyrene of molecular weight 550,000. Thus the growth rate, G, depends on the type and the concentration of the added plasticizer as well as the temperature of crystallization. Data scatter from duplicate measurements indicates that the growth rate under normal conditions is reproducible to within ± 5%.

3. Melting Temperature Measurement

Thin films of isotactic polystyrene/plasticizer, crystallized at a variety of temperatures, were individually heated on a Kofler hot stage at a rate between 0.5°C and 1.0°C per minute until the crystalline birefrigence totally disappeared. The temperature at which the birefringence disappeared was designated as the optical melting temperature. The same films were not recrystallized for a second melting point determination because excessive loss of volatile plasticizer significantly affected the concentration ratio and hence the observed melting temperature. Thin films of isotactic polystyrene/diluent, prepared for the threshold crystallization study, were either shadowed with platinum at 30° or vertically decorated with gold at 90° and then examined in a JEM-6A electron microscope for the first signs of crystalline structure. The characteristics of the electron microscope and discussions of the shadowing and decoration techniques are recorded in Chapter II.

C. Results

1. Morphology

Electron microscope examination of crystallized thin films of isotactic polystyrene/plasticizer shows that the spherulites are made up of fibrous structures similar to those observed in spherulites grown from mixtures of isotactic/atactic polystyrene, Figure 15 on page 74. Under crossed polarizers in the optical microscope, the crystals are birefringent

with a normal maltese cross extinction pattern. The spherulites develop from small 1 to 2 micron symmetrically round fibrous nuclei. In the plasticized system, there is no evidence of the hexagonal hedrite nuclei observed under certain conditions in mixtures of isotactic/atactic polystyrene. Spherulites grown from plasticized mixtures have the same fine fibrous texture as spherulites of pure isotactic polystyrene. This is in agreement with the observations of Boon and Azcue [5] for spherulites grown from mixtures of isotactic polystyrene/benzophenone.

2. Effect of Temperature

The spherulitic growth rate of isotactic polystyrene/plasticizer is linear with respect to time over a wide range of temperatures, as indicated in an example shown in Figure 16. The growth rate curve for this particular mixture reaches a clear maximum at approximately 160°C and is depressed at both higher and lower temperatures, Figure 17. In general, the growth rate becomes non-linear only under the conditions in which the diffusion of the crystallizable constituent becomes rate controlling, which starts to occur when spherulites impinge upon one another. There is no evidence of a non-linear growth rate caused by increased plasticizer concentration at the growing crystal interface.

3. Effect of Diluent Concentration

As noted in Figure 17, when the concentration of di-methyl phthalate is increased, the maximas in the growth

rate curves shift to lower temperatures, the amount of shift being proportional to the amount of plasticizer added. This result is in general agreement with the effects reported by Boon and Azcue [5] in the isotactic polystyrene/benzophenone system. In addition, it should be noted that the growth rate maximas for the diluted di-methyl phthalate system are substantially higher than the maxima for the pure system and reach an overall optimum growth rate at about 20 to 30% dilution, Figure 20. This optimum is also observed when the maximum growth rates are plotted as a function of concentration in the isotactic polystyrene/benzophenone system, Figure 18. In this case, the overall optimum growth rate, according to the data of Boon and Azcue [5], occurs at 20% dilution and is in general agreement (better than 10%) with data taken on the present equipment at the same temperatures using mixtures of isotactic polystyrene (molecular weight 550,000) and benzophenone.

4. Effect of Diluent Type

When di-decyl phthalate is added to isotactic polystyrene, the resulting radial growth rate curves do not have the same characteristics as observed when benzophenone and di-methyl phthalate are used as the added diluent, Figure 19. As the concentration of di-decyl phthalate increases, the growth rate maximas shift to lower temperatures in accordance with the amount of plasticizer added. However, above 20% dilution the growth rate maximas remain fixed at about 145°C for dilutions up to 80% plasticizer, while in

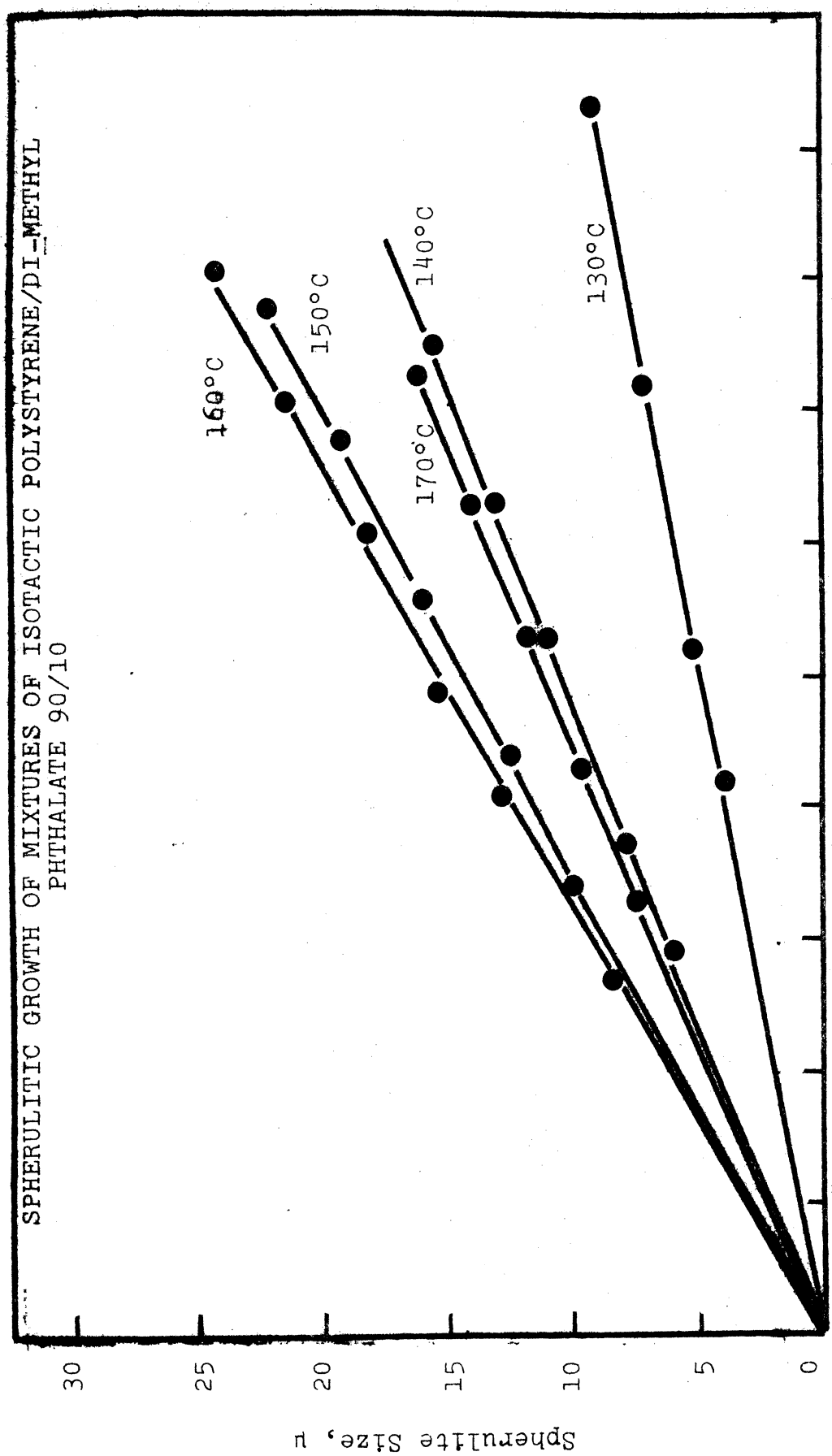
SPHERULITIC GROWTH OF MIXTURES OF ISOTACTIC POLYSTYRENE/DI-METHYL PHTHALATE 90/10
160°C
150°C
140°C
130°C
170°C
Spherulite Size, μ
Time, minutes
0
5
10
15
20
25
30
35
40
45
50

Figure 16

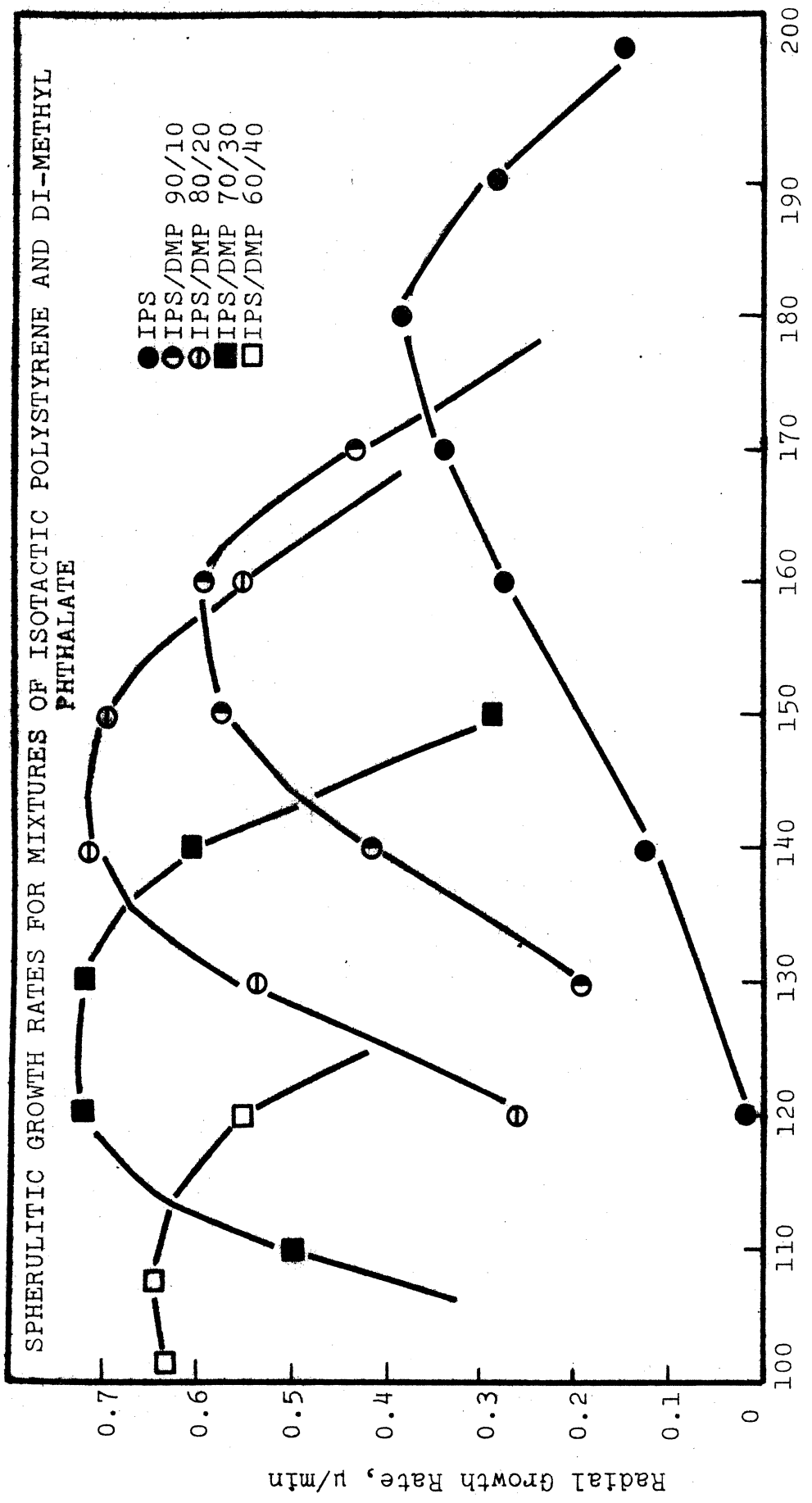
SPHERULITIC GROWTH RATES FOR MIXTURES OF ISOTACTIC POLYSTYRENE AND DI-METHYL PHTHALATE
IPS
IPS/DMP 90/10
IPS/DMP 80/20
IPS/DMP 70/30
IPS/DMP 60/40
Radial Growth Rate, μ/min
0
0.1
0.2
0.3
0.4
0.5
0.6
0.7
100
110
120
130
140
150
160
170
180
190
200
Temperature, °C

Figure 17

the case of benzophenone and di-methyl phthalate, they continue to shift to lower temperatures, Figure 17.

The magnitude of the overall optimum growth rate at comparable concentrations (20%) is considerably higher for the di-decyl phthalate system than for the benzophenone and di-methyl phthalate systems; 1.1 microns per minute as compared to 0.76 and 0.73 microns per minute respectively, Figure 20. In addition, it should be noted that the sharp overall maximum at 20% dilution for the benzophenone system is considerably more diffuse for the di-methyl phthalate system, and is actually quite dispersed between 20% and 40% dilution for the di-decyl phthalate system. These observations will be examined in more detail in the discussion section.

5. Melting Temperature Determination

Figure 21 shows the relationship between the optical melting temperature and the concentrations of plasticizer in crystallized thin films of isotactic polystyrene/di-methyl phthalate. In general, the melting temperature is depressed with increasing concentration of added impurity. Also indicated in Figure 21 is the effect of added plasticizer on the glass transition temperature of the mixture, based on the dynamometric balance data of Taeger and Suvorova [57]. The temperature range between the optical melting temperature and the glass transition temperature increases with increasing plasticizer concentration because the glass transition temperature is depressed more rapidly

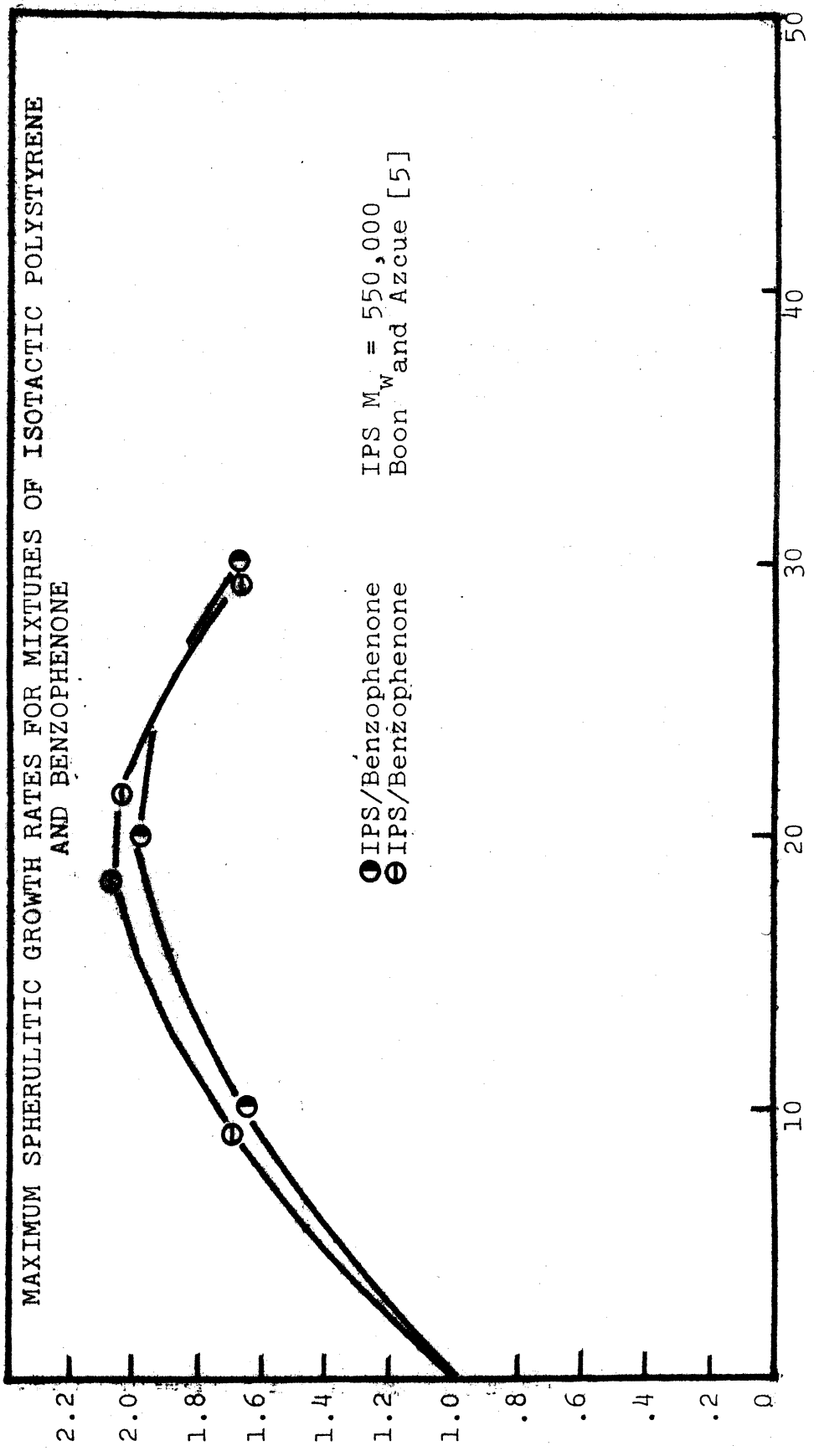
MAXIMUM SPHERULITIC GROWTH RATES FOR MIXTURES OF ISOTACTIC POLYSTYRENE AND BENZOPHENONE
IPS/Benzophenone
IPS/Benzophenone
IPS M_w = 550,000
Boon and Azcue [5]
Maximum Radial Growth Rate, G(diluted)/G(undiluted)
% Benzophenone
0
.2
.4
.6
.8
1.0
1.2
1.4
1.6
1.8
2.0
2.2
10
20
30
40
50

Figure 18

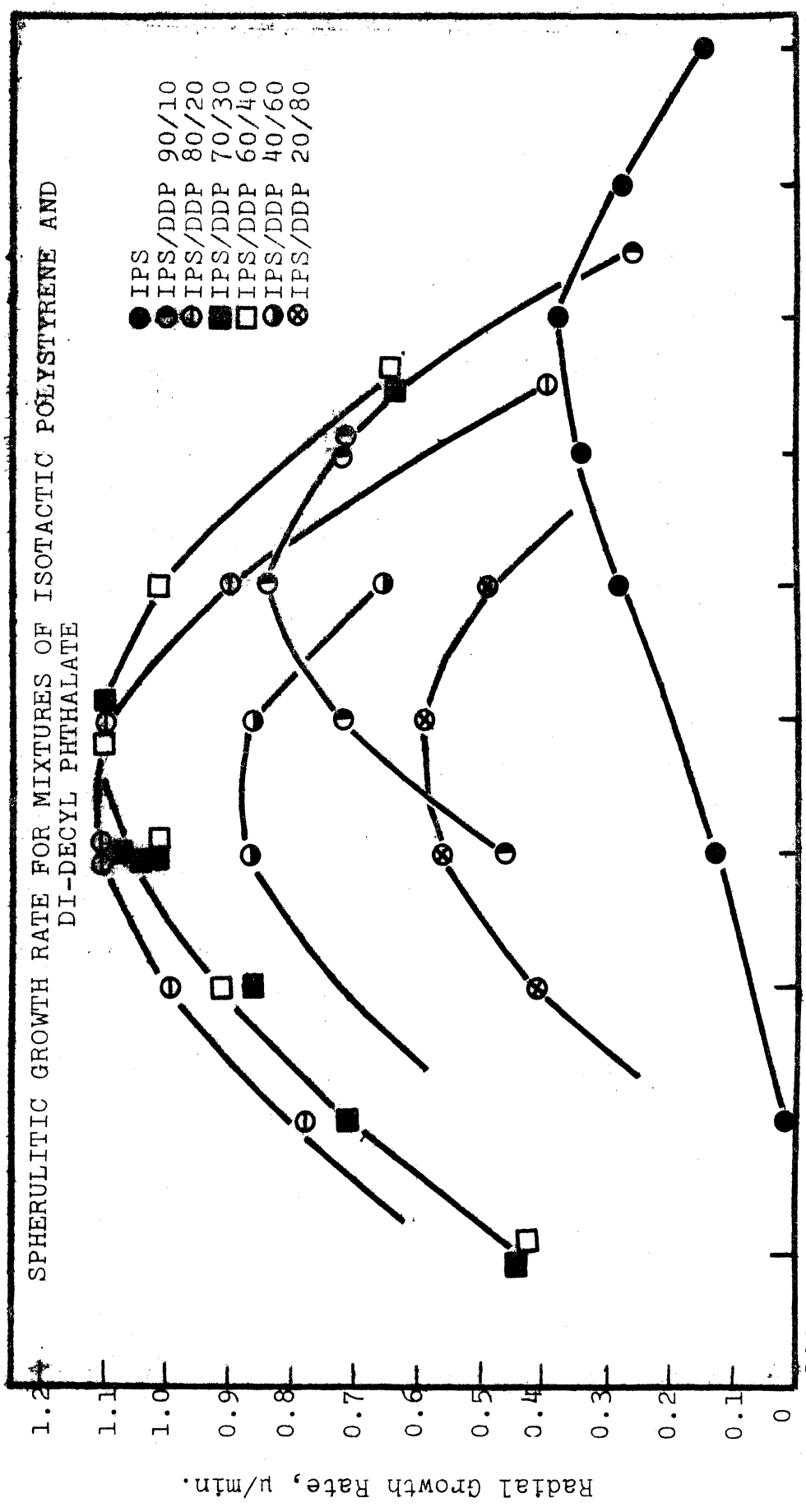
SPHERULITIC GROWTH RATE FOR MIXTURES OF ISOTACTIC POLYSTYRENE AND DI-DECYL PHTHALATE
IPS
IPS/DDP 90/10
IPS/DDP 80/20
IPS/DDP 70/30
IPS/DDP 60/40
IPS/DDP 40/60
IPS/DDP 20/80
Radial Growth Rate, μ/min.
Temperature, °C
1.2
1.1
1.0
0.9
0.8
0.7
0.6
0.5
0.4
0.3
0.2
0.1
0
100
110
120
130
140
150
160
170
180
190
200

Figure 19

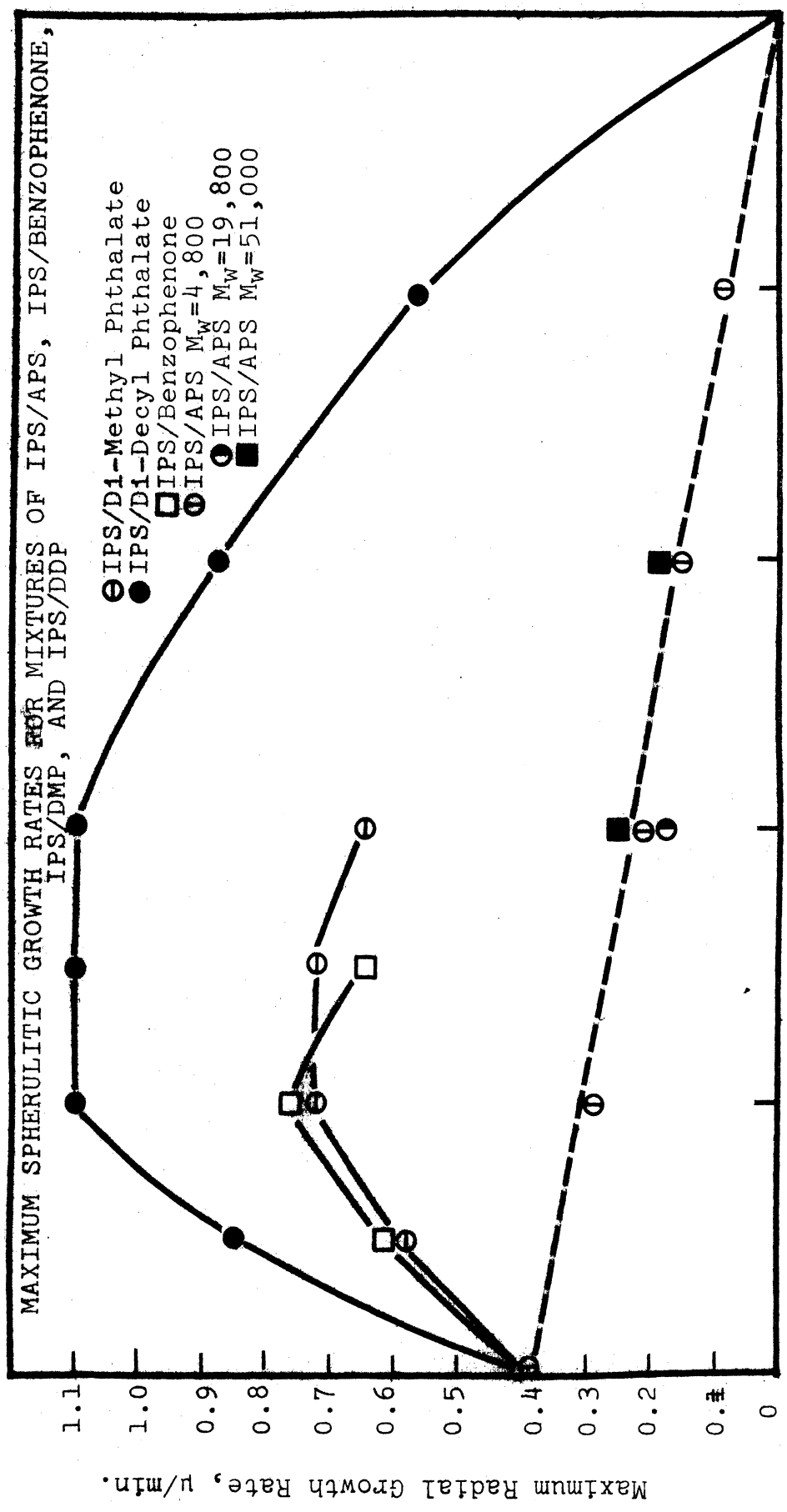
MAXIMUM SPHERULITIC GROWTH RATES FOR MIXTURES OF IPS/APS, IPS/BENZOPHENONE, IPS/DMP, AND IPS/DDP
IPS/D1-Methyl Phthalate
IPS/D1-Decyl Phthalate
IPS/Benzophenone
IPS/APS M_w=4,800
IPS/APS M_w=19,800
IPS/APS M_w=51,000
Maximum Radial Growth Rate, μ/min.
% Diluent
0
0.1
0.2
0.3
0.4
0.5
0.6
0.7
0.8
0.9
1.0
1.1
0.0
0.2
0.4
0.6
0.8
1.0

Figure 20

than the melting temperature. This trend was also noted by Boon and Azcue [5] for the isotactic polystyrene/benzophenone system and served as an important basis for their explanation of the overall growth rate maxima observed in Figure 18.

The relationship between di-decyl phthalate concentration and the optical melting temperature of crystallized thin films is shown in Figure 22. Also indicated in this figure is the effect of added plasticizer on the glass transition temperature of the mixture, based on the data of Taeger and Suvorova [57]. Although the melting temperature is consistently depressed with increasing plasticizer concentration, the glass transition temperature appears to have a minimum around 20% to 30% dilution and actually increases slightly for higher dilutions. Taeger and Suvorova attribute this anomalous behavior to macroscopic ($> 2000\text{Å}$) phase separation which starts to occur at about 10% dilution. For this system, the temperature range between the melting temperature and the glass transition temperature sharply increases up to 20% dilution where it levels off and slightly diminishes for higher dilutions.

In the two systems studied (di-methyl and di-decyl phthalate) the greater melting temperature depression (at comparable concentrations) is observed for di-methyl phthalate, which also happens to be the better solvent, according to the phase separation temperatures reported by Taeger and Suvorova [57]. This result is consistent with the findings of Mandelkern [42] who noted that (at comparable concentrations)

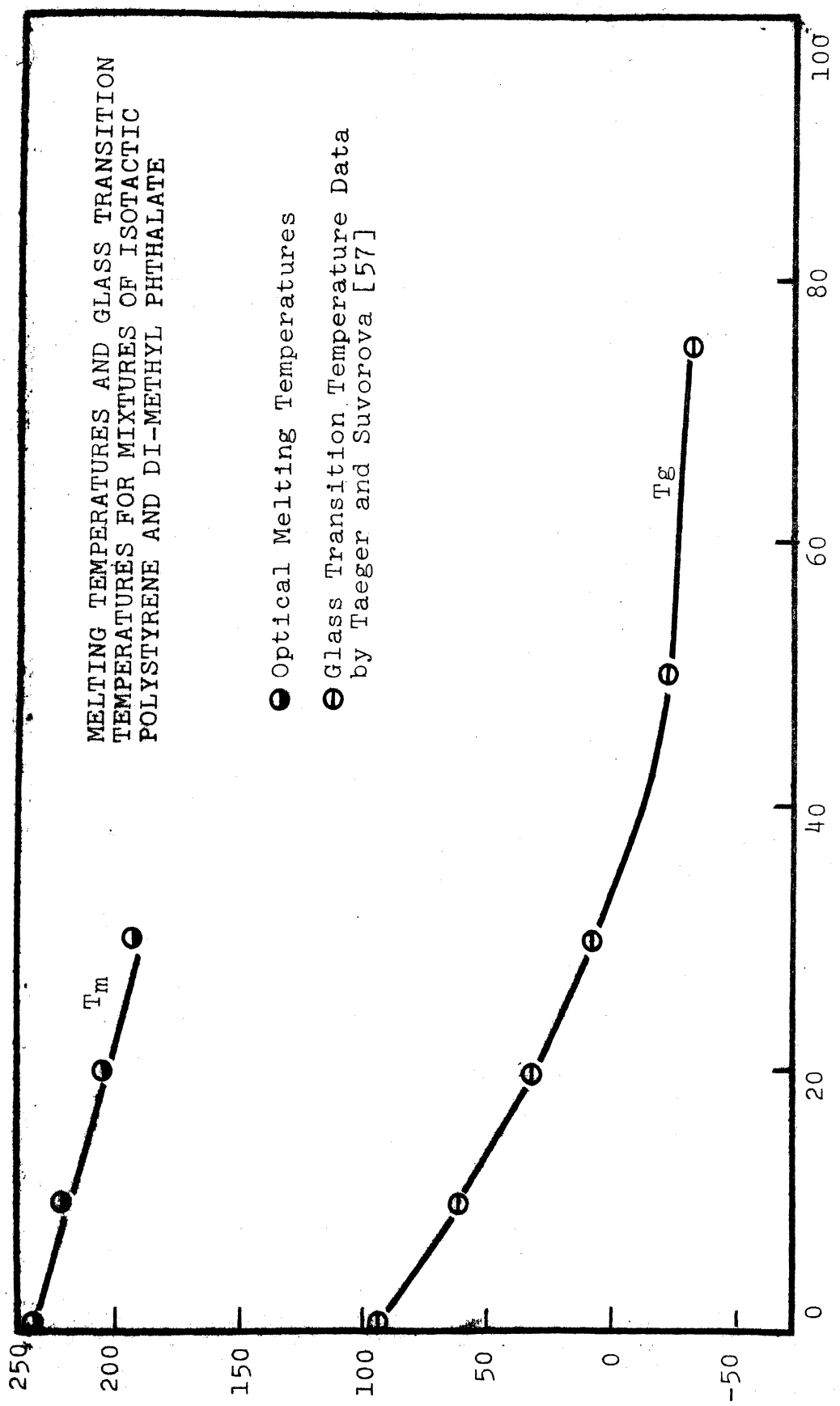
MELTING TEMPERATURES AND GLASS TRANSITION TEMPERATURES FOR MIXTURES OF ISOTACTIC POLYSTYRENE AND DI-METHYL PHTHALATE
Optical Melting Temperatures
Glass Transition Temperature Data by Taeger and Suvorova [57]
Tm
Tg
Melting Temperature or Glass Transition Temperature, °C
250
200
150
100
50
0
-50
0
20
40
60
80
100
% Di-Methyl Phthalate

Figure 21

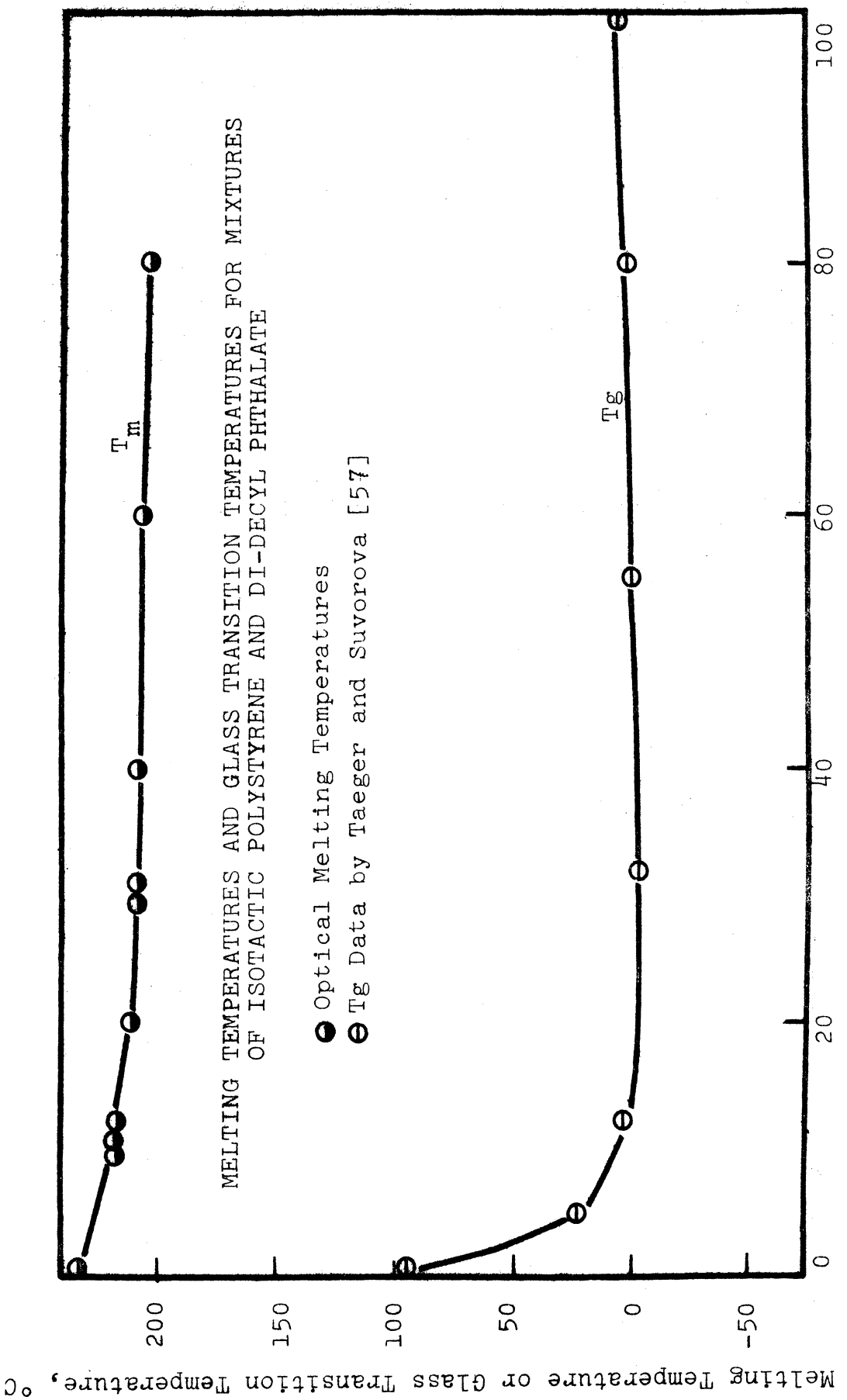
MELTING TEMPERATURES AND GLASS TRANSITION TEMPERATURES FOR MIXTURES OF ISOTACTIC POLYSTYRENE AND DI-DECYL PHTHALATE
Optical Melting Temperatures
Tg Data by Taeger and Suvorova [57]
T_m
Tg
Melting Temperature or Glass Transition Temperature, °C
200
150
100
50
0
-50
0
20
40
60
80
100
% Di-Decyl Phthalate

Figure 22

low molecular weight diluents which are good solvents depress the melting temperature of linear polyethylene more than diluents which are poor solvents.

6. Threshold Crystallization Study

The threshold crystallization temperature is characterized as the annealing temperature at which the first crystalline structures appear from the glassy amorphous state after a long annealing time. For the present study, a 24 hour annealing time was judged to be sufficiently long to induce crystallization at threshold temperatures. At this characteristic temperature molecular chain segments start to orient and pack together in such a way as to form a few discrete bundles of crystalline fibrils fanning out from a central nucleus region, Figure 23. Less than 2°C above this temperature, these discrete bundles develop into extensive spherulitic structures while slightly below this threshold temperature (~ 2°C), there are no signs of crystalline morphology whatsoever.

The first appearance of fibril structure characteristic of the onset of polymer crystallization is most easily detected by electron microscope examination of the surfaces of platinum shadowed or gold decorated thin films, rather than by electron diffraction, which generally shows an amorphous pattern. Values of the threshold crystallization temperature for mixtures of isotactic/atactic polystyrene are recorded in Table III. The glass transition temperature, Tg, and melting temperature, Tm, values are based on the

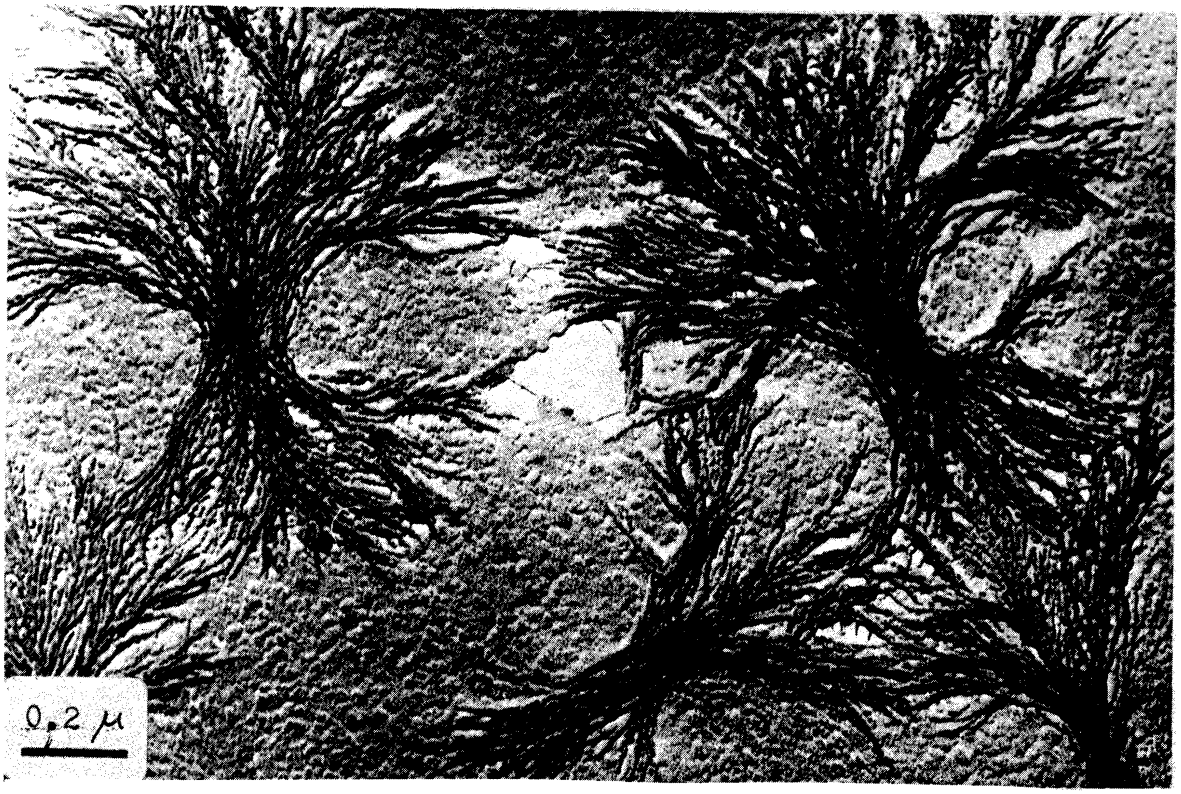

Figure 15: Isotactic polystyrene/benzophenone 50/50, crystallized from the glassy amorphous state at 40°C. Platinum shadowed at 30°.

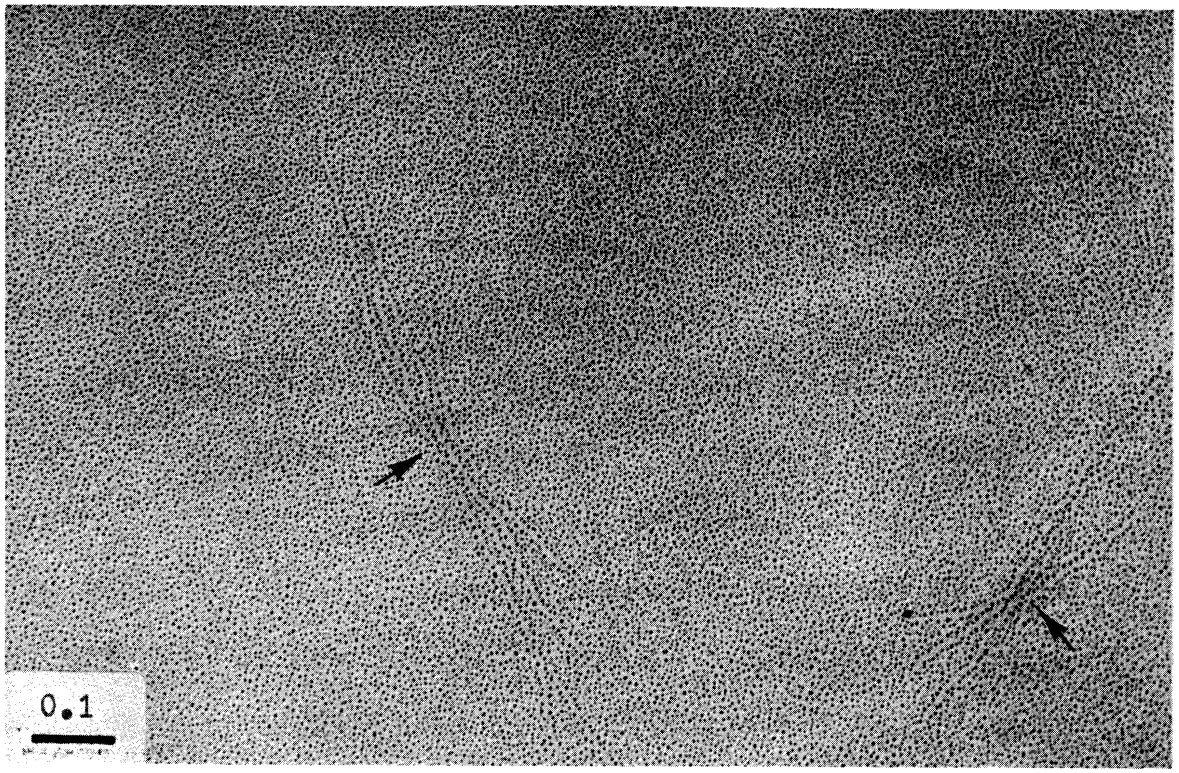

Figure 23: Isotactic polystyrene/benzophenone 80/20, crystallized from the glassy amorphous state at 82°C. Gold decorated at 90°.

results of Boon and Azcue [5], while the threshold crystallization temperature, T_T, values were experimentally measured to within ± 2°C. Analysis of these results in terms of the equations describing the theoretical growth rate kinetics will be considered in the discussion section.

Table III

Threshold Crystallization Temperatures for Mixtures of IPS/Benzophenone and IPS/APS

Concentration	*Tg,°C	**Tm,°C	T_T, °C	T_T-Tg
IPS/benzo. 50/50	-15	180	30	46
IPS/benzo. 60/40	- 2	190	42	46
IPS/benzo. 65/35	8	196	52	44
IPS/benzo. 70/30	16	201	63	47
IPS/benzo. 75/35	26	208	75	49
IPS/benzo. 80/20	36	213	82	46
IPS/benzo. 90/10	58	227	98	40
IPS/APS M_w4,800 10/90	-	-	104	-
IPS/APS M_w4,800 50/50	85	230	105	20
IPS/APS M_w4,800 100/0	85	240	113	28

*Data from Boon and Azcue [5]

**Data from Dedeurwaerder and Oth [14]

D. Discussion

1. Growth Rate Phenomena

The spherulitic growth rate in diluted systems is dependent upon the melting temperature, Tm, and the glass transition temperature, Tg, of the mixture as well as the

concentration of the crystallizable constituent, υ_2, according to equation 10. Dilution of isotactic polystyrene with di-methyl or di-decyl phthalate causes a substantial depression of both the melting and glass transition temperatures, Figures 21 and 22.

At a given crystallization temperature, depression of Tg increases the molecular mobility which leads to a more rapid spherulitic growth rate. However, simultaneous depression of the melting temperature reduces the driving force for secondary nucleation (or growth rate), thus tending to reduce the increase of growth rate expected due to depression of the glass transition temperature. The third effect of dilution is to depress the rate of secondary nucleation (or growth rate) by reducing the probability of interaction between crystallizable polystyrene molecules. At a given temperature and concentration, the interaction of these three effects (Tm, Tg, and υ_2) principally determines the magnitude of the spherulitic growth rate, resulting in the behavior noted in Figures 17 and 19.

Shifting of the maximas of the growth rate curves, T_{max}, to lower temperatures with increasing plasticizer concentration can be correlated with melting temperature, Tm, depression over the same range of concentrations, since the maximas occur at temperatures ranging from 0.84 Tm to 0.89 Tm, Table IV. This correlation is in general agreement with the results found for most crystallizable polymers [41]. The fact that the growth rate maximas remain fixed at about 145°C (± 2°C) for di-decyl phthalate concentrations above

20% (Figure 18) is reflected in the levelling off of the melting temperature curve over the same range of concentrations, Table IV.

Table IV

Relationship Between T_{max} and Tm for Mixtures of IPS/Plasticizer

Concentration	T_m,°C	T_{max},°C	T_{max}/T_m, (°K/°K)
IPS	233.0	178.0	0.890
IPS/DMP 90/10	219.0	157.0	0.875
IPS/DMP 80/20	205.0	145.0	0.875
IPS/DMP 70/30	194.5	122.0	0.844
IPS/DDP 90/10	218.0	160.0	0.872
IPS/DDP 80/20	212.0	143.0	0.858
IPS/DDP 70/30	208.0	147.0	0.871
IPS/DDP 60/40	208.0	147.0	0.871
IPS/DDP 40/60	206.0	145.0	0.870
IPS/DDP 20/80	202.5	145.0	0.878

For the isotactic polystyrene/benzophenone system, Boon and Azcue [5] attribute the increase in spherulitic growth rate for dilutions below 20% to the widening temperature difference between the melting and glass transition temperatures, i.e., the effect due to the increased molecular mobility outweighs the depressive effect due to the reduced rate of nucleation. This growth rate reaches a maximum at 20% dilution (Figure 18) and is depressed at higher benzophenone concentrations because the effect of the reduced

probability of molecular interaction overwhelms other growth factors, thereby causing a marked depression in the overall spherulitic growth rate. Presumably similar forces are operative in the isotactic polystyrene/di-methyl or di-decyl phthalate systems, although in the case of di-decyl phthalate, the curve shows a characteristic flattening of the growth rate over a wide diluent concentration range (20% to 40%), Figure 20. This tendency for curve flattening at the maximum growth rate cannot be accounted for by the behavior of the glass transition and melting temperatures because these parameters remain essentially invariant for diluent concentrations exceeding 20%, Figure 22. Under these conditions (invariant T_m and T_g), if the isotactic polystyrene/di-decyl phthalate system forms a "homogeneous" phase, then the probability effect of dilution would tend to cause a monotonic (not necessarily linear) depression of the growth rate in direct proportion to the increasing diluent concentration. This type of monotonic depression is observed for increasing concentrations of diluent in the isotactic/atactic polystyrene system, Figure 8.

For the present system, however, it appears that the isotactic polystyrene is not being uniformly diluted over the concentration range in question (20% to 40% di-decyl phthalate), Figure 20, since the growth rate is not being depressed. This result suggests that the crystallizing melt might actually form a microscopic two phase mixture over this concentration range. A model based on phase separation between an isotactic polystyrene rich phase and a di-decyl

phthalate phase is consistent with the observation that the crystalline phase is apparently not being diluted by the addition of di-decyl phthalate over this particular concentration range. For diluent concentrations exceeding 40%, it is most likely that some phase separation still exists, as indicated by the lack of melting temperature depression (Figure 22, also see page 72).

There is no evidence suggesting macroscopic (> 2000Å) phase separation in any of the thin films studied, since no signs of optical turbidity were observed in films diluted with either atactic polystyrene or low molecular weight plasticizer at the isothermal crystallization temperature prior to crystallization. The crystallization temperature for mixtures diluted with either di-methyl or di-decyl phthalate were at least 100°C above the macroscopic phase separation temperatures (ranging from 0° to 80°C) reported for these respective mixtures by Taeger and Suvorova [57].

However, there are some indications that a microscopic phase separation might exist in these systems, particularly the di-decyl phthalate system. As mentioned earlier, Taeger and Suvorova [57] proposed the existence of a structured polystyrene phase as being a reasonable model to explain why polystyrene/di-decyl phthalate mixtures have a lower glass transition temperature than comparable concentrations of polystyrene/di-methyl phthalate. Structures which might be regarded as phase separation structure have actually been observed by Gezovich and Geil [18] in poly(vinyl chloride) plasticized with di-octyl phthalate and chlorinated parafin.

They reported spherical structures on the order of 0.1 to 5.0 microns diameter in bulk samples brittle fractured under vacuum at liquid nitrogen temperatures and then ion etched. In addition, they also detected such structures by small angle x-ray scattering methods.

A direct comparison of the spherulitic growth rates for isotactic polystyrene diluted with a 20% concentration of either atactic polystyrene or low molecular weight plasticizer suggests that there might be a difference in the microscopic structure of these two systems, Figure 24. The growth rate for the atactic polystyrene system is only slightly affected by the molecular weight of the atactic diluent. However, the system similarly diluted with comparable concentrations of plasticizer, particularly di-decyl phthalate, shows a spectacular 100% to 200% increase in growth rate, Figure 24. At this point it might be argued that the difference in the growth rate for these two systems is essentially due to the difference in the molecular weight of the diluent. In order to clarify this issue, it is necessary to extrapolate the behavior of the isotactic/atactic polystyrene system to very low diluent molecular weights (~ 450). An extrapolation based on the Hoffman and Weeks [23] relationship ($G\alpha(1/M_n)^y$), giving y the maximum value of 1.0, results in a 20% increase in growth rate between diluent molecular weights 900 and 450.

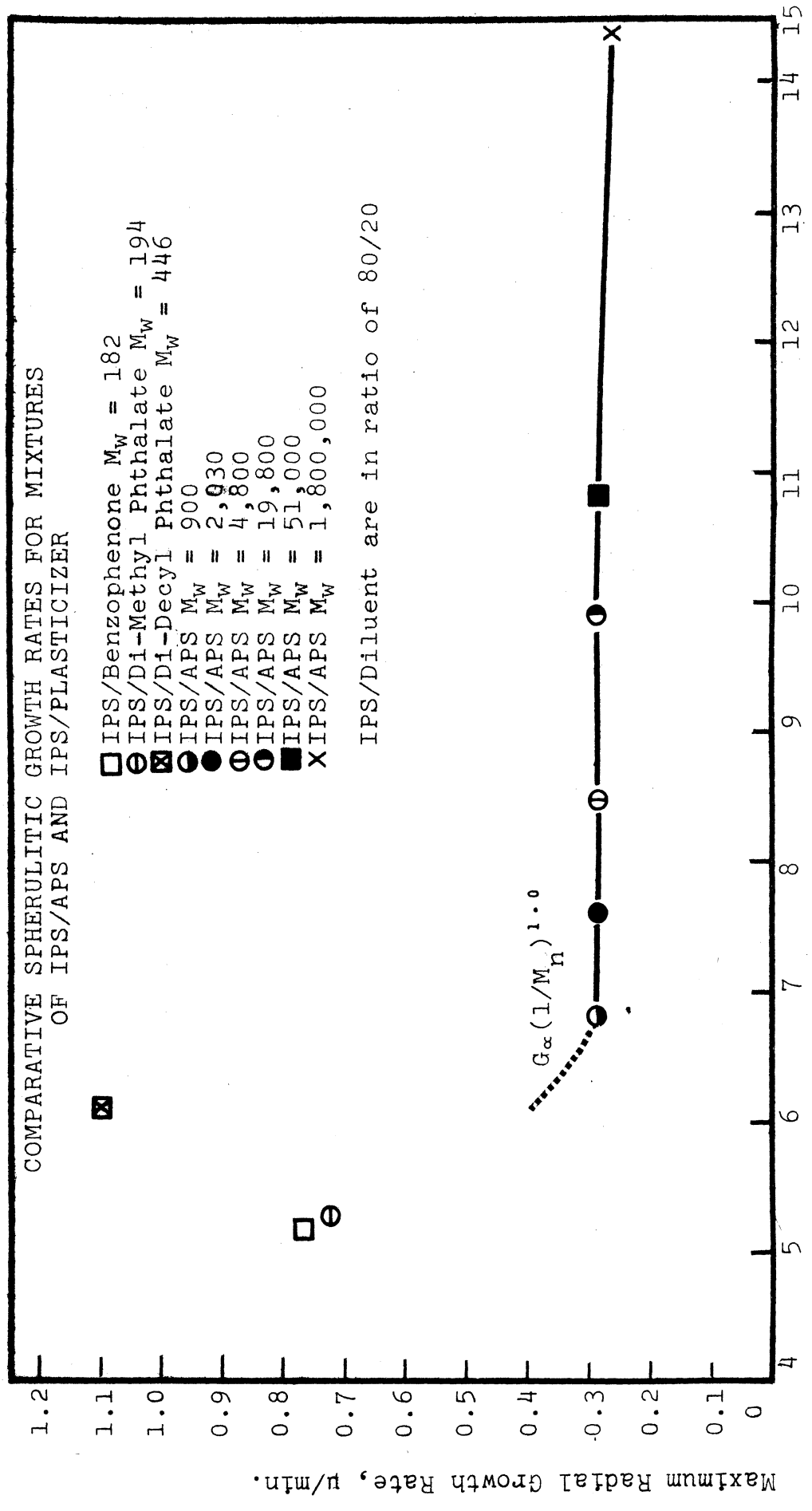
COMPARATIVE SPHERULITIC GROWTH RATES FOR MIXTURES
OF IPS/APS AND IPS/PLASTICIZER
IPS/Benzophenone M_w = 182
IPS/Di-Methyl Phthalate M_w = 194
IPS/Di-Decyl Phthalate M_w = 446
IPS/APS M_w = 900
IPS/APS M_w = 2,030
IPS/APS M_w = 4,800
IPS/APS M_w = 19,800
IPS/APS M_w = 51,000
IPS/APS M_w = 1,800,000
IPS/Diluent are in ratio of 80/20
$G\alpha(1/M_n)^{1.0}$
Maximum Radial Growth Rate, μ/min.
Ln Diluent Molecular Weight
0
0.1
0.2
0.3
0.4
0.5
0.6
0.7
0.8
0.9
1.0
1.1
1.2
4
5
6
7
8
9
10
11
12
13
14
15

Figure 24

This extrapolation obviously does not explain the spectacular increases in growth rate observed for the mixture diluted with di-decyl phthalate.

It is now apparent that the difference in the behavior of these two systems (isotactic/atactic polystyrene and isotactic polystyrene/plasticizer) is related to the microstructure of the mixture. As mentioned earlier, the system diluted with atactic polystyrene apparently forms a "homogeneous" phase, since the resulting growth rate is monotonically depressed with increasing diluent concentration. However, the system diluted with di-decyl phthalate, at least over certain concentration ranges, apparently forms a two phase mixture. If we assume that in the latter case we actually do have a two phase system, then how can we explain the spectacular increase in growth rate associated with the plasticized system? If we consider the terms in equation 2, it is apparent that upon the creation of a two phase system either the viscous transport term, E_D, or the free energy of nucleus formation, ΔF^*, must be significantly altered. We will try to distinguish between these two possibilities in the following discussion of the activation energy for viscous transport.

B. Activation Energy for Viscous Transport

At threshold crystallization conditions, the spherulitic growth rate is principally controlled by the activation energy required for viscous transport across the liquid-nucleus interface, E_D, equation (2). Thus, the results of

the threshold crystallization study for mixtures of isotactic polystyrene/benzophenone and isotactic/atactic polystyrene may be analyzed by the theoretical growth rate equation 10 developed from equation 2 in the introduction of Chapter III with specific terms evaluated by Boon and Azcue [5]:

$$G(dil) = 9.1x10^{6}\upsilon_2 \exp\left[\frac{-2080}{75+T-Tg}\right] \exp\left[\frac{-279T_m}{T(Tm-T)} + \frac{0.2T_m \ell n \upsilon_2}{(Tm-T)}\right] \quad , \mu/min. \tag{14}$$

where υ_2 and T_m are the volumetric concentration of isotactic polystyrene and the melting temperature of the mixture respectively. In this form they assume that the empirical constant, $C_2 = 75°K$, in the viscous transport activation energy term (I) has the same value for both pure and diluted isotactic polystyrene systems. We also assume that the value of G_o is constant (page 13) and that the first approximation of the Δf_u term (equation 9) is valid for the temperature range being considered [56]. The spherulitic growth rate for threshold crystallization, G_T, can be experimentally measured from electron micrographs of thin films crystallized at the threshold temperature for 24 hours, Figure 23. The values of the threshold growth rates, G_T, for all mixtures are recorded in Table V.

Table V

Threshold Growth Rates for Mixtures

of IPS/Benzophenone and IPS/APS

Concentration	Spherulite Sizes, μ	G_T, μ/min	$G/9.1X10^6\upsilon_2$	(I+II+III)
IPS/Benzo. 90/10	1.09	$7.57X10^{-4}$	$9.25X10^{-11}$	-23.00
IPS/Benzo. 80/20	.59	$4.10X10^{-4}$	$5.63X10^{-11}$	-23.60
IPS/Benzo. 75/25	.71	$4.95X10^{-4}$	$7.26X10^{-11}$	-23.35
IPS/Benzo. 70/30	.87	$6.04X10^{-4}$	$9.48X10^{-11}$	-23.05
IPS/Benzo. 65/35	.84	$5.83X10^{-4}$	$9.86X10^{-11}$	-23.00
IPS/Benzo. 50/50	.68	$4.72X10^{-4}$	$10.41X10^{-11}$	-22.95
IPS/APS 100/0	.75	$5.18X10^{-4}$	$5.72X10^{-11}$	-23.55
IPS/APS 50/50	.62	$4.34X10^{-4}$	$9.52X10^{-11}$	-23.05

The following analysis will be based on the threshold growth rate for the isotactic polystyrene/benzophenone 80/20 mixture, $G_T = 4.10X10^{-4}$/min (Table V). If the value of the growth rate, G_T, for this particular mixture is substituted into equation 14, we have the following result:

$$4.10X10^{-4}=9.1X10^{6}(0.8)\exp(I)\exp(II+III) \qquad (15)$$

$$5.63X10^{-11}=\exp(I+II+III)$$

$$-23.60=(I+II+III) \qquad (16)$$

The complete solution of equation 16 requires a trial and error procedure based on the assumption of various crystallization temperatures. The following table indicates the approximate values of the exponential terms of equation 14 as a function of various assumed threshold crystallization temperature, T_T, using Tm = 213°C and Tg = 36°C (Table III).

Assumed Threshold Temperature (°K), T_T	I	II	III	(I+II+III)
325	-22.85	-2.60	-.135	-25.58
330	-21.85	-2.63	-.139	-24.42
335	-20.60	-2.68	-.145	-23.42

A threshold crystallization temperature of 334°K(61°C) satisfies equation 16 for the isotactic polystyrene/benzophenone 80/20 mixture. However, the experimentally measured threshold temperature, T_T, for this particular mixture is 82°C (Table III), some 21°C higher than indicated by an analysis based on the theoretical kinetics equation. This discrepancy can be resolved by adjusting the value of C_2 while leaving C_1 invariant in the activation energy viscous transport term (I) in equation 14. This constant can be reevaluated by recalculating the values of exponential terms II and III for a crystallization temperature of 82°C and substituting the results into equation 16:

$$I-2.920-.165=-23.60 \tag{17}$$

$$I=-20.520$$

$$\frac{-2080}{C_2+T-Tg} = -20.52 \tag{18}$$

According to equation (18), when T_T = 82°C and Tg = 36°C (Table III), the recalculated value is C_2 = 55.5°K. If we use the third approximation for the Δf_u term ($d(\Delta C_p)/dT$=constant) [56] in equation 14, the resulting value of C_2 following the same type of analysis would be C_2 = 57.7°C. Thus, we can see that the calculated value of C_2 is relatively independent of the assumed form of the free energy of fusion.

A question might be raised at this point as to whether this new value of C_2 is also valid for other concentrations of benzophenone in isotactic polystyrene. Calculated values of the threshold crystallization temperature using equation 18, with C_2 = 55.5°K, and data in Table III are compared to the experimentally measured values in Table VI. Examination of Table VI shows that the value of C_2 = 55.5°K, is independent of the benzophenone concentrations exceeding 20%. This result is also reflected in the relative independence of the temperature difference between the threshold crystallization temperature and the glass transition temperature, Tx-Tg, (Table III), as well as the threshold growth rate, G_T, (Table V) to the respective benzophenone concentrations.

The value of the exponential term (I) for the activation energy for viscous transport at threshold crystallization may also be calculated for the pure isotactic polystyrene system (Table V), using values of T_m and Tg as recorded in Table III.

$$I-2.53-0.00=-23.55 \qquad (19)$$

$$I=-21.02$$

If we use the appropriate value of the activation energy term (I) together with the experimentally measured threshold crystallization temperatures (Table III), we can calculate the values of the activation energy empirical constant, C_2, using T_g = 85°C.

$$\frac{-2080}{C_2+T-Tg} = -21.02 \qquad (20)$$

Table VI

Threshold Crystallization Temperature,

Experimental and Calculated

Concentration	T_T, °C exp.*	T_T, °C, Cal.	**C_2,°K	***C_2°K
IPS/Benzo. 50/50	30	31.0	55.5	6.5
IPS/Benzo. 60/40	42	43.8	55.5	6.5
IPS/Benzo. 65/35	52	53.7	55.5	6.5
IPS/Benzo. 70/30	63	62.2	55.5	6.5
IPS/Benzo. 75/25	75	72.0	55.5	6.5
IPS/Benzo. 80/20	82	82.0	55.5	6.5
IPS/Benzo. 90/10	98	98.0	62.0	12.8
IPS/APS M_w=4,800 10/90	104	--	--	--
IPS/APS M_w=4,800 50/50	105	105.0	79.2	33.2
IPS/APS M_w=4,800 100/0	113	113.0	71.2	25.4

* ±2°C.

**Calculated according to the values of G_o and C_1 used by Boon and Azcue [5].

***Calculated for values of G_o, C_1, and K reported by Suzuki and Kovacs [56].

The values of the empirical constant, C_2, are 71.2°K and 79,2°K for the IPS/APS 100/0 and IPS/APS (M_w=4,800) 50/50 mixtures respectively. These values are in general agreement with the value of C_2 = 75.0°K, reported by Boon and Azcue [5] for the pure isotactic polystyrene system.

If we follow a similar analysis using the values of the empirical constants G_o, C_1=1.5cal./mole, and $K = 4b_o\sigma_u\sigma_e/k\Delta H_f$ in equation 14 as determined by Suzuki and Kovacs [56] for the isotactic polystyrene system, then C_2 = 6.5°K for the benzophenone mixtures and C_2 = 25.4°K and 33.2°K for IPS/APS 100/0 and IPS/APS (M_w=4,800) 50/50 mixtures respectively, Table VI. For pure isotactic polystyrene, Suzuki and Kovacs [56] found that C_2 = 30.7°K. The difference in the magnitude of the values of C_2 for the methods of Boon and Azcue [5] and Suzuki and Kovacs [56] is related to the type of analysis used to evaluate the other empirical constants in the growth rate equation. Suzuki and Kovacs [56] also reported that according to their analysis, $C_2 = fg/\alpha_f$ where fg is the fractional free volume at the glass transition temperature and α_f is the coefficient of thermal expansion. Bueche [10] indicates that fg = 0.025 for almost all glass forming substances and $\alpha_f = 10^{-4}$ for most polymers. In addition Bueche [10] found that α_f is approximately 10^{-3} for low molecular weight plasticizers. Thus, by using the values of the free volume parameters (fg, α_f) reported by Bueche [10], we can see that the value of C_2 should be depressed by the addition of low molecular weight plasticizer, a result experimentally verified for the benzophenone system.

Regardless of the analysis technique used, it is apparent that the empirical constant C_2 in the activation energy for viscous transport term (I) is significantly lower for the system diluted with benzophenone than for the isotactic/atactic polystyrene system. In effect this means that for equivalent values of T_T-Tg (crystallization temperature-glass transition temperature) in the range near T_g, where the growth rate is principally controlled by the activation energy for viscous transport (term I), the resulting growth rate for the isotactic/atactic polystyrene system will actually be higher than the rate for benzophenone system. However, in the range closer to the maximum growth rate where the free energy term exerts a stronger influence, we know that the benzophenone system has a growth rate substantially higher than the equivalent rate for the isotactic/atactic polystyrene system, Figure 20. The only way we can reconcile these experimental results with the derived form of the spherulitic growth rate equation (4) is to suggest that the free energy of critical nucleus formation is uniformly lower for the benzophenone system than for the atactic polystyrene system at equivalent dilutions. Apparently, the creation of a two phase plasticized mixture tends to lower the free energy of critical nucleus formation ΔF^* by decreasing the interfacial free energies σ_u and σ_e (equation 7) associated with the formation of a critical nucleus.

Although the exact mechanism of nucleus formation is presently unknown, it would seem reasonable to suggest that in the case of isotactic polystyrene plasticized with benzophenone and perhaps with di-decyl phthalate, the growth mechanism involves

the addition of whole structural units (with a lower free energy of critical nucleus formation) rather than segments of single molecules, onto the crystalline growth front. For the isotactic/atactic polystyrene system, however, the "homogeneous" phase growth rate behavior and growth rate magnitude would suggest a non-structured nucleation process or one of smaller magnitude, which perhaps involves the addition of single molecules or small groups of loosely bound molecules onto the growth front.

E. Conclusions

1. For the isotactic polystyrene/di-methyl or di-decyl phthalate systems, the dependence of growth rate on temperature is very similar to that for the undiluted polymer, i.e., the growth rate curves are generally gaussian in shape with a sharp maximum at the optimum crystallization temperature.
2. As the concentration of di-methyl phthalate is increased, the crystallization range shifts to lower temperatures, the amount of shift being proportional to the amount of plasticizer added.
3. The overall maximum growth rate for the isotactic polystyrene/di-methyl phthalate system occurs between 20 and 30% dilution.
4. As the concentration of di-decyl phthalate is increased, the crystallization range shifts to lower temperatures for up to 20% dilution. Above 20% dilution, the maximum growth rates remain fixed at about 145°C (± 2°C) for dilutions up to 80% plasticizer. Apparently, the curves

no longer shift to lower temperatures because the melting temperature over this concentration range is nearly constant (Figure 22).

5. The overall maximum growth rate for mixtures of isotactic polystyrene and di-decyl phthalate is relatively flat between 20% and 40% dilution, suggesting a microscopic phase separation between an isotactic polystyrene rich phase and a di-decyl phthalate phase over this concentration range.

6. The optical melting temperatures for mixtures of isotactic polystyrene/di-methyl or di-decyl phthalate are uniformly depressed with increasing plasticizer concentration, the amount of depression being greatest for comparable concentrations of di-methyl phthalate.

7. A direct comparison of the spherulitic growth rates for mixtures of isotactic/atactic polystyrene and isotactic polystyrene/di-decyl phthalate over the same diluent concentration and molecular weight range suggests that there is a basic difference in the microstructure of these two blends. It is suggested that the former mixture behaves as a "homogeneous" phase since the growth rate (concentration of isotactic polystyrene) is monotonically depressed with increasing concentrations of atactic polystyrene. The latter mixture, however, appears to behave as a two phase system, at least over certain concentration ranges. Thus, since the optimum spherulitic growth rate for the plasticized mixture is much higher than the comparable rate for the atactic mixture, the creation of a two phase system apparently effects either the viscous transport mechanism or the free energy of critical nucleus formation

in the spherulite growth process.

8. According to an analysis of the threshold crystallization temperatures for mixtures of isotactic/atactic polystyrene and isotactic polystyrene/benzophenone, the empirical constants C_1 and C_2 in the WLF form of the viscous transport term in the growth rate equation take on different values for these two mixtures. If we consider C_1 to be invariant for both systems, then C_2 is significantly lower for the benzophenone system, according to the methods of Boon and Azcue [5] and Suzuki and Kovacs [56]. The magnitude of this constant (C_2), however, is dependent upon which method is used. If the derived form of the spherulitic growth rate equation (equation 4) is correct, then the free energy of critical nucleus formation must also be lower for the benzophenone system in order to explain the higher maximum growth rates observed.

Thus, it is suggested that the spherulitic growth mechanism for plasticized systems involves the addition of whole structural units (with a lower free energy of critical nucleus formation) to the growth front, while the mechanism for the atactic polystyrene system is a nonstructural nucleation process involving the addition of single molecules or small groups of loosely bound molecules to the growth front.

CHAPTER V

STRAIN INDUCED CRYSTALLIZATION

A. Introduction

Melt extrusion or injection molding of a crystallizable polymer often introduces an oriented crystalline morphology which is quite different than the type of morphology normally found in random spherulitic crystallization. Recent studies designed to elucidate the nature of this structure have concentrated on strain induced crystallization from the melt state. However, some crystalline polymers, particularly those having a slow spherulitic growth rate, can also be crystallized from the glassy or rubbery states. Therefore, in order to more fully understand the nature of strain induced crystallization, a comprehensive study was undertaken to examine the influence of extension ratio, substrate, annealing temperature, plasticizer, and annealing time on the morphology of strain induced crystallization of isotactic polystyrene from the glassy and rubbery amorphous states.

In the work most directly related to the present study, Yeh and Geil [61] observed strain induced crystallization from the glassy amorphous state of poly(ethylene terephthalate). They reported that strain induced crystallization occurs by rotation, alignment, and perfection of

the internal order of 75Å paracrystalline ball-like structures originally present in the amorphous material. Thin films of amorphous poly(ethylene terephthalate) became two dimensionally ordered when drawn 500% even at temperatures below the nominal glass transition Tg. This appearance of crystallinity below Tg coincides with the alignment of ball-like structures at angles ranging from 45° to 50° to the stretch direction. Subsequent heat treatment for 15 minutes at temperatures ranging up to 260°C increased the amount of crystallinity as well as the internal ordering of the ball-like structures, as indicated by small angle x-ray diffraction. Thin films annealed while in contact with a substrate (glass slide) developed row type structures oriented perpendicular to the stretch direction, with the crystalline fibers (rows of ball-like structures) prominently rising above the surface of the film. Dark field electron micrographs of thin films heat set at 240°C and 260°C, using the (010) and ($1\bar{1}0$) reflections, show 75Å diffracting regions, but no evidence of any extended chain nuclei oriented parallel to the stretch direction.

In experiments involving strain-induced crystallization of natural rubber from the melt state, Andrews [1] observed the change from spherulitic morphology in unstrained films to fibrillar morphology in highly stretched films. Thin films stretched to low elongations at room temperature and subsequently cooled to -26°C developed fibrous row structures oriented perpendicular to the stretch direction, while similar films stretched to high elongations, 400% to

700%, develop fibril type structures aligned parallel to the stretch direction. Recent work by Luch [34] on the strain induced crystallization of natural rubber from the melt state shows structures similar to those observed by Andrews [1], although they appear to differ in detail. In addition, Luch noted that the fibillar structures in highly stretched thin films can be reversibly transformed to perpendicular structures by suitable thermal treatment.

Keller and Machin [33] have examined strain induced crystallization of lightly crosslinked polyethylene from the rubbery melt state. In highly stretched films, they observed very fine structures or lamallae arranged perpendicular to the draw direction. In films stretched to lower elongations prior to crystallization, however, the perpendicular lamallae assumed a twisting conformation similar to those often observed in normal spherulitic crystallization. Their explanation for this behavior is that when the stress is low, the crystalline ribbons can freely twist as they grow, but as the stress is increased, the twisting becomes progressively more difficult because an increasing overall crystallization rate generates a higher fiber density. Keller and Machin [33] also suggest that line nuclei are probably present in the observed row structures and that the line nuclei are most likely made up of extended chain crystals. This would indicate that the resulting growth mechanism for row structures involves epitaxial growth of folded chain fibers perpendicular to these extended chain nuclei.

Pennings and Kiel [47], among others, have produced

Shish-Kebab type row structures by shear induced crystallization of dilute solutions of polyethylene in xylene. These structures appear to be made up of platelet type lamallae superimposed on a filamentary ribbon backbone. The structure of the filamentary ribbon backbone is presently under intensive research by numerous investigators. For polyethylene shear crystallized at small supercoolings from dilute solution, Wikjord and Manley [59] succeeded in removing the lamallar row structures by nitric acid oxidation and selective toluene dissolution, leaving naked filamentary ribbons. Differential thermal analysis of these ribbon structures suggests a dual molecular conformation of both folded and extended chains. Thermal and oxidative behavior of polyethylene prepared at lower crystallization temperatures suggests a greater content of chain folds in the central ribbon as the degree of supercooling is increased.

Row structures are also frequently found in bulk material prepared by melt extrusion or by injection molding [49]. Clark and Garber [13] observed that row structures are characteristic of the highly oriented surface of molded bars of polyoxymethylene while random spherulitic crystallization occurs in the unoriented interior. Some evidence suggesting the presence of fibril nuclei in blown films of polyoxymethylene was also reported by Clark and Garber [13]. They observed 300Å diameter fibrils oriented parallel to the stretch direction in the same field as crystalline row structures oriented perpendicular to the stretch direction. They suggest that the fibrils, supposedly generated by high

stress, are responsible for the row structure morphology, but the chain conformation within these fibrils has not been established.

From the above discussion, we can see that the exact nature of line nucleation and the mechanism for the growth of row structures is not clearly understood at the present time. The results of Wikjord and Manley [59] indicate that the nature of the filamentary ribbon backbone in shear crystallized polyethylene is quite complex, consisting of both folded and extended chains. Dark field micrographs of strain crystallized poly(ethylene terephthalate) by Yeh and Geil [61] also indicate a segmented rather than an extended type structure. Thus, the backbone structures aligned parallel to the orientation direction---if they exist---are certainly more complex than the simple extended chain model suggested by Keller [33]. In addition, it is not clear whether the mechanism for the growth of row structures involves epitaxial growth on some type of line nucleus or a rearrangement of previously existing crystalline structures. In the present study, we have tried to expand our knowledge of strain induced crystallization by examining the detailed behavior of isotactic polystyrene strain crystallized from the amorphous glassy and rubbery states under a wide variety of conditions. In particular, we have examined thin films stretched up to 500% elongation by adding 40% benzophenone to isotactic polystyrene in order to reduce the glass transition temperature of the mixture to -2°C, in effect making the isotactic polystyrene/benzophenone 60/40

thin films rubbery at room temperature. We have used bright and dark field electron microscopy and electron diffraction to study stretched thin films which were either shadowed with platinum, decorated with gold, or mildly etched with amyl acetate, in order to remove the noncrystallizable diluent and expose the underlying crystalline structure. Since the gold decoration technique in particular is not well understood, we have carried out additional studies on crystallized holey films of isotactic polystyrene in order to elucidate the mechanism of gold decoration with respect to fiber orientation.

B. Experimental

Thin films of amorphous isotactic polystyrene with a large number of small holes were made by preparing dilute 0.2% solutions of isotactic polystyrene in diethylene chloride. After complete dissolution of polystyrene, several drops of water were added, and the combined solution was vigorously shaken until a finely dispersed emulsion was formed. Drops of the emulsion were cast onto glass slides coated with sodium hexa-meta phosphate, a water soluble replica releasing agent, and drained in such a way as to cause the resulting film to have a graduated thickness. While the emulsion thin films were drying, moist breathing on the film surface helped to create large numbers of tiny holes 0.1 to 10 μ in diameter. After complete drying, the amorphous holey films of isotactic polystyrene were floated off onto a water surface and picked up on specimen grids for

subsequent annealing at 140°C in a controlled temperature hot air oven (± 2°C) for 10 to 15 minutes. The crystallized holey films were prepared for electron microscope examination by either shadowing the surface with platinum, or decorating it with gold.

Rubbery thin films capable of being stretched 500% on a water surface were cast from dilute 0.4% solutions of isotactic polystyrene/benzophenone 60/40 in benzene made by pipetting together proper ratios of 0.4% isotactic polystyrene and 0.4% benzophenone in benzene solutions. Thin films approximately 1,000 to 1,200Å thick, as judged by light reflections, were cast onto glass slides coated with sodium hexa-meta phosphate. After air drying at room temperature for 20 minutes, these films were floated off onto a clean water surface. Insufficient drying caused these films to shrink and thicken upon contacting the water surface. On the other hand prolonged drying tended to remove excess amounts of volatile benzophenone, making the films brittle at room temperature.

Thin films having yellowish-orange light reflections, 1200Å, were most successfully stretched to elongations ranging from 100% to 500% by means of a pair of modified draftsman dividers, described by Yeh and Geil [62]. Specimen grids were placed on the surface of the stretched film and picked up by plunging a finger down through the water surface and scooping up the grids. These stretched films were annealed at 125°C, 155°C, or 175°C in a temperature controlled hot air oven (± 2°C) from 1 to 60 minutes and

then prepared for electron microscope examination by either shadowing with platinum or decorating with gold.

Films of unplasticized isotactic polystyrene were cast directly onto a Mylar substrate and stretched 50 to 100% in a small mechanical stretching device especially designed for this purpose, Yeh and Geil [62]. After stretching, these films were annealed at 155°C or 175°C for 20 minutes and shadowed with platinum or decorated with gold. The stretched films were then removed from the Mylar substrate by stripping with a layer of poly(acrylic acid) dried down from a 10% aqueous solution. The stripped films were backed with 200Å-300Å of carbon and the poly(acrylic acid) was redissolved in water, leaving the extraction replica to be picked up on specimen grids.

The method for selective etching, similar to that used by Padden [46], involved mounting stretched thin films of isotactic polystyrene/benzophenone 60/40 on pieces of freshly cleaved mica and crystallizing the films in the same manner as before. After crystallization, the pieces of mica were plunged into a bath of amyl acetate, at 23°C, for times normally ranging from 20 to 30 seconds, drained, and then air dried. Other solvents such as xylene, acetone, and methyl ethyl ketone were also tried at various temperatures and etching times, but room temperature amyl acetate was found to be the most suitable because it did not cause solvent induced crystallization in noncrystalline amorphous thin films. After selective etching, the stretched films were shadowed with platinum, coated with carbon, and floated

off onto a water surface to be picked up on grids.

Films of isotactic/atactic polystyrene stretched on Mylar substrate were also selectively etched. After crystallization, the thin films mounted in the stretching device were plunged into a bath of amyl acetate, at 23°C, for times normally ranging from 20 to 30 seconds. They were then drained and air dried. The etched films were shadowed with platinum and then removed from the mylar substrate by stripping with poly(acrylic acid).

C. Results

1. Morphology of Holey Films

Electron microscopy examination of thin holey films of isotactic polystyrene, crystallized while being supported on 200 mesh copper grids, shows radial fibers uniformly distributed around the edges of 0.1 to 10.0 μ diameter holes, as illustrated in Figure 25. The measured width of radial fibers, as well as the non-oriented fibers, is 110-120Å in platinum shadowed holey films crystallized at 140°C. This result is in general agreement with the 127Å small angle x-ray long period reported by Manley and Blais [43].in bulk isotactic polystyrene crystallized at 140°C. Similar holey films crystallized while being supported on a substrate (glass slide) do not develop the radial fiber conformation, Figure 26. Andrews [1], upon observing similar radial fiber formation in thin films of natural rubber, attributed the radial orientation to the concentric stress field which is locally generated around the edge of

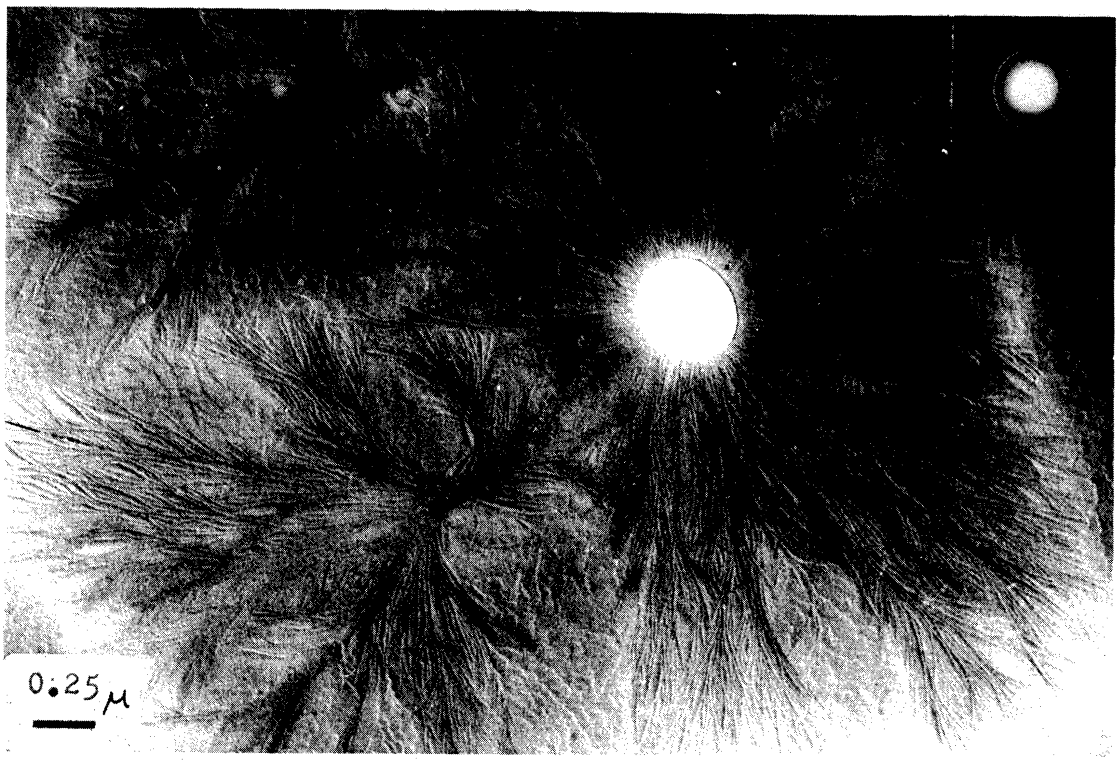

Figure 25: Isotactic polystyrene holey film crystallized at 140°C for 5 minutes. Platinum shadowed at 30°.

Figure 26: Isotactic polystyrene holey film crystallized on glass slide at 140°C for 10 minutes. Gold decorated at 90°.

each hole. Apparently, the effect of the substrate in Figure 26 is to relieve this local stress field, thus causing a random fiber orientation.

2. Gold Decoration of Holey Films

Gold decoration of crystallized isotactic polystyrene holey films shows a tri-layer decorative pattern which appears to coincide with the radial fiber orientation, as illustrated in Figure 27. Examination of Figure 27 will clearly show that the tri-layer decorative pattern consists of two lines of gold particles, 45Å in diameter, on either side of a completely vacated region, measuring 60Å between the edges of the aligned gold particles. It is of interest to note that our value of 60Å is about the same as the value of 65Å reported by Haller and Magill [20] for the vacated width of gold decorated fibers of polysiloxane crystallized at 130°C from the melt state.

It is well known that the equilibrium width of crystalline fibers is a strong function of crystallization temperature. Accordingly, thin films of isotactic polystyrene were crystallized at three different temperatures and the resulting average dimensions of the platinum shadowed and gold decorated fibers are compared in Table IV (see Figures 25, 27, 28, 29).

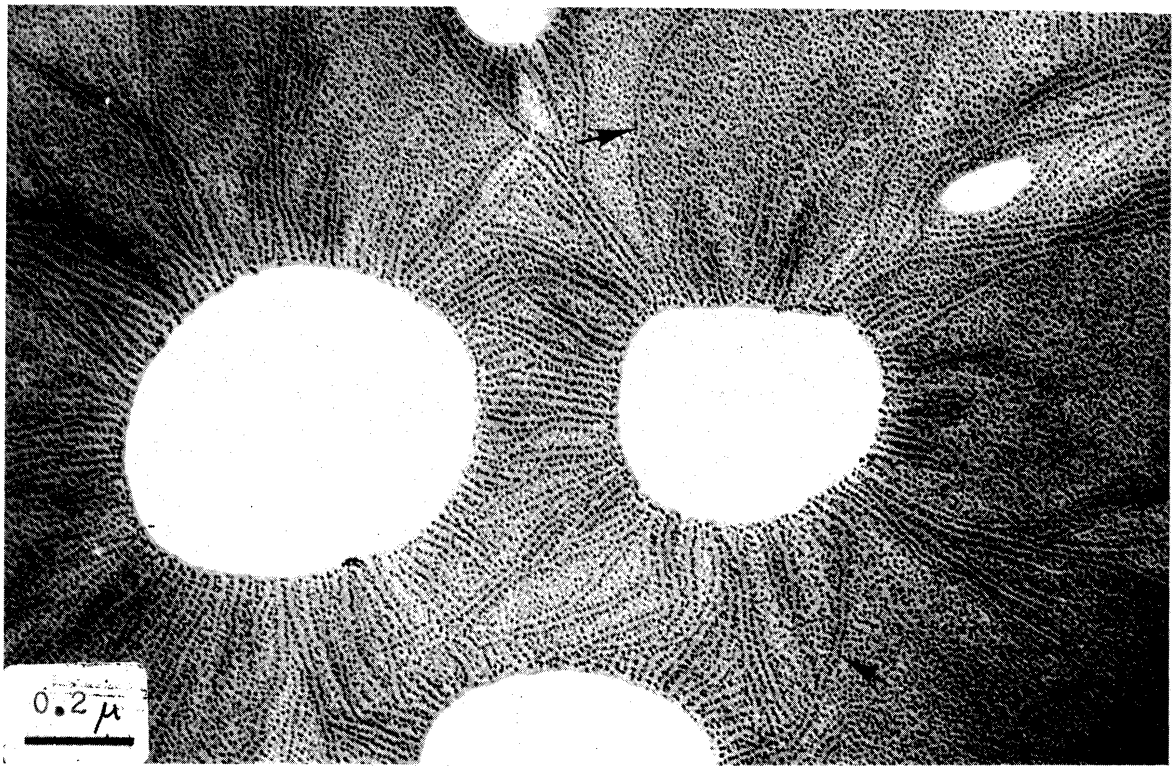

Figure 27: Isotactic polystyrene holey film crystallized at 140°C for 10 minutes. Gold decorated at 90°. Arrows indicate tri-layer decorative pattern.

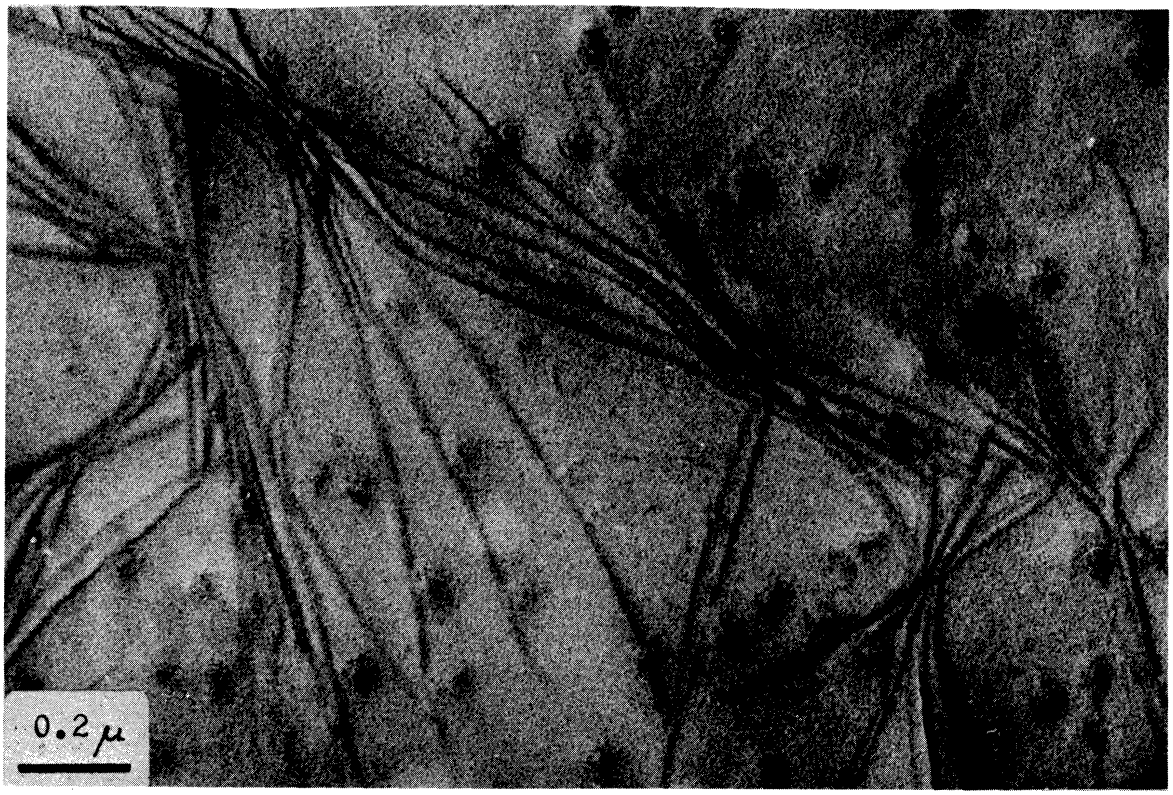

Figure 28: Isotactic polystyrene thin film crystallized at 210°C for 5 hours. Platinum shadowed at 30°.

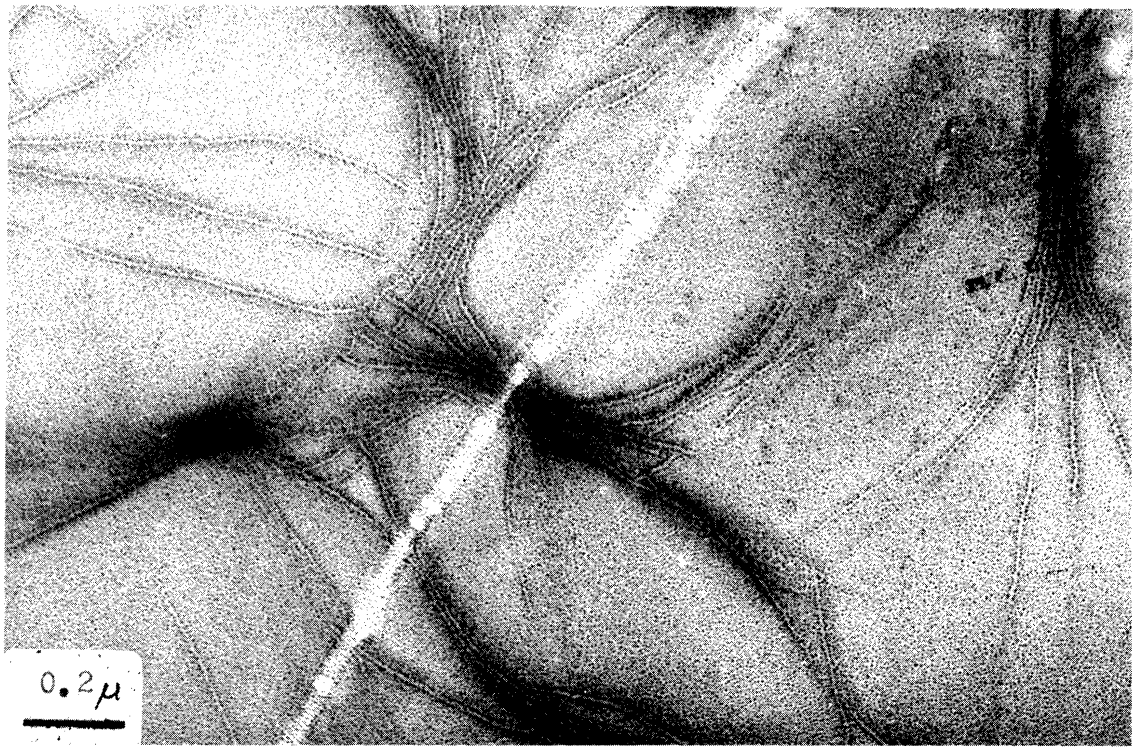

Figure 29: Isotactic polystyrene thin film crystallized at 210C for 5 hours. Gold decorated.

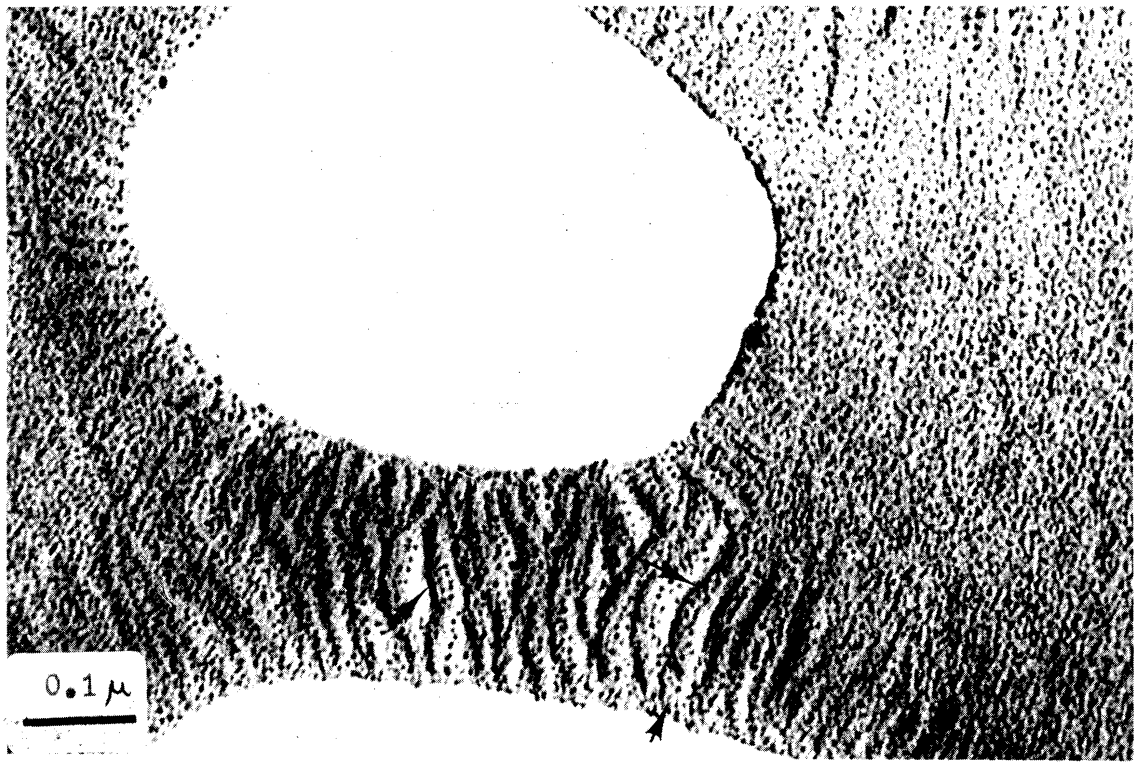

Figure 30: Isotactic polystyrene holey film crystallized at 140C for 10 minutes. Platinum shadowed on one side and gold decorated on reverse side. Arrows indicate area where platinum stacks up.

Table VII

Parameters of Gold Decorated Fibers

Temperature, °C	Pt.	Au vacant Area	Au particle	X-ray*
140	110-120Å	60-65Å	50-55Å	127Å
175	150-165Å	55-60Å	45-50Å	160Å
210	200-210Å	55-60Å	45-50Å	215Å

*Small angle x-ray data, Manley and Blais [43].

Although the dimensions of the platinum shadowed fibers are in general agreement with the small angle x-ray data of Manley and Blais [43], the width of the vacated region in similar films decorated with gold appears to be insensitive to lamallar thickness or crystallization temperature. This result appears to be in conflict with the observations of Spit [55], who noted that in thin films of crystallized nylon 6, the gold particles and phosphotungstic acid stain seem to be sensitive to one and the same region, presumably the amorphous layer adjacent to the crystalline fiber.

In a separate experiment, we tried to establish whether the gold decoration particles stack up along the bottom edge of raised crystalline fibers, as does platinum, or perhaps are sensitive to surface structure on top of the crystalline fibers. Figure 30 shows a crystallized holey film of isotactic polystyrene shadowed with platinum on one side and decorated with gold on the reverse side. Careful examination will show that the gold decoration particles tend to stack up in about the same region as the platinum

material (± 25Å) and perhaps a little toward the center of the crystalline fibers. Thus, with this type of experiment it cannot be clearly established exactly where the gold particles reside, i.e., in the middle or on the edge of lamallae. Figure 31 shows a high resolution micrograph of a very thin holely film of crystallized isotactic polystyrene decorated with gold. The dark radial fibers can be associated with crystalline fibrous regions oriented edge on for maximum electron scattering density. Adjacent regions are either completely amorphous or only partially crystalline, and in any case have a lower electron density or mass thickness. In most areas, the tri-layer decorative pattern appears to coincide directly with the most dense regions in the thin film, the crystalline fibers. However, in some areas, particularly where the radial fibers are closely packed together, the line of gold particles actually appears to reside on top of the dense crystalline fibers. Although these results are not conclusive, it appears that the tri-layer decorative pattern may in some instances be sensitive to the surface structure of the fibers, perhaps even along the crystalline core regions, as indicated by these experiments and the data in Table VII.

3. Morphology of Films Stretched on Mylar

Thin films of isotactic polystyrene stretched 100% on a Mylar substrate at room temperature are amorphous according to surface morphology and corresponding electron diffraction patterns. However, when these stretched films

Figure 31: Isotactic polystyrene holey film crystallized at 140°C for 10 minutes. Gold decorated at 90°. Dense crystalline regions are indicated by arrows.

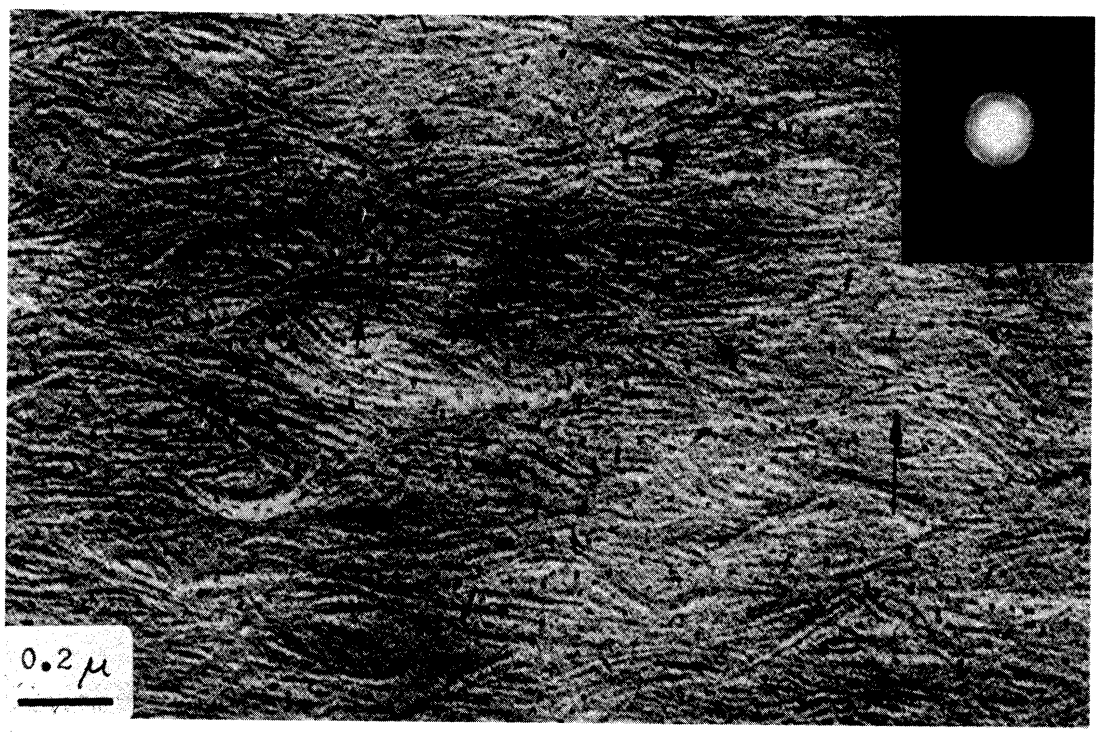

Figure 32: Isotactic polystyrene stretched 100% on mylar, annealed at 175°C for 20 minutes. Platinum shadowed. Stretch direction is verticle and crystalline fibers are indicated by small arrows.

are annealed at 175°C, a uniform field of crystalline fibers grow perpendicular to the original draw direction, Figure 32. These platinum shadowed fibers range in width from 170 to 190Å, which is somewhat larger than the small angle x-ray long period of 160Å reported by Manley and Blais [43] for bulk unoriented isotactic polystyrene crystallized at 175°C.

Examination of Figure 32 indicates that the fibrous structures are somewhat discontinuous, perpendicular to the stretch direction, as in PET [61], and evidently twist into the plane of the film at various random locations. The selected area electron diffraction pattern corresponding to the area in Figure 32 shows a strong (102) reflection (within 9° of the (001) chain axis [9]) parallel to the draw direction and strong equitorial reflections which correspond to the (300), and (220) planes, Figure 33. This result indicates that the molecular chain C axis is oriented parallel to the original stretch direction, which is consistent with the molecular orientations found by Natta [44] in stretched fibers of isotactic polystyrene. This molecular orientation and the width of the fibers (170Å along the stretch direction) would tend to suggest that the fibrous row structures have a folded chain conformation across the 170Å width of the fiber. The folded chain conformation is also found in crystalline structures of other polymers [17]. Finally, Miller and Buchanan [9] reported that the average theoretical crystallite size, based on (102) x-ray line broadening data, is about 85Å to 100Å in direction parallel to stretch for oriented isotactic polystyrene.

Gold decoration of similarly crystallized films of oriented isotactic polystyrene shows fibrous row structures mostly aligned perpendicular to the original stretch direction, Figure 34. The width of the vacated region in the tri-layer pattern measures 60-65Å. The fact that the decorated row structures appear to be somewhat more continuous perpendicular to the stretch direction is probably related to the lower fiber density in the decorated film (compared to Figure 32). Figure 35 illustrates the effect of selective amyl acetate etching of a film of isotactic polystyrene stretched 100% and annealed at 175°C. The clearly defined row structures actually appear to be stacks of lamallar ribbon structures oriented edge on perpendicular to the original draw direction. These etched fibers range in width from 160 to 180Å, which is in good agreement with the results noted for unetched films crystallized under similar conditions.

A finely distinguished Shish-Kebab structure is found in thin films of isotactic/atactic polystyrene/benzophenone 10/80/10 cast from solution onto Mylar substrate and crystallized under stress at 155°C from the glassy amorphous state, Figure 36. We have selectively etched this thin film (Figure 36) to preferentially remove the noncrystalline impurity. In many areas of this film the crystalline structure appears to develop quite independently of any common extended line nuclei. The long shish-kebab structures, oriented parallel to the stretch direction, have lamallae overgrowths attached perpendicular to some type of common

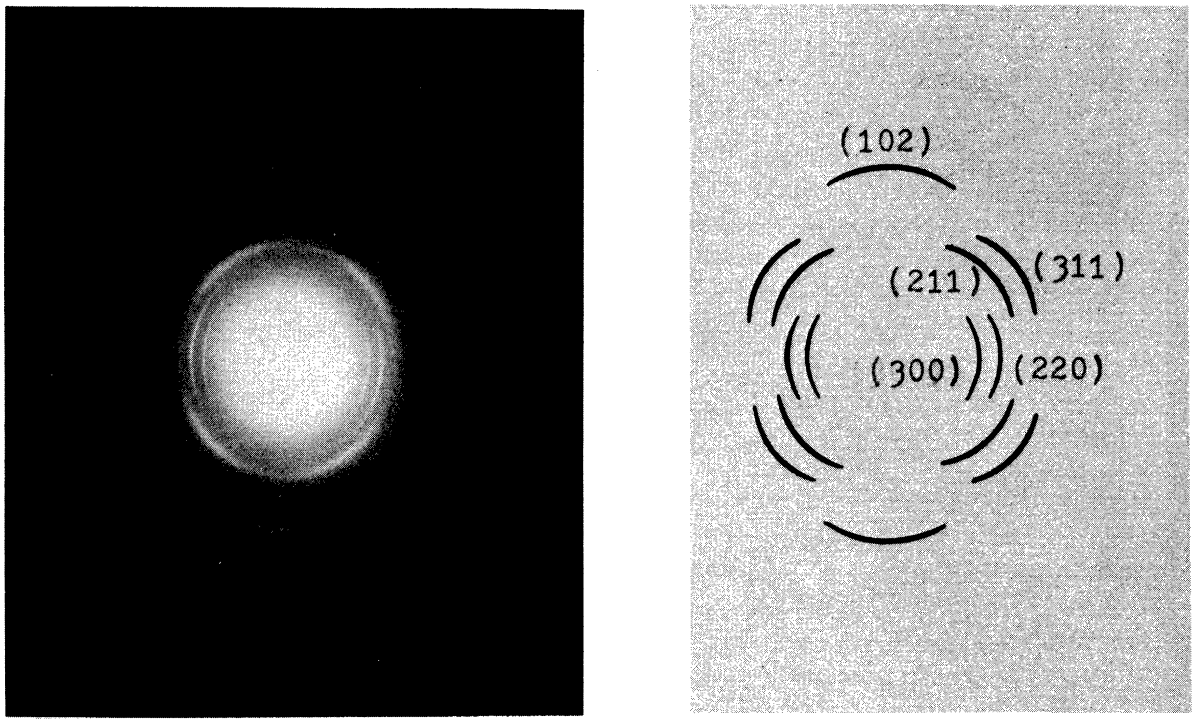

Figure 33: Isotactic polystyrene stretched 100% on mylar, annealed at 175°C for 20 minutes. Electron diffraction pattern. Sketch indicates lattice designations for crystalline reflections.

Figure 34: Isotactic polystyrene stretched 100% on mylar, annealed at 175°C for 5 minutes. Gold decorated. Stretch direction is verticle. Small arrows indicate tri-layer decorative pattern.

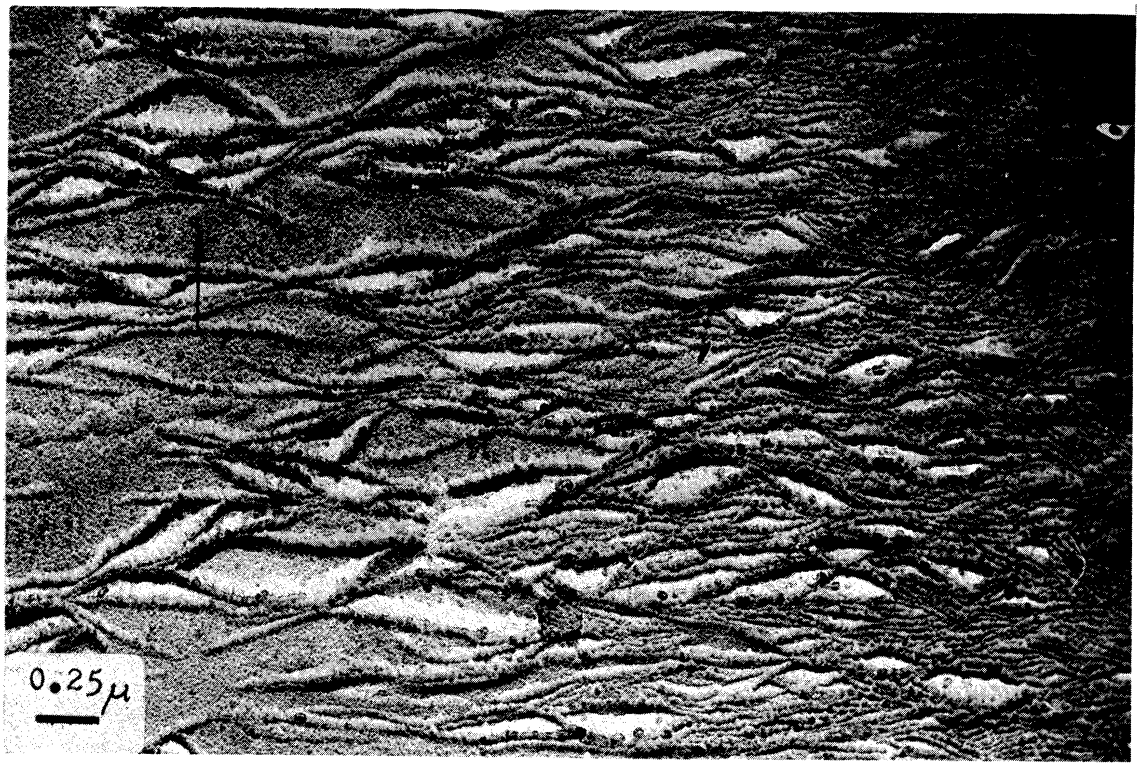

Figure 35: Isotactic polystyrene stretched 100% on mylar, annealed at 175°C for 20 minutes, amyl acetate etched for 20 seconds. Platinum shadowed at 30°. Stretch direction is verticle.

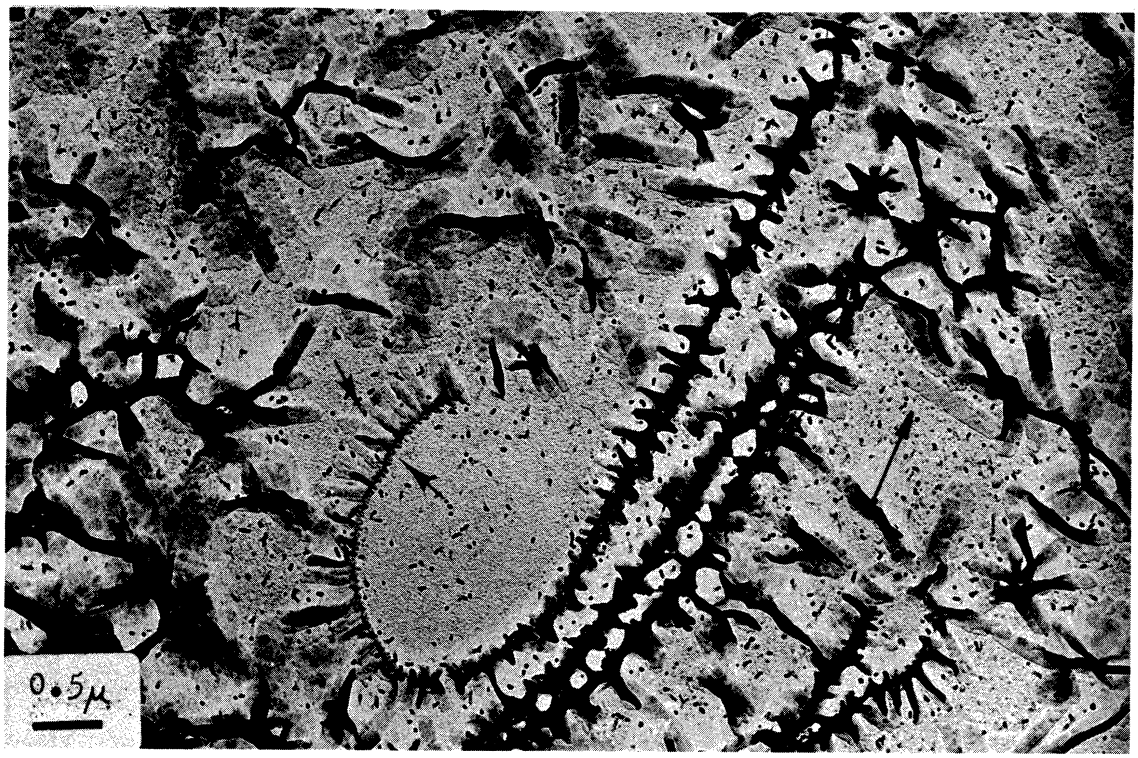

Figure 36: IPS/APS/benzophenone 10/80/10 stretched 100% on mylar, annealed at 155°C for 20 minutes, amyl acetate etched for 10 seconds. Platinum shadowed. Stretch direction indicated by large arrow.

backbone. These lamallae overgrowths measure 140 to 160Å in thickness, which is somewhat larger than the small angle x-ray long period of 135Å reported by Manley and Blais [43] for bulk unoriented isotactic polystyrene crystallized at 155°C. The ends of strongly etched shish-kebab structures often appear to curl around some 180°. The reason for this behavior is unknown, but might be related to redeposition after etching. In a separate experiment, we optically measured the comparative growth rates at 175°C for oriented lamallae in shish-kebab type structures and randomly oriented lamallae in spherulites of isotactic/atactic polystyrene molecular weight 900. The growth rates for the two structures are essentially the same in a thin film (60 μ thick) which has an indeterminate stress field.

4. Morphology of Films Stretched on Water

Unfortunately, thin films stretched on Mylar substrates are limited to extensions less than 100%. In order to investigate the effect of greater extension, up to 500%, as well as annealing temperature and time, thin films of isotactic polystyrene plasticized with a 40% concentration of benzophenone (Tg = -2°C) were stretched on a water surface, mounted on grids, and annealed at different temperatures and times, Tables VIIIA, VIIIB, VIIIC.

Unannealed films stretched up to 500% show no signs of crystallinity, either with regard to the appearance of surface structure or a discrete electron diffraction pattern. However, after annealing a film stretched 100% for 2 minutes

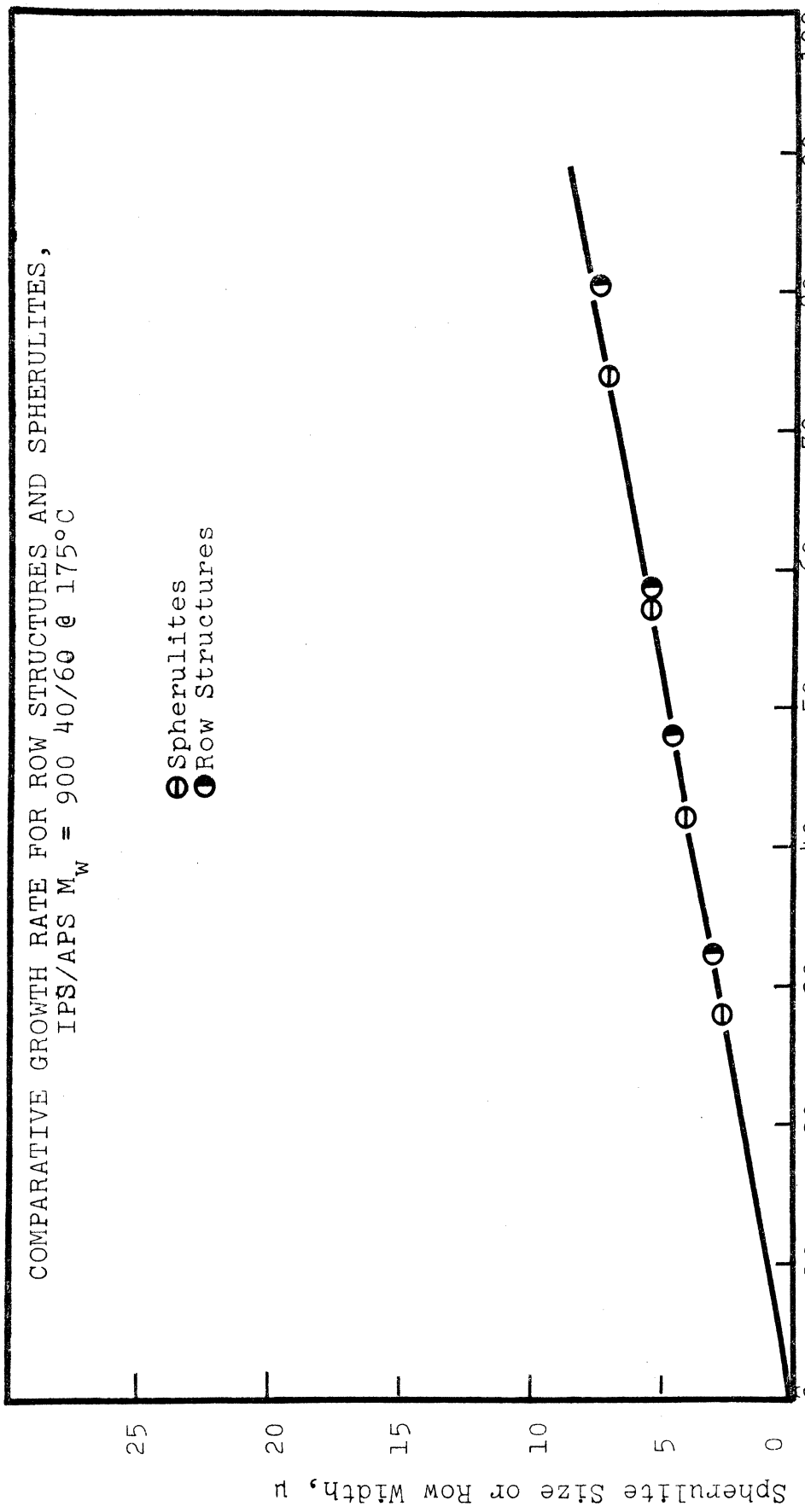
COMPARATIVE GROWTH RATE FOR ROW STRUCTURES AND SPHERULITES,
IPS/APS M_w = 900 40/60 @ 175°C
Spherulites
Row Structures
Spherulite Size or Row Width, μ
0
5
10
15
20
25
0
10
20
30
40
50
60
70
80
90
100
Time, Minutes

Figure 37

Table VIIIA

Strain Induced Crystallization of Thin Films of IPS/Benzophenone 60/40 Stretched on Water at Room Temperature, Platinum Shadowed

Ta,°C	Stretch	ta,min.	⊥ structure, (dia.) Å	∥ fibrils, (dia.) Å	Lateral, μ	Length, μ
125	200%	4	120	-	.69	.13-2.8
125	200%	5	110	-	.75	.10-2.4
125	200%	10	120	-	-	-
125	200%	20	115	-	.72	.16-2.2
125	300%	2	---	-	-	-
125	300%	2	120	-	.62	.15-2.0
125	300%	4	115	-	.69	.09-1.4
125	300%	6	120	-	.77	.12-2.3
155	100%	2	145	-	-	-
155	100%	2	140	-	-	-
155	100%	4	---	-	-	-
155	100%	6	145	-	.46	.15-2.7
155	200%	2	134	-	.66	.11-1.8
155	200%	4	137	-	.39	.09-1.8
155	200%	6	144	-	-	-
155	300%	2	137	-	.48	.07-1.4
155	300%	6	135	-	.74	-
155	300%	6	136	-	.61	.17-2.3
155	300%	8	140	-	.54	.15-2.9
155	400%	2	137	-	.34	-
155	400%	6	135	160	-	-
155	400%	30	138	-	-	-
155	400%	60	140	-	-	-
175	100%	6	148	-	-	-
175	200%	4	151	152	-	-
175	500%	2	152	145	.45	3.0+
175	500%	6	---	143	-	-
175	500%	6	---	147	-	-

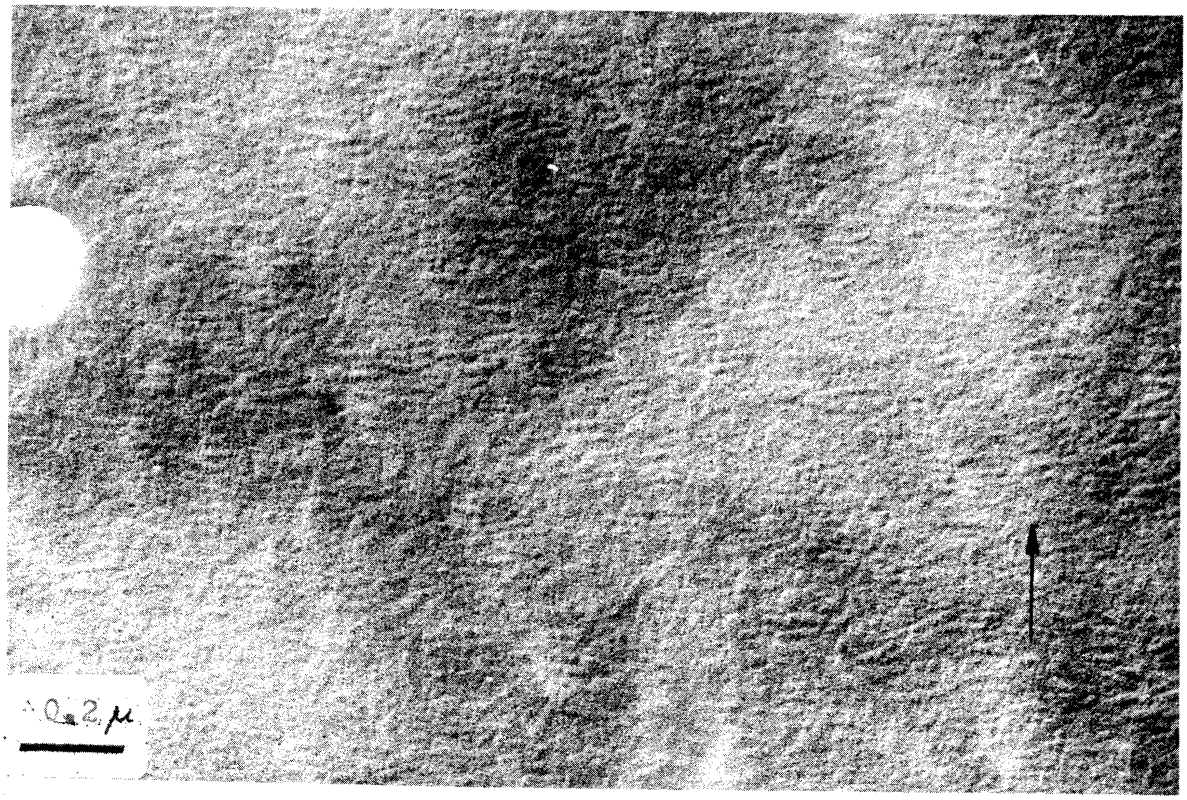

Figure 38: Isotactic polystyrene/benzophenone 60/40 stretched 100%, annealed at 155°C for 2 minutes. Platinum shadowed at 30°. Stretch direction indicated by arrow.

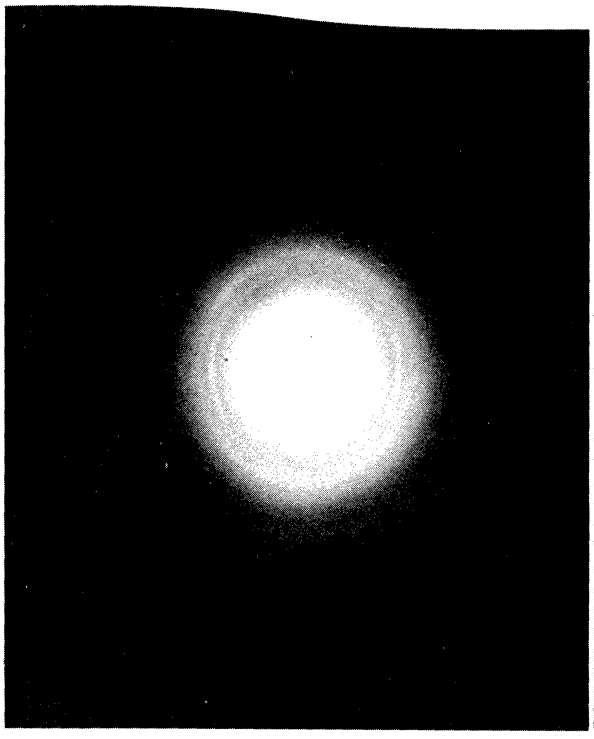

Figure 39:
Electron diffraction pattern corresponding to Figure 38.

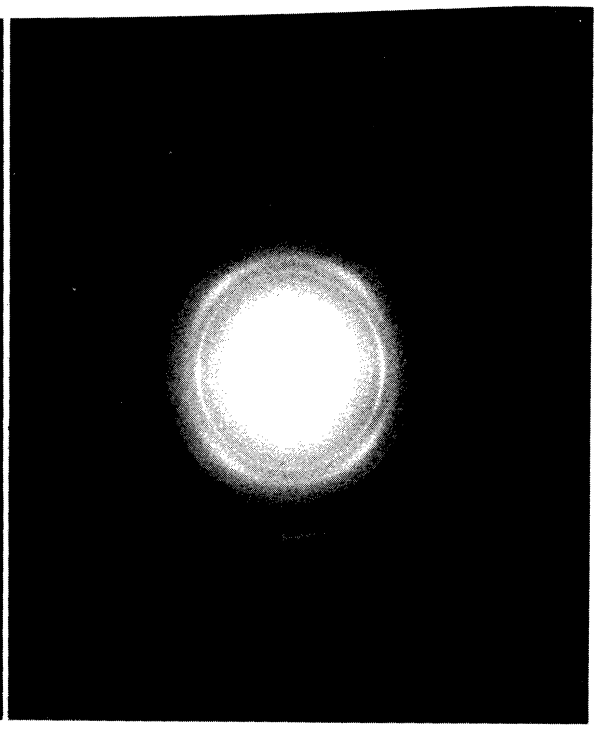

Figure 40:
Electron diffraction pattern corresponding to Figure 44.

Figure 41:
IPS/benzophenone 60/40 stretched 300%, annealed at 125°C for 4 minutes. Platinum shadowed at 30°. Stretch direction is verticle.

Figure 42:
IPS/benzophenone 60/40 stretched 300%, annealed at 125°C for 6 minutes. Platinum shadowed at 30°. Stretch direction is verticle.

Figures 32 and 38. Instead, groups of oriented fibers appear to be arranged into column structures aligned parallel to the stretch direction. After 6 minutes annealing time under these conditions, Figure 42, the crystalline surface structure is now more extensive with perpendicularly oriented fibers being arranged, not only in small groups extending from 0.1 to 0.5 μ along the stretch direction, but also along column structures extending 2 to 3 μ or more. Even small groups of fibers, however, appear to reach a more or less uniform lateral width of 0.6 to 0.8 μ (independent of annealing time) before impinging upon neighboring structures, Table VIIIA. Earlier results suggest that the spherulitic growth rate for these mixtures should be about 0.6 μ per minute, which would indicate that impingement probably occurs within the first minute of growth. Apparently the nucleation density for these films is too high to correlate the increase in lateral width with the growth rate kinetics. The measured thickness of individual fibers in films annealed at 125°C ranges from 110Å to 120Å, as shown in Figure 43. This value is in good agreement with the small angle x-ray long period of 120Å reported by Manley and Blais [43] for unoriented bulk isotactic polystyrene crystallized at 125°C.

When a film stretched 300% is annealed at 155°C for 6 minutes, the surface crystallization appears to be complete with the entire surface of the film being covered with fibrous structures, Figure 44. This surface morphology does not appear to be altered by extended annealing time up to 60

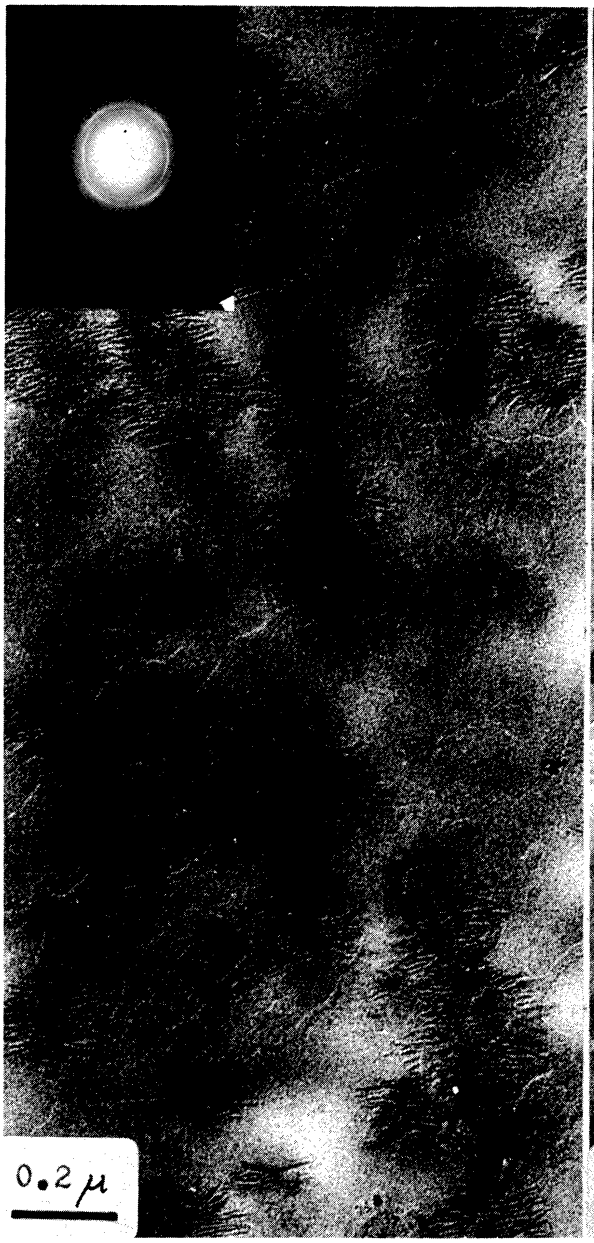

Figure 43:
IPS/benzophenone 60/40 stretched 300%, annealed at 125°C for 6 minutes. Platinum shadowed at 30°.

Figure 44:
IPS/benzophenone 60/40 stretched 300%, annealed at 155°C for 6 minutes. Platinum shadowed at 30°. Stretch direction is verticle, as indicated by electron diffraction pattern.

minutes once the crystallization is complete. Most of the surface structure in Figure 44 can be associated with extended column structures 2 to 3 μ long aligned parallel to the stretch direction, but interspersed among these columns are small independently developed groups of oriented structures, not necessarily related to any common line nucleus. The typical electron diffraction pattern corresponding to this area, Figure 40, has a sharper and more intense (102) reflection parallel to the draw direction, indicating a higher degree of molecular alignment than observed in films stretched 100%, Figure 39. A direct comparison of the surface morphology of films stretched 100% and 300% indicates that the higher elongations also tend to generate more extended column type structures than found in films stretched 100%, compare figures 32, 38 and 44.

The lateral width of oriented structures in stretched films annealed at 155°C reaches a more or less uniform value of 0.3 to 0.6 μ (independent of annealing time) before neighboring structures impinge upon one another, Table VIIIA. The measured thickness of individual fibers in films annealed at 155°C ranges from 135 to 145Å, which is in general agreement with the small angle x-ray long period of 137Å reported by Manley and Blais [43] for unoriented bulk isotactic polystyrene crystallized at 155°C. Apparently elongations ranging from 100% to 400% and annealing times up to 60 minutes have no significant influence on the resulting thickness of perpendicular structures, Table VIIIA.

Selective etching of a thin film stretched 300% and annealed at 155°C for 6 minutes reveals the underlying crystalline structure beneath the surface, Figure 45. Within the same field of view, we can see extended column structures (I), small groups or bundles of oriented fibers (II), and stacks of lamallae lying in the plane of the film (III). The extended column structures seem to be made up of long rows of perpendicularly oriented fibers which appear to have a common line nucleus. In nearby regions we can see small bundles of fibers mostly oriented perpendicular to the stretch direction, but not necessarily having a common line orientation. In between these fibrous structures, we can see stacks of lamallae lying in the plane of the film. This type of lamallar structure is commonly observed in thin films crystallized while not under stress. This result would suggest that extended column structures might be associated with areas of high stress while bundle structures, and particularly lamallae structures might correspond to low stress areas.

When thin films stretched 500% are annealed at 175°C for 2 minutes, fibril type structures aligned parallel to the stretch direction are usually observed, Figure 46. Similar fibril structures have been found by Luch [34] in highly stretched thin films of natural rubber crystallized from the melt state. The fibril structure in isotactic polystyrene (140 to 150Å in diameter) is particularly prominent at higher extensions and higher annealing temperatures (Table VIIIA). Occasionally, they are found at

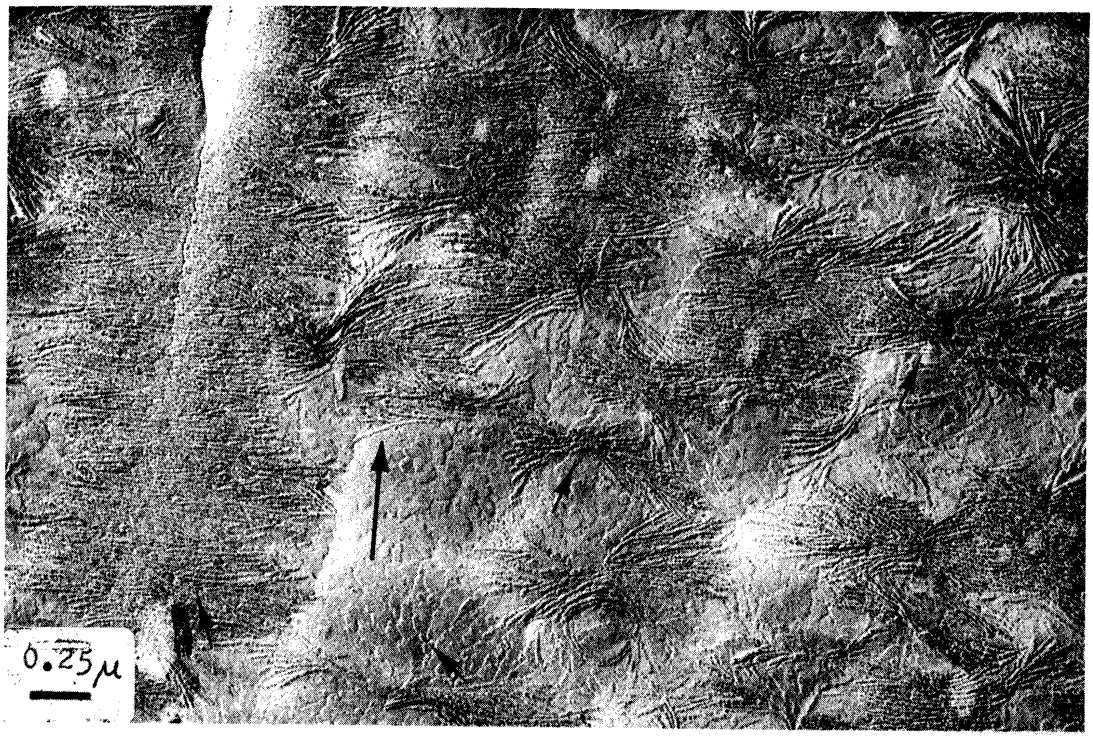

Figure 45: Isotactic polystyrene/benzophenone 60/40 stretched 300%, annealed at 155C° for 6 minutes, amyl acetate etched for 30 seconds. Platinum shadowed. Stretch direction is verticle. Small arrows indicate important structural features.

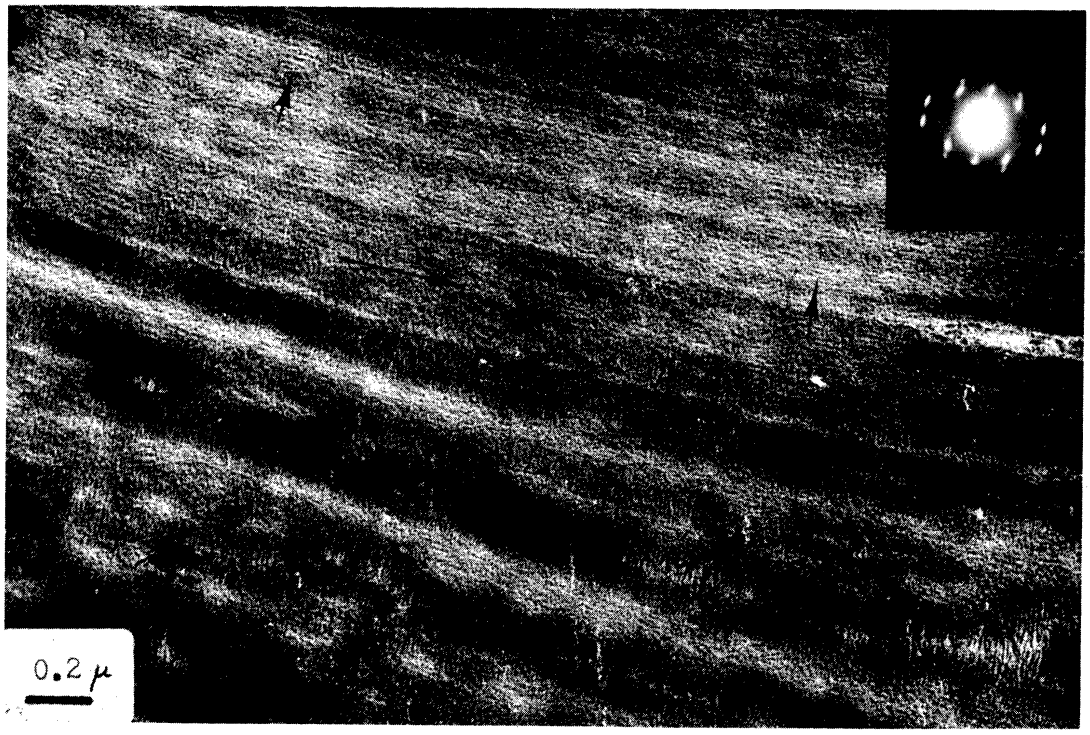

Figure 46: Isotactic polystyrene/benzophenone 60/40 stretched 500%, annealed at 175C° for 2 minutes. Platinum shadowed. Stretch direction is nearly horizontal, as indicated by electron diffraction pattern.

elongations as low as 200%, when stretched films are crystallized at 175°C, Figure 47. Otherwise, the annealing temperature apparently has little discernible effect on the type of morphology (other than fiber thickness) observed in annealed films having the same elongation prior to crystallization.

Higher magnifications of Figure 46 shows that fibril structures are generally discontinuous on the surface for distances greater than 0.5μ, Figure 48. It should also be noted that along the border of the extended column structures, the parallel fibrils appear to closely intermingle with the perpendicularly oriented fibers. The typical electron diffraction pattern corresponding to Figure 46 shows a splitting of the very intense (102) reflection, indicating a very high degree of molecular alignment parallel to the stretch direction, Figure 49. The angle between the (102) reflection and the C axis measures 9°, in good agreement with the angular relationship found by Buchanan and Miller [9] in stretched bulk films of isotactic polystyrene. The spacing of the layer lines along the stretch direction equals 6.54Å, which agrees with the C axis unit cell parameter, as determined by Natta [44].

Gold decoration of a thin film stretched 500% and annealed at 155°C for 4 minutes also indicates parallel fibril structures, as suggested by the vacated areas aligned parallel to the stretch direction (see arrows), Figure 50. The vacated areas vary in length from 0.07 to 0.5 μ parallel to the stretch direction and have widths ranging from 70 to

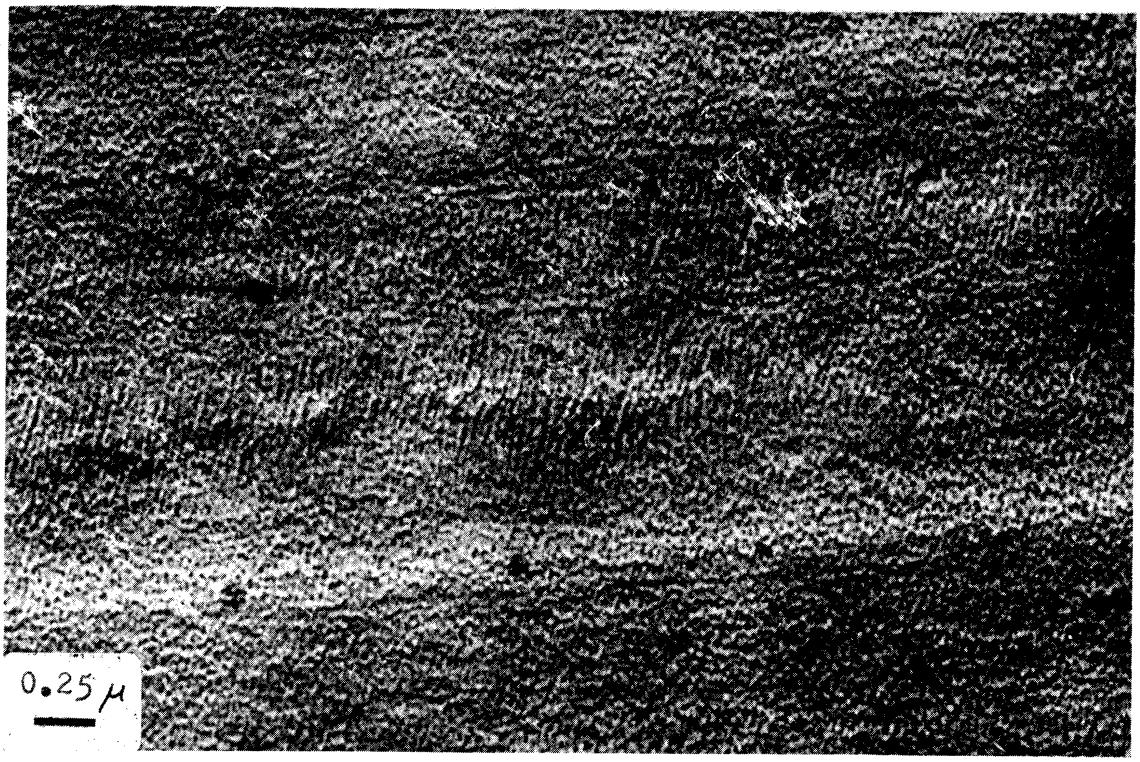

Figure 47: Isotactic polystyrene/benzophenone 60/40 stretched 200%, annealed at 175°C for 4 minutes. Platinum shadowed at 30°. Stretch direction is indicated by large arrow.

Figure 48: Isotactic polystyrene/benzophenone 60/40 stretched 500%, annealed at 175°C for 2 minutes. Platinum shadowed at 30°. Stretch direction is horizontal.

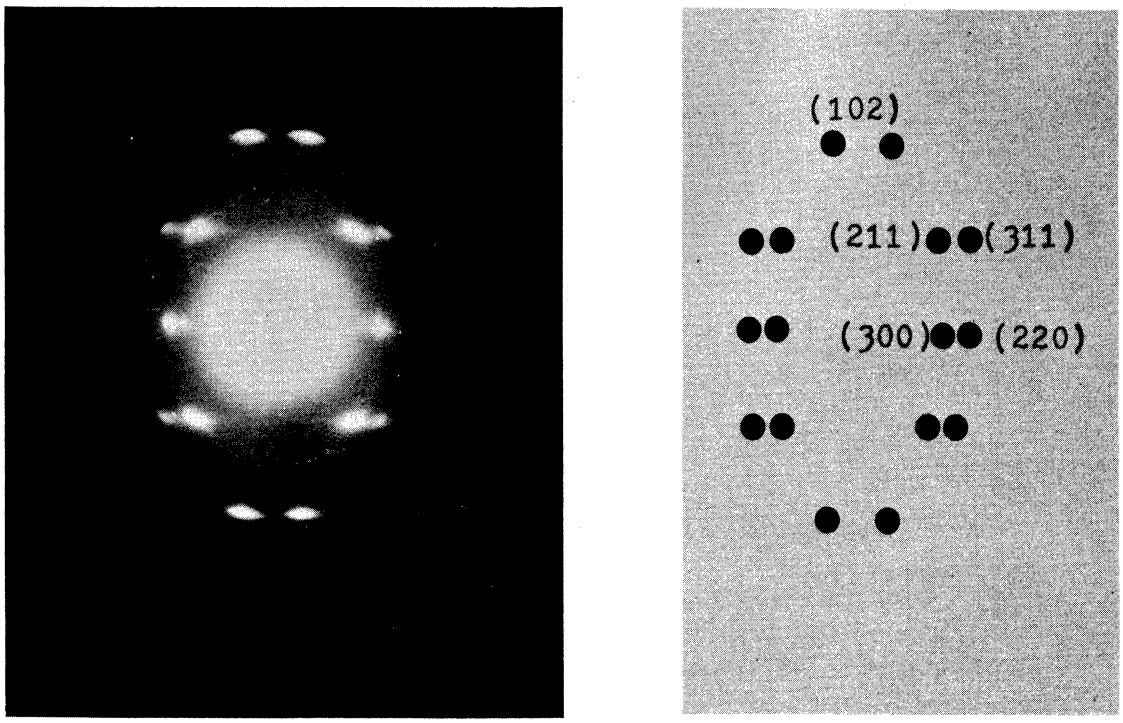

Figure 49: Isotactic polystyrene/benzophenone 60/40 stretched 500%, annealed at 155C for 4 minutes. Electron diffraction pattern. Sketch shows lattice designations for crystalline reflections.

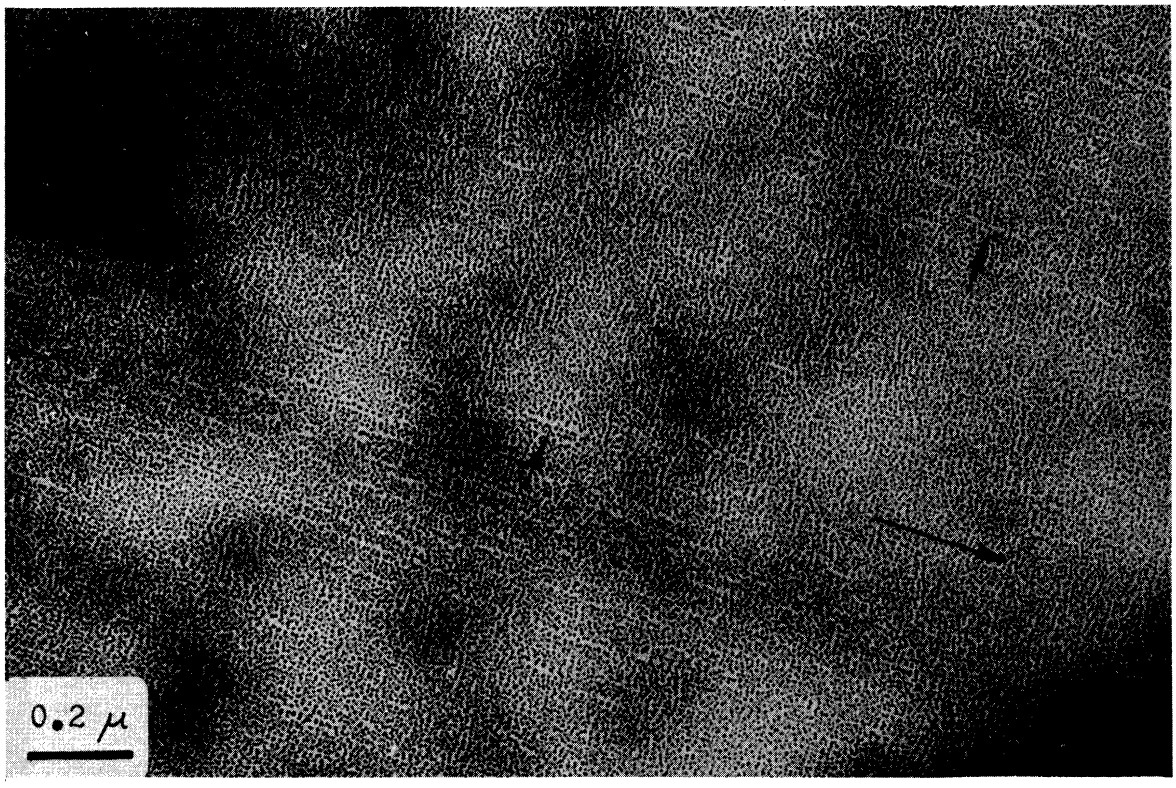

Figure 50: Isotactic polystyrene/benzophenone 60/40 stretched 500%, annealed at 155C for 4 minutes. Gold decorated. Stretch direction is indicated by large arrow.

100Å between parallel lines of gold particles. Careful examination of Figure 50 will also show that the parallel fibrils and perpendicular fibers (indicated by vacated areas perpendicular to the stretch direction), although growing in separate regions, closely intermingle on the border separating them. Selective etching of a thin film stretched 400% and annealed at 155°C for 6 minutes reveals the internal structure of the extended columns, as illustrated in Figures 51 and 52. Along the backbone of the extended column structures we can see common line nuclei measuring 100 to 110Å in diameter (see arrows). The lamallar overgrowths attached perpendicularly to the line nuclei measure 110 to 120Å in width, somewhat less than unetched row structures prepared under similar conditions. Apparently, in this case, the etching solvent also attacks the regions in between the lamallar overgrowths.

Figures 53 and 54 show a bright field-dark field pair of micrographs from the same region of a thin film stretched 500% and crystallized at 155°C for 4 minutes. The dark field uses the (102) reflection which should show the areas of the crystalline structure in which the molecules are most strongly aligned in the stretch direction. Although the resolution of the dark field micrograph is marginal, it is still possible to distinguish individual diffracting areas, indicated by the dark spots in the negative print, some 150 to 200Å in diameter. The individual diffracting regions do not appear to be elongated in the stretch direction, although in some cases they appear to align (see arrow A). In the corresponding bright field area (Figure 53)

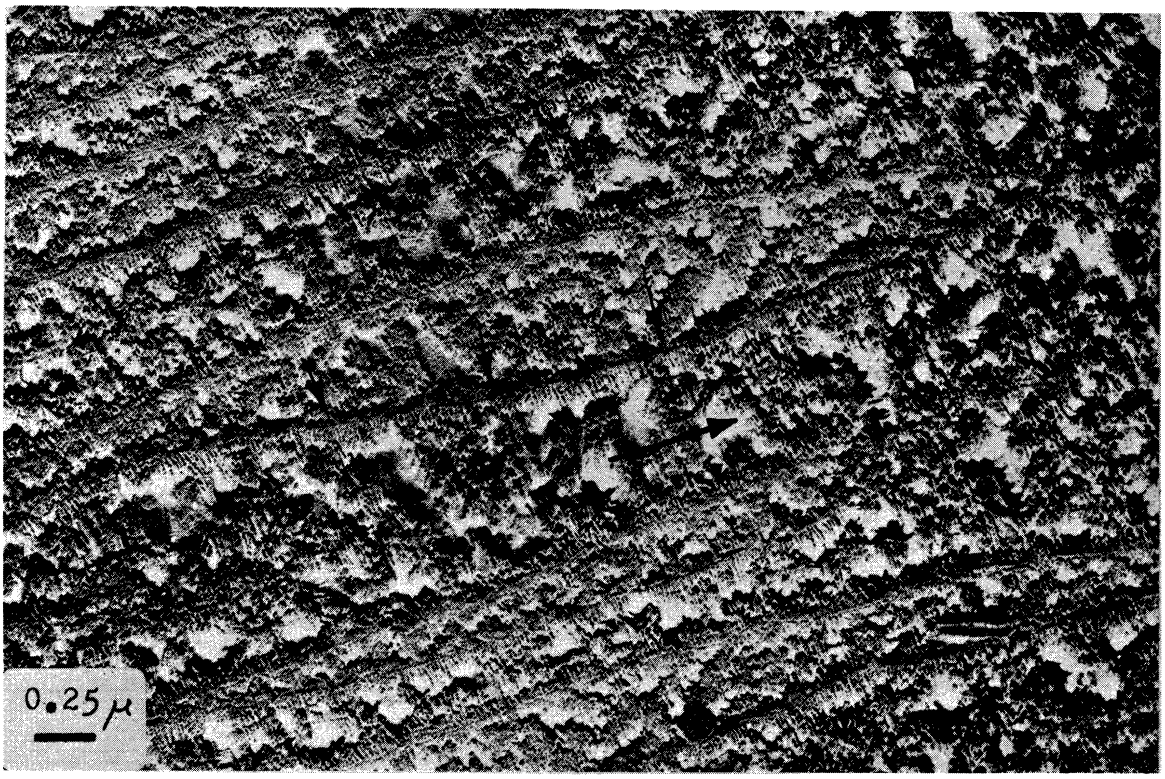

Figure 51: Isotactic polystyrene/benzophenone 60/40 stretched 400%, annealed at 155°C for 6 minutes, amyl acetate etched for 30 seconds. Platinum shadowed. Stretch direction is indicated by large arrow.

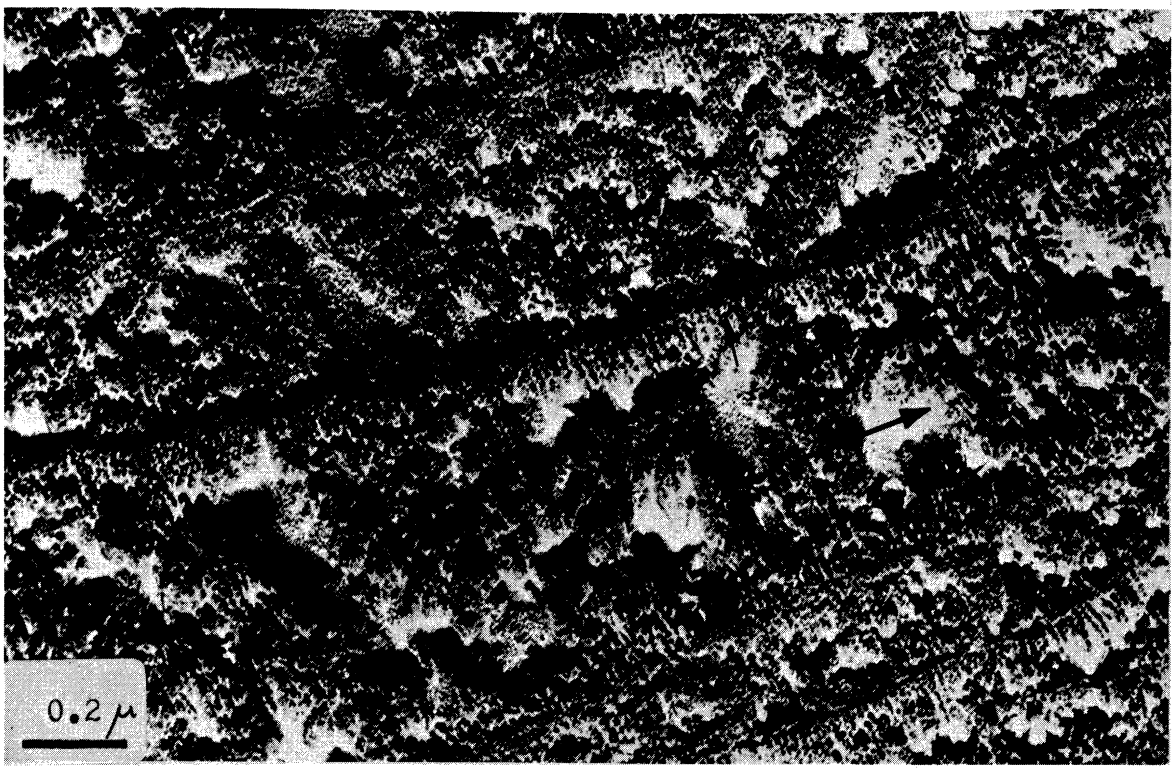

Figure 52: Isotactic polystyrene/benzophenone 60/40 stretched 400%, annealed at 155°C for 6 minutes, amyl acetate etched for 30 seconds. Platinum shadowed. Stretch direction is indicated by large arrow.

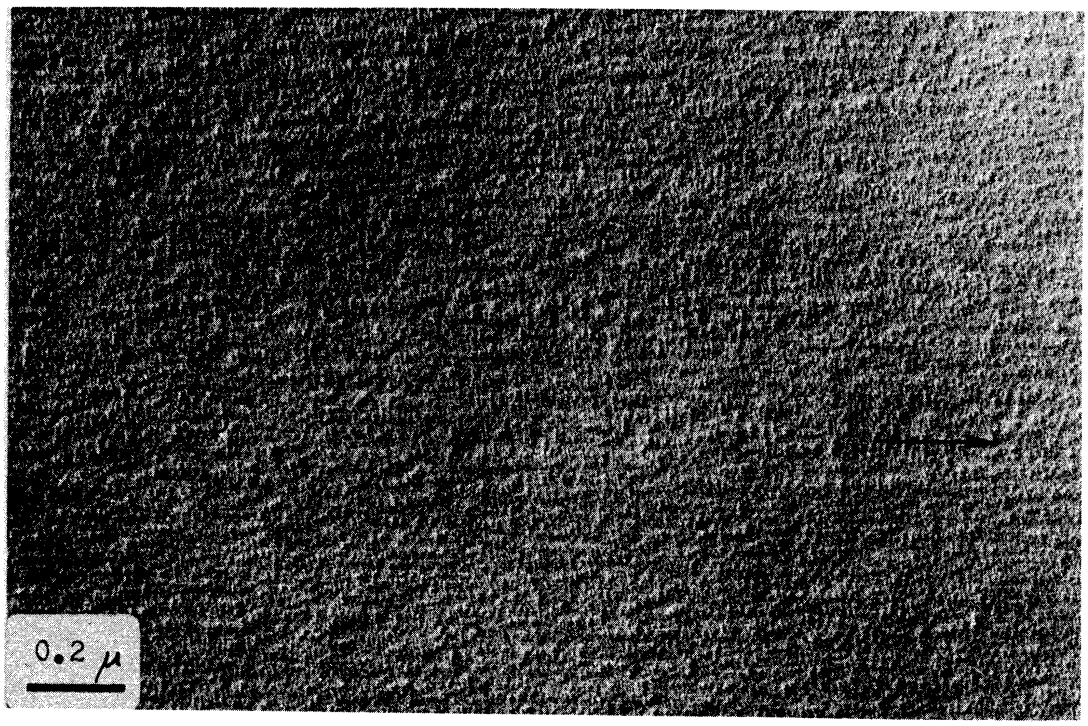

Figure 53: Isotactic polystyrene/benzophenone 60/40 stretched 500%, annealed at 155°C for 6 minutes. Platinum shadowed at 30°. Stretch direction is horizontal.

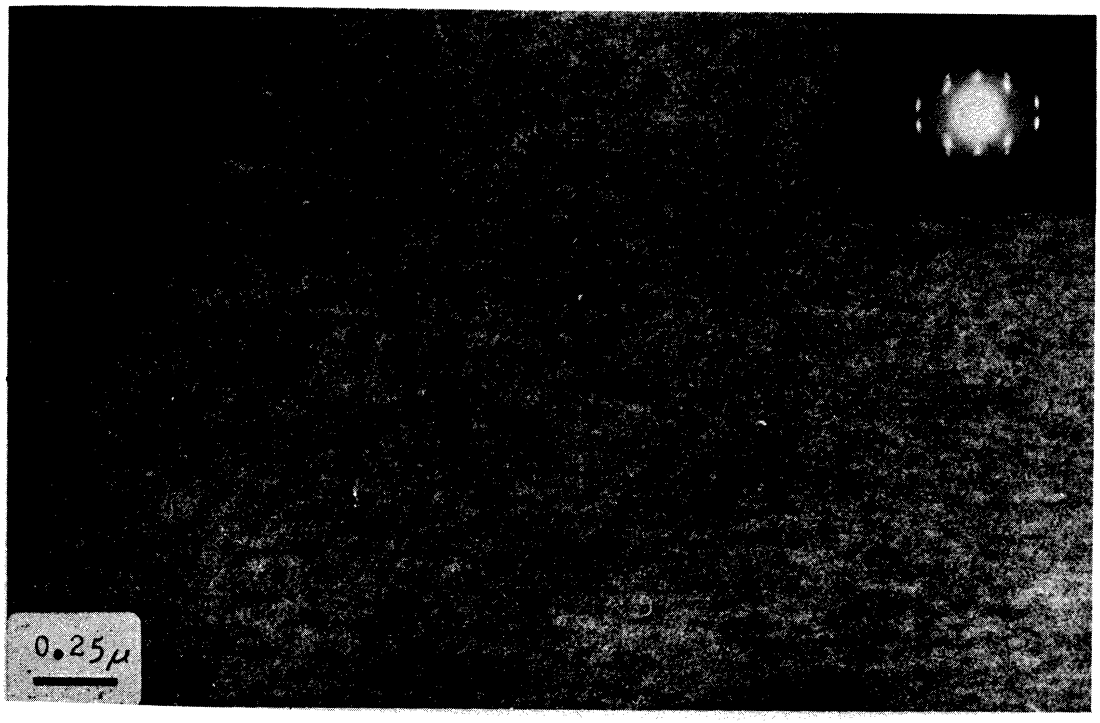

Figure 54: Isotactic polystyrene/benzophenone 60/40 stretched 500%, annealed at 155°C for 6 minutes. Platinum shadowed. Dark field of figure 53 using (102) reflection. Stretch direction is horizontal, as indicated by electron diffraction pattern.

indistinct fibril structures aligned parallel to the stretch direction measure 150Å in width. Theoretical calculations based on the line broadening of the (102) reflection by Buchanan and Miller [9] indicate a crystallite size ranging from 85-100Å, considerably smaller than the diffracting areas observed in the dark field print. Perhaps the discrepancy here is partially due to the relatively poor resolution obtained by the apperture technique in dark field microscopy. In any case, it is apparent that the fibril structures have segmented diffracting regions, indicating that the molecular structure is predominately folded chain rather than extended chain. This result is in agreement with the findings of Yeh and Geil [61] who observed 75Å ball-like diffracting regions, but no extended chain nuclei, in strain crystallized PET from the glassy state.

D. Discussion

1. Characterization of Structure

Bassette [3] and Spit [55] both indicated that gold decoration of spherulitic structure in crystallized polymer films reveals a layered decorative effect which appears to be sensitive to crystalline fibers. In addition, Spit [55] demonstrates in crystallized thin films of nylon 6, that gold particles and phosphotungstic acid stain seem to be sensitive to one and the same region, presumably the amorphous layer adjacent to the crystalline fiber.

In the present study, gold decoration of dispersed

crystalline fibers of isotactic polystyrene reveals a tri-layer decorative pattern which consists of two lines of gold particles on either side of a completely vacated region, Figure 27. In the region near the hole where the fibers impinge on one another the gold particles appear to lie on top of the fibers. Experiments involving both platinum shadowing and gold decoration of opposite sides of the same thin film suggest that the decorative pattern is sensitive to the crystalline fibers, but not necessarily the raised edges of these fibers. Other results show that the decorative pattern coincides with the most dense regions in a crystallized film, the crystalline fibers oriented edge on to the plane of the film. Finally, we found that the width of the vacated region, 60Å, is apparently insensitive to crystallization temperature over a range of temperatures where the crystalline fibers increase in width from 127 to 210Å. Although these results are not conclusive, it appears that the tri-layer decorative pattern may in some instances be sensitive to the surface structure of the fibers, perhaps even along the crystalline core, as indicated by these experiments and data in Table VII.

In all strain induced crystallization experiments, the molecular orientation, as determined by electron diffraction, is found to be more or less parallel to the stretch direction, while the most common morphological structure seems to be arranged perpendicular to the stretch direction. The folded chain model reconciles the orientation of these two structural features by specifying that molecular chains, approximately 24,000Å long, must have chain folds in order

to fit into crystalline fibers ranging from 110Å to 160Å thick. Other models such as the fringed micelle, in which most chains tend to extend from one fiber to the next with few fold backs, do not apply in this case because selective etching experiments have clearly established the separate lamallar identity of each perpendicular fiber, Figure 36.

If the molecular structure in these fibers is somehow different than the folded chain structure normally found in lamallar ribbons, then the resulting crystalline growth rates for row structures and spherulites should reflect this difference, since the growth rates are controlled by the rate of secondary nucleation at the growing interface. Figure 37 shows that the growth rates for row structures and spherulites are equal under the same conditions, thus implying that their molecular structures are also identical. We should point out that in this case we may be comparing epitaxial growth in row structures to normal spherulitic growth. Growth rates for strain induced crystallization of polymers are seldom obtainable. In any case, all of these results suggest that the crystalline fibers aligned perpendicular to the stretch direction in strain crystallized films have a folded chain molecular structure.

The microstructures generated as a result of strain induced crystallization may be separated into three loosely defined categories. Type I structure is made up of small groups or bundles of fibers growing more or less perpendicular to the orientation direction, but developing independently of any common extended line nuclei, Figure 45. Such

structures are most commonly found in films stretched to low elongations (100%), but also are found in films at higher elongations (200% to 300%). The electron diffraction pattern corresponding to this structure indicates a preferential molecular alignment more or less parallel to the stretch direction. Extended column type structures found in Figures 44 and 46 are designated as being of type II. This structure appears to be made up of rows of crystalline fibers growing perpendicular to some type of common line nucleus, Figures 51 and 52. Column structures are usually observed at elongations greater than 200%, while the corresponding electron diffraction pattern indicates a somewhat higher degree of molecular alignment than found in type I structure.

Fibril structures aligned parallel to the stretch direction are designated as type III structures. These fibrils, 140 to 150Å wide and extending 0.07 to 0.5 μ in the stretch direction, are generated at high elongations (400 to 500%) and high annealing temperatures, Table VIII. The electron diffraction corresponding to these structures suggests a high degree of molecular alignment parallel to the stretch direction, while dark field studies using the (102) reflection indicate that the internal structure of these fibrils is segmented. This latter result suggests that the molecular conformation of these fibrils is predominately folded chain rather than extended chain. Gold decoration and selective etching experiments indicate that type III fibrils often occur in regions closely adjacent to type II structures.

2. Mechanism of Strain Induced Crystallization

Keller [49] has proposed that the mechanism of strain induced crystallization basically involves the epitaxial growth of folded chain fibers on an extended chain nucleus backbone as depicted in the following diagram. Experimental

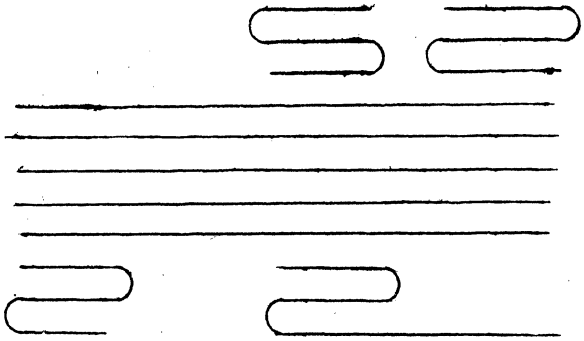

Row Structures

evidence indicating the existence of these proposed nuclei was recently presented by Wikjord and Manley [59], who observed that filamentary ribbon structures remain after the selective dissolution of oxidated polyethylene row structures produced by shear induced crystallization from dilute xylene solutions. Differential thermal analysis and selective oxidation behavior suggests that the ribbon structures observed in polyethylene have a dual molecular conformation of both folded and extended chains. Wikjord and Manley also established that the folded chain character of these filamentary ribbons increases as the crystallization temperature is lowered. Fibril type structures have also been observed in other studies by Andrews [1] and Luch [34], but there is no clear evidence relating these structures to the extended chain nuclei proposed by Keller.

In the present study, fibril (type III) structures,

aligned parallel to the stretch direction, were observed in highly stretched thin films of isotactic polystyrene. Dark field studies using the (102) reflection indicate that the internal structure of these fibrils is segmental, suggesting a predominately fold chain molecular conformation.

In the study on strain induced crystallization of isotactic polystyrene, the degree of supercooling for fibril structures grown at 155°C was approximately $\Delta T = 35°C$, considerably higher than the supercooling used by Wikjord and Manley [59] for shear induced crystallization of polyethylene row structures from dilute xylene solution. These results suggest that a folded chain molecular conformation for fibril structures grown from the amorphous rubbery state is not inconsistent with the experimental evidence on solution grown row structures by Wikjord and Manley.

We also observed a filamentary backbone in mildly etched column (type II) structures of strain crystallized isotactic polystyrene, Figures 51 and 52. The dimensions and the orientation of this backbone structure suggest that it might be the line nucleus responsible for the generation of extended column structures, a mechanism proposed by Keller [49]. However, there is no evidence at the present time indicating what type of internal structure the filamentary backbone might have and no evidence indicating the mechanism for the growth of row structures along the backbone.

E. Conclusions

1. The dimensions of the gold tri-layer decorative pattern for crystalline fibers of isotactic polystyrene appear to be insensitive to crystallization temperature over the range of temperatures where the fibers increase in width from 127 to 210Å. This result suggests that gold decoration may be sensitive to the surface structure of these fibers, perhaps even the crystalline core region.

2. Crystalline fibers aligned perpendicular to the stretch direction in strain crystallized thin films appear to have a folded chain molecular structure.

3. Fibril type structures 140 to 150Å wide and aligned parallel to the stretch direction are found in thin films of isotactic polystyrene/benzophenone 60/40 stretched 400 to 500% and annealed at 175°C from the rubbery amorphous state. The electron diffraction pattern corresponding to these films indicates a high degree of molecular alignment parallel to the stretch direction while dark field studies using the (102) reflection indicate that the internal structure of these fibrils is segmented. This latter result suggests that the molecular conformation in the fibrils is predominately folded rather than extended chain.

4. In thin films stretched to lower elongations (300%) prior to crystallization from the glassy amorphous state, extended column type structures are often observed. These column structures are made up of rows of crystalline fibers 120 to 160Å thick, growing perpendicular to a common

filamentary backbone.

5. In thin films strain crystallized at very low elongations (100%), small groups or bundles of fibers aligned more or less perpendicular to the orientation direction appear to develop independently of any common line nucleus.

CHAPTER IV

CRYSTALLIZATION OF ISOTACTIC POLYSTYRENE/PLASTICIZER BLENDS

A. Introduction

Spherulitic crystallization from mixtures of crystallizable polymer and low molecular weight plasticizer has received very limited attention, compared to the numerous studies on spherulitic crystallization of homopolymers. Mixtures of polymer and low molecular weight plasticizer are often commercially important systems because the mechanical properties of some polymers can be favorably altered by the addition of plasticizer [45]. Therefore, it was decided to examine the influence of di-methyl and di-decyl phthalate, as well as benzophenone on the spherulitic crystallization kinetics of isotactic polystyrene and to compare these results to those obtained in Chapter III. We also determined the threshold crystallization temperatures for mixtures of isotactic/atactic polystyrene as well as isotactic polystyrene/benzophenone. The threshold crystallization temperature (T_T) is the lowest temperature at which the onset of crystallization can be detected. This temperature gives us a relative measure of the magnitude of the viscous transport term in the theoretical growth rate equation.

styrene butadiene rubber. In the case of polisobutylene, they observed that ultra-sonic treatment, while reducing the molecular weight of the material, does not appreciably affect the size of the resulting microstructure.

In closely related work, Yeh and Geil [62] observed a 75Å nodular structure in bulk and thin films of amorphous poly(ethylene terephthalate), PET. They found that upon drawing thin films some 500%, these nodular structures tend to align approximately 50° to the draw direction. Careful dark field microscopy using the inner amorphous ring suggests that these structures have a paracrystalline-type order. Crystallization at temperatures near Tg occurs by movement, aggregation, and alignment of these structures into spherical patches which then seem to form tree-like branches. In later stages of development, small bundles of spherulitic fibers in which the nodules are aligned perpendicular to the fiber axis are commonly observed. The small angle x-ray long period is found to increase as expected with annealing temperature, suggesting a regularization of the irregular folds originally present in the ball-like nodules.

Frank and Stuart [16] reported a 100Å nodular microstructure in bulk amorphous polycarbonate from bisphenol A. This structure, unobservable under normal conditions, was detected by ion etching of bulk films which had been annealed just below Tg. They were able to correlate the presence of this structure with a slight change in the temperature dependence of the mechanical loss angle in amorphous polycarbonate.

Similar 125Å nodular structures have been observed in thin films of polycarbonate from bisphenol A by Carr and Geil [12]. They noted that upon annealing just below Tg, these nodules enlarge to 250Å. Tensile deformation of a cast thin film causes the nodules to break down into 60Å units which align perpendicular to the stretch direction. Annealing of the film prior to deformation, however, causes these nodules to align along shear lines. In an extension of this work, Siegman and Geil [53] examined the crystallization of polycarbonate A from the glassy amorphous state. They found that crystallization near Tg occurs by aggregation of the enlarged nodules into irregularly shaped lamallae single crystals which, in later stages, develop fibril type structures characteristic of spherulitic crystallization. They indicate that subsequent growth of these fibrils occurs by interfacial addition of nodules.

In the study of a plasticized system, Gezovich and Geil [18] observed a 200Å nodular structure in mixtures of poly(vinyl chloride) and di-octyl phthalate, by means of brittle fracturing at liquid nitrogen temperatures followed by ion etching under vacuum. Large structures on the order of 0.1 μ and 5 to 10 μ were observed when chlorinated paraffin was used as the plasticizer. The small angle x-ray long period was found to increase with increasing plasticizer concentration, suggesting that the structures were becoming separated by a greater distance as the plasticizer content increased.

B. Experimental

Solutions containing 0.2% polystyrene in appropriate solvent (benzene, dichlorobenzene, or cyclohexanone) were made by dissolving a weighed amount of either isotactic or atactic polystyrene in a measured volume of boiling solvent. Once the solution had cooled to room temperature, amorphous thin films 400Å to 600Å thick, as judged by light reflection, were cast onto glass slides coated with sodium hexa-meta phosphate, a water soluble releasing agent. Annealing and crystallization experiments were carried out on some of these films in a temperature controlled (± 2°C) hot air oven at temperatures up to 140°C for periods of time ranging from 1 to 60 minutes. These thin films were then floated off onto a water surface and picked up on copper grids for subsequent study in the electron microscope. Most films were either shadowed with platinum or decorated with gold. However, a number of unshadowed films were also examined.

Occasionally, crystallized thin films of isotactic polystyrene were selectively etched in room temperature amyl acetate. The etching procedure, similar to the one used by Padden [46], involves dipping the film covered glass slide into a bath of etching solvent for times ranging from 10 to 120 seconds, draining the slide, and allowing it to air dry. The etched films were then shadowed with platinum, coated with about 200Å of carbon, and floated off onto a water surface to be picked up on specimen grids.

Oriented thin films of amorphous polystyrene were

prepared by stretching on Mylar substrate in the same manner as discussed in Chapter V. These films were either shadowed with platinum or decorated with gold and then stripped off the Mylar with a 10% aqueous solution of poly(acrylic acid).

Bulk samples of atactic polystyrene were examined by surface replication and ultra-microtoming. Pellets of commercial atactic polystyrene were melted on a glass slide and annealed at 190°C, 205°C, and 220°C in a hot air oven for 30 minutes before quenching in either a -70°C mixture of ethanol-dry ice, ice water, or the ambient atmosphere. One stage surface replicas of these quenched bulk samples were made by shadowing the surface with platinum and stripping the replica with a 10% aqueous solution of poly (acrylic acid). The replica was then coated with about 200Å of carbon backing and floated onto a water surface in order to redissolve the poly(acrylic acid). A Cambridge Ultramicrotome device was used to shave ultra thin 700-900Å sections from the same commercial polystyrene which were then shadowed with platinum and examined in the electron microscope. Specimen preparation and microtoming techniques are fully discussed in Sjostrand [54] and will not be dealt with here.

C. Results

1. Amorphous Structure

An unshadowed 20Å grainy microstructure was observed in all of the thin films of amorphous polystyrene examined in a JEM-6A electron microscope. The average diameters and center to center distance between these structures for a

variety of conditions is recorded in Table XII. According to these results, none of the major conditions studied (variation of molecular weight, solvent, annealing temperature) has a significant influence on the size of the observed microstructure. When similar unshadowed thin films were examined in a Phillips EM300 electron microscope with a much higher resolution, smaller structures on the order of 7Å to 8Å were observed in atactic polystyrene. Because of the difficulties involved in the interpretation of phase contrast images and the need for a high resolution microscope (which was not always available) these structures were not investigated further.

When amorphous thin films of isotactic polystyrene were shadowed with platinum, sharp 30Å grainy microstructures were observed, Figure 55. The average diameter and the center to center distance between these structures in shadowed amorphous thin of several different polymers prepared under different conditions is recorded in Table XIII. It appears, based on these results, that the size of the platinum shadowed microstructure is essentially invariant with respect to the conditions examined.

Orientation of amorphous thin films should cause the resulting microstructure to align into some type of preferred orientation. Accordingly, thin films of polystyrene were stretched 50 to 100% on a Mylar substrate and either shadowed with platinum or decorated with gold, Figures 56 and 57. Because of the effect of residual astigmatism at high magnification (30,000) on the alignment

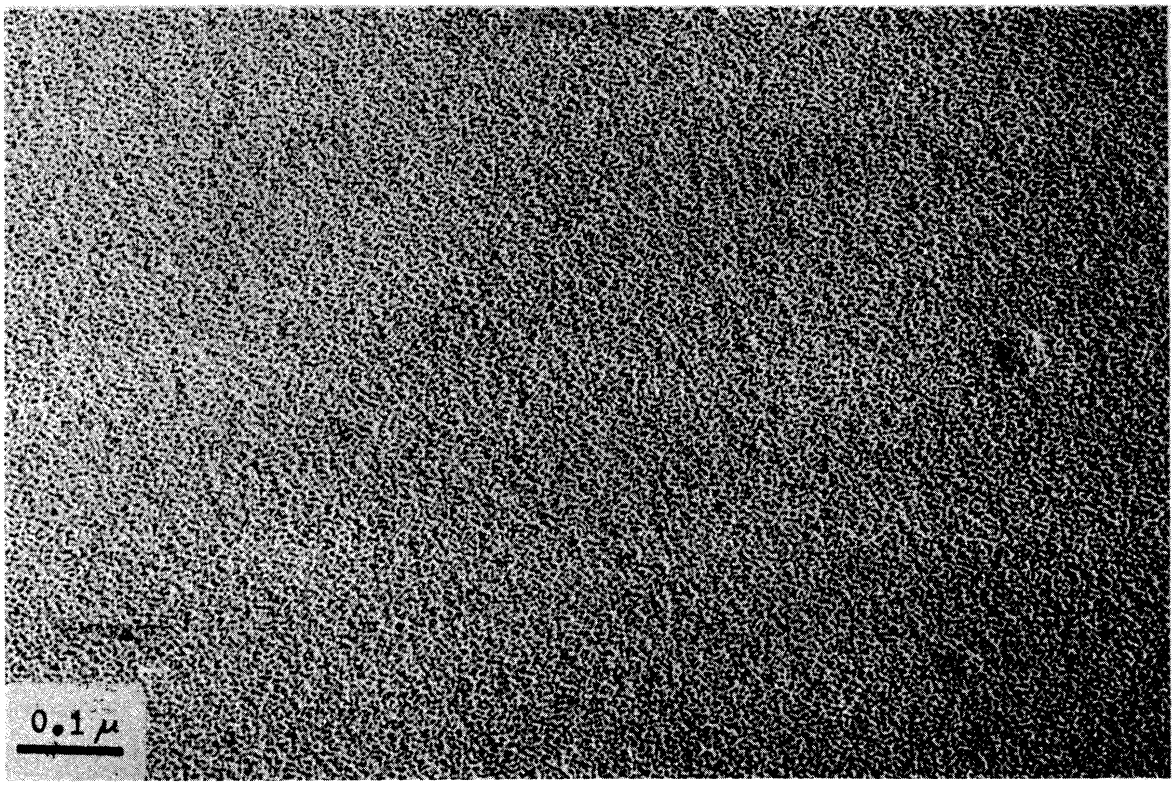

Figure 55: Isotactic polystyrene M_w=1,200,000 amorphous film cast from dichlorobenzene solution. Platinum shadowed at 30°.

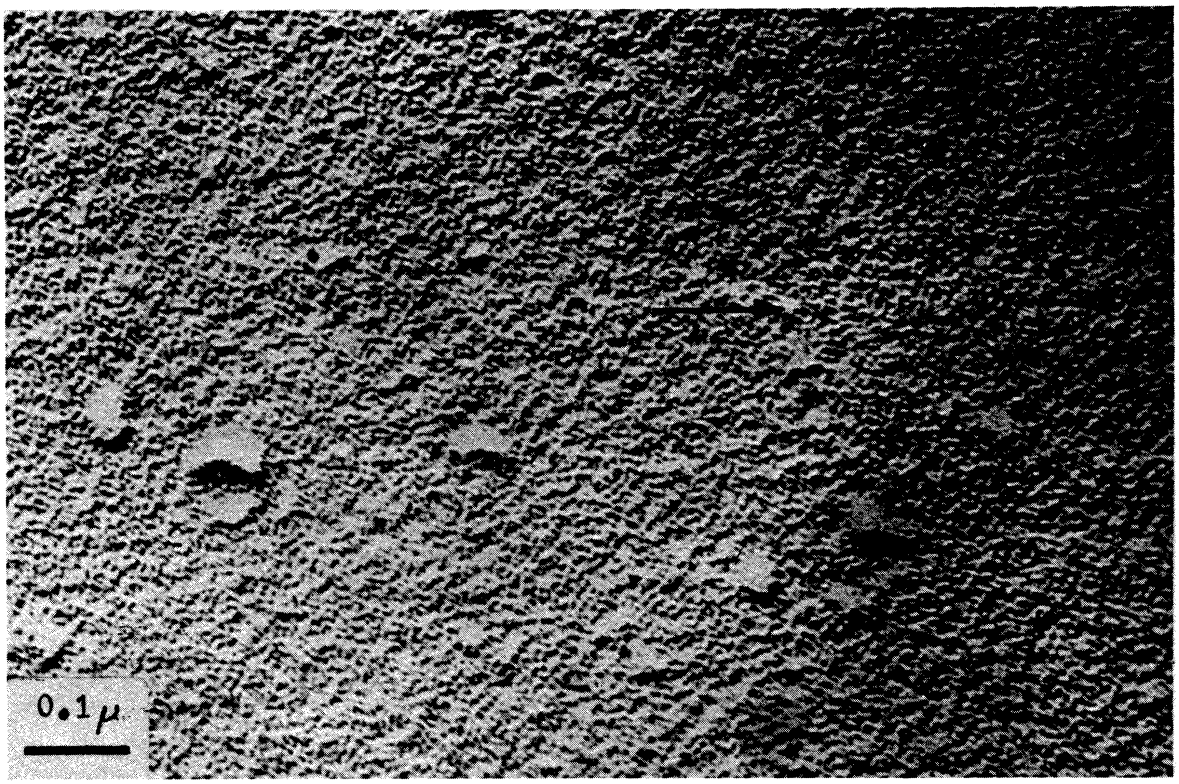

Figure 56: Atactic polystyrene M_w=1,800,000 stretched 100% on mylar. Platinum shadowed at 30°. Stretch direction is horizontal.

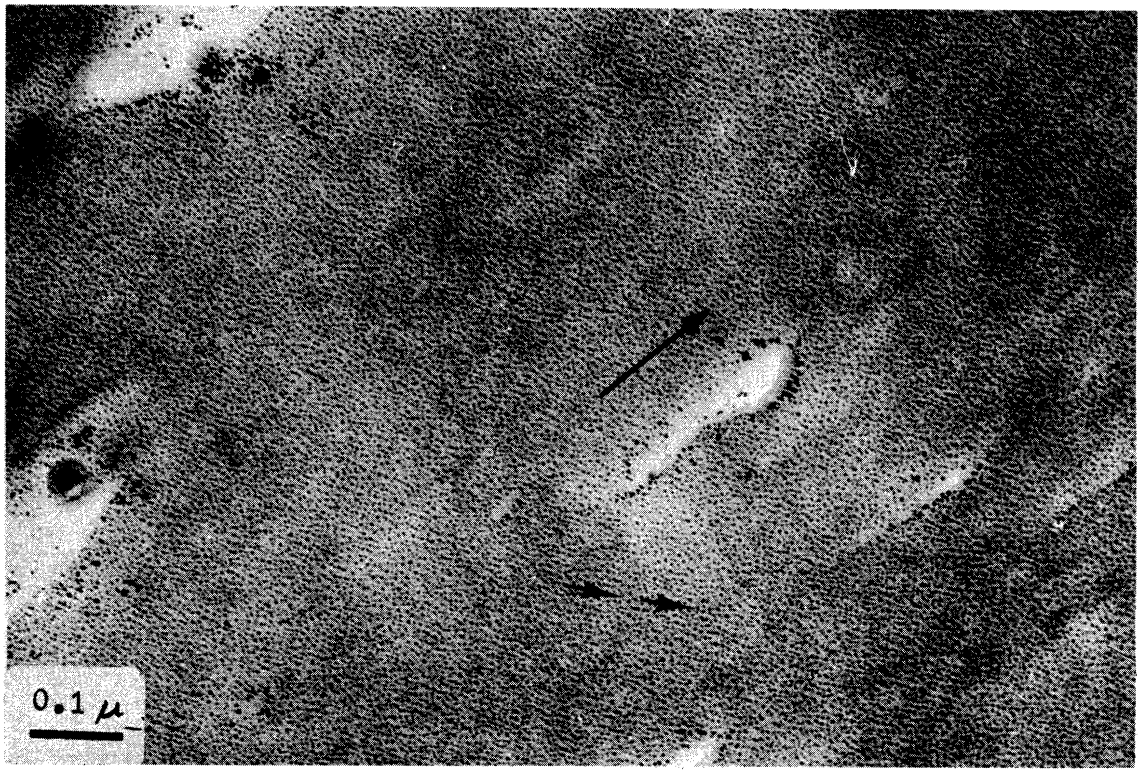

Figure 57: Atactic polystyrene M_w=1,800,000 stretched 100% on mylar. Gold decorated. Stretch direction indicated by large arrow. Small arrows show alignment of gold particles.

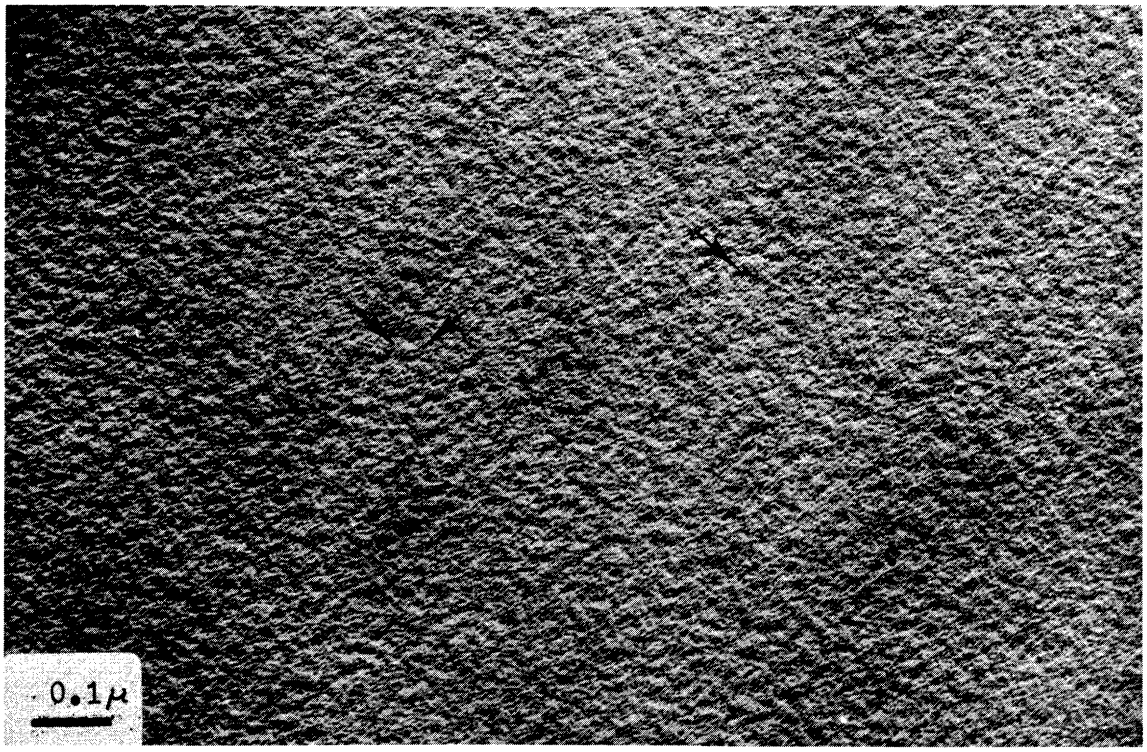

Figure 58: Atactic polystyrene annealed 30 minutes at 220°C, ice water quench. Platinum shadowed at 30°.

of closely spaced particles, it was difficult to clearly establish with any degree of certainty whether or not platinum shadowed microstructures tended to align preferentially, Figure 56. In stretched films decorated with gold, however, the gold particles did show a definite tendency to align at angles ranging from 30° to 70° to the stretch direction, Figure 57. It was established, by means of through focus micrographs, that this alignment of gold particles is independent of astigmatism.

In bulk samples of atactic polystyrene annealed at 220°C for 30 minutes and quenched in ice water, a nodular structure on the order of 150Å is observed, Figure 58. Similarly prepared samples annealed under the same conditions and quenched in ethanol-dry ice mixtures (-70°C), however, do not show this structure. Figure 59. In other experiments using similar samples annealed at a lower temperature (190°C), ice water quenching does not generate this same nodular structure observed at higher annealing temperatures, Figure 60. Thus, the appearance of an enlarged microstructure under one set of conditions, suggests that isolation and examination of an amorphous microstructure in general is highly dependent upon the experimental conditions used.

Thin sections of commercial atactic polystyrene (sectioned at room temperature) were shadowed with platinum parallel to the cutting direction and examined in the electron microscope, Figure 61. The column of segmented dark areas (parallel to the arrow) is thought to be an artifact generated

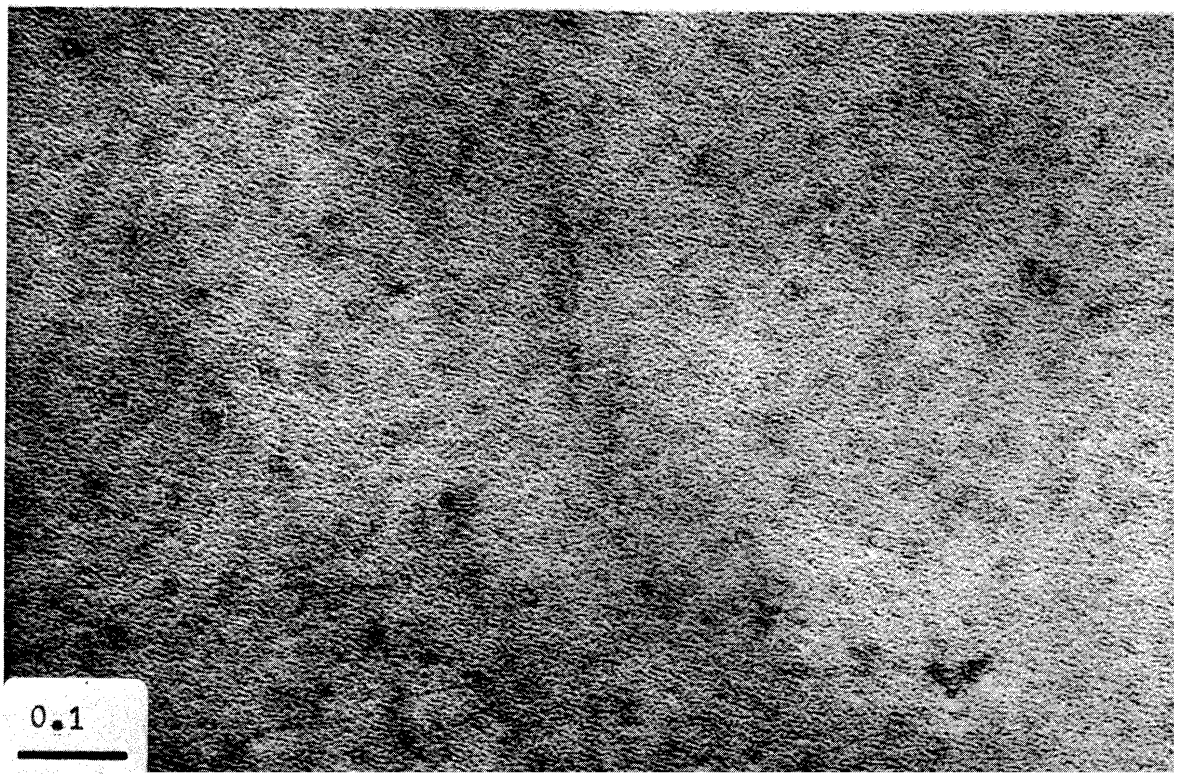

Figure 59: Atactic polystyrene annealed 30 minutes at 220°C, ethanol-dry ice quench. Platinum shadowed at 30°.

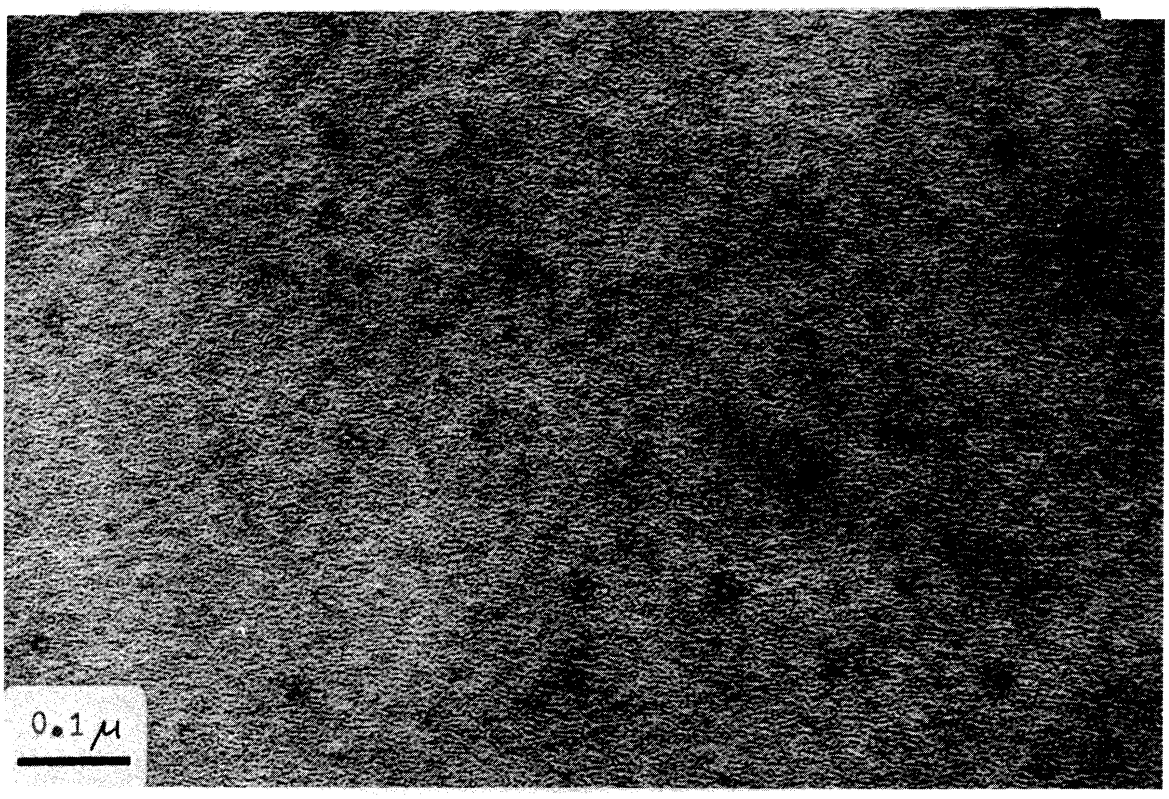

Figure 60: Atactic polystyrene annealed 30 minutes at 190°C, ice water quench. Platinum shadowed at 30°.

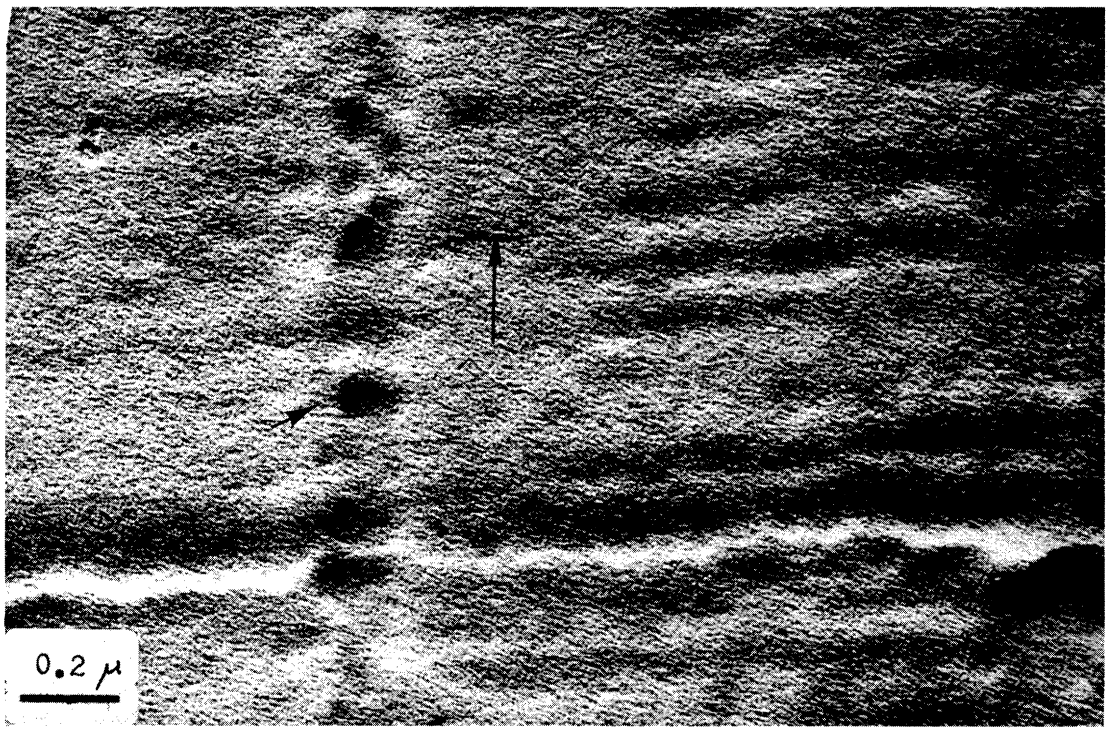

Figure 61: Atactic polystyrene thin section.
Platinum shadowed at 30°. Cutting direction is verticle

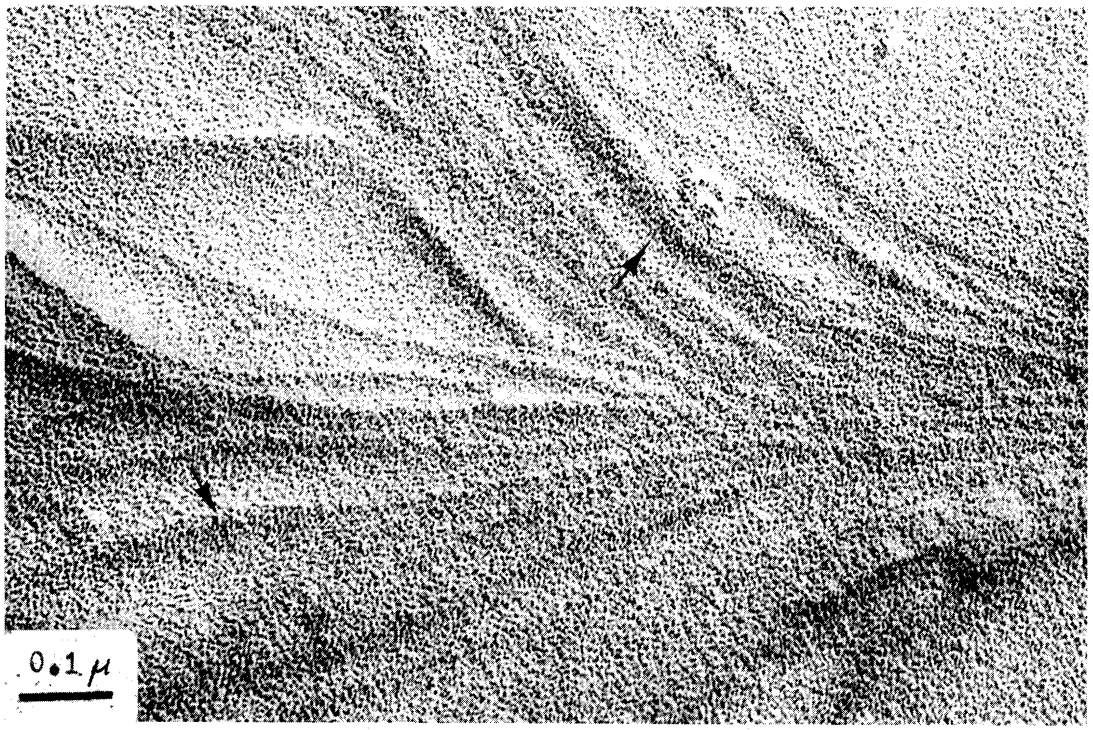

Figure 62: Isotactic polystyrene crystallized at 140°C
for 20 minutes. Platinum shadowed at 30°.

by the glass knife blade as it cuts through the sample. Dark striations perpendicular to the knife blade artifact are probably caused by compressive deformation of the thin section, as indicated by Sjostrand's [54] discussion on the mechanism of thin sectioning. The background platinum shadowed structure is on the order of 30Å, approximately the same size as observed in shadowed thin films of atactic polystyrene, Table XIII.

2. Crystallization of Unoriented Isotactic Polystyrene from the Glassy Amorphous State

When thin films of amorphous isotactic polystyrene are annealed 35°C to 40°C above the glass transition temperature Tg for 10 to 15 minutes, dark fibrous structures characteristic of spherulitic crystallization start to form on the film surface. Crystalline thin films of isotactic polystyrene shadowed with platinum show the splaying fibrous bundle structure observed in spherulitic crystallization of other polymers [17], Figure 3. Examination of these fibers at high magnification indicate that the platinum shadowed microstructure does not preferentially align itself into a crystallograph orientation, Figure 62. The thickness of the fibers in thin films crystallized at 140°C ranges from 110 to 120Å, which is in general agreement with the small angle x-ray long period of 127Å reported by Manley and Blais [43] for bulk isotactic polystyrene crystallized at 140°C.

The typical electron diffraction pattern for the area

in Figure 3 has concentric rings with Bragg spacings of 11.02Å 6.41Å, 5.56Å, 4.80Å, 4.12Å, and 4.04Å, which correspond to the (110), (300), (220), (211), (410) and (311) planes of isotactic polystyrene respectively, Figure 63. Gold decoration of films partially crystallized at 125°C shows the splaying fibrous structure with a tri-layer vacated area measuring 55Å, Figure 64. A more detailed discussion of the effects of gold decoration can be found in Chapter V.

Quite often it is difficult to observe fine crystalline structure in thin films because the overlying uncrystallized amorphous material partially obscures it. Therefore, efforts were made to use selective etching techniques to preferentially remove this overlying amorphous material. Figures 65 and 66 show a thin film of isotactic/atactic polystyrene 50/50 crystallized at 125°C and selectively etched with amyl acetate before shadowing with platinum. The irregularly shaped structures appearing on the surface of crystalline lamallae measure 120-150Å diameter, while the background regions adjacent to the lamallae do not have any nodular structure. In other crystalline thin films prepared under similar conditions, nodular structures ranging from 140 to 170Å primarily appear along the backbone edge of crystalline fibers, Figure 67.

These nodular structures along the edge or the surface of crystalline lamallae, however, are not observed in all etched films. When more dilute mixtures of isotactic/atactic polystyrene 10/90 are crystallized at 145°C and selectively etched with amyl acetate, the resulting crystalline fibers

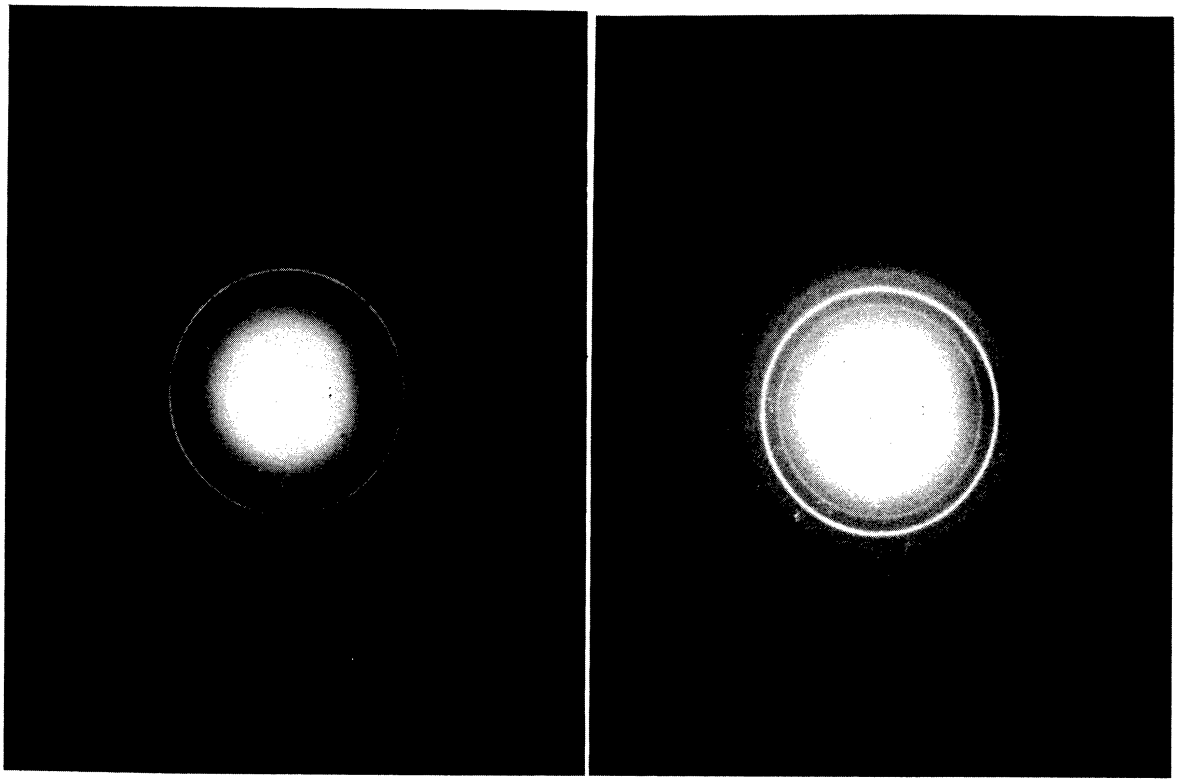

Figure 63: Isotactic polystyrene crystallized at 140°C for 20 minutes. Electron diffraction pattern. Prints show pattern developed at different intensities.

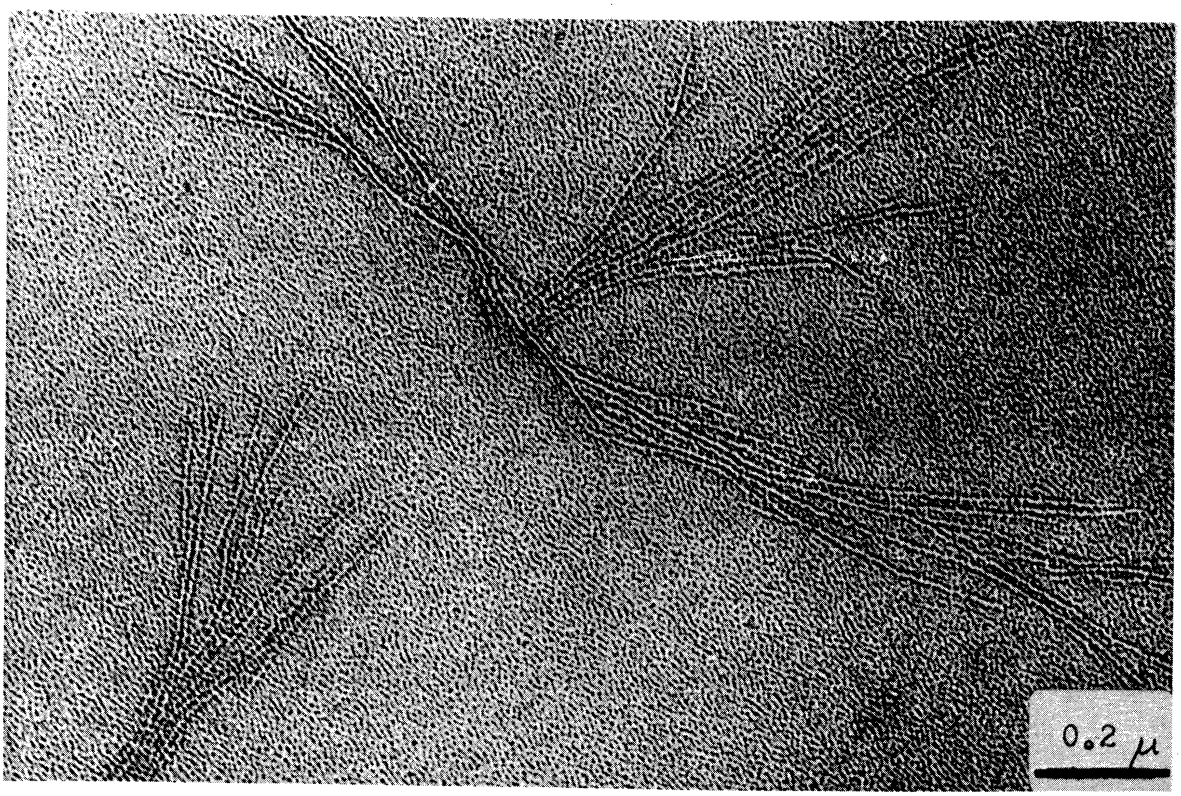

Figure 64: Isotactic polystyrene/atactic polystyrene 50/50 crystallized at 125°C for 60 minutes. Gold decorated.

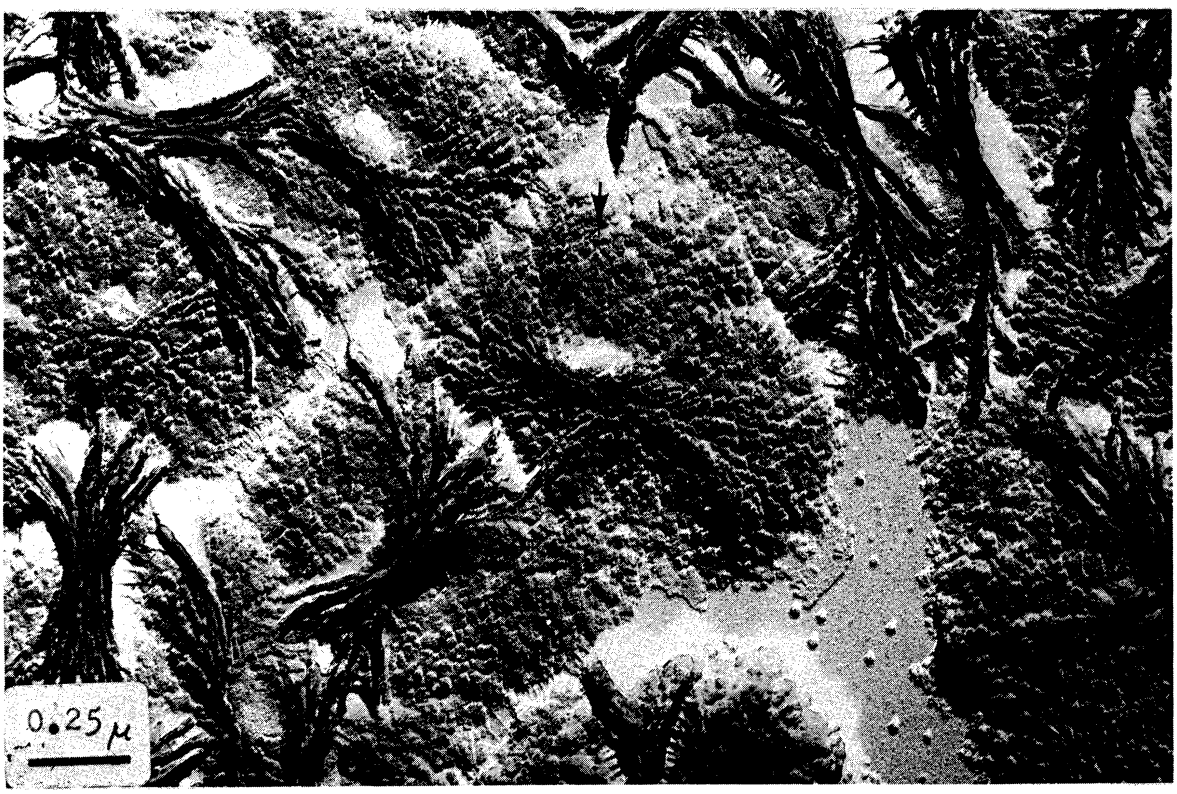

Figure 65: Isotactic polystyrene/atactic polystyrene 50/50 crystallized at 125°C for 120 minutes, amyl acetate etch for 20 seconds. Platinum shadowed at 30°.

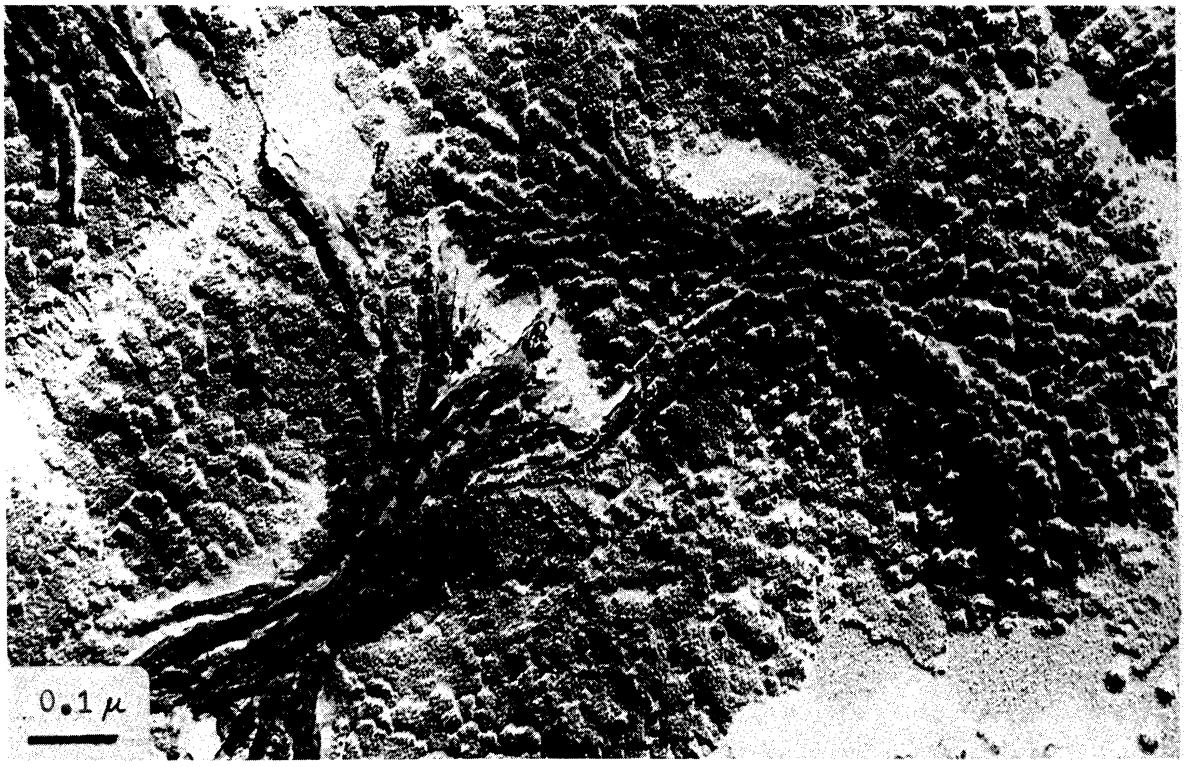

Figure 66: Isotactic polystyrene/atactic polystyrene 50/50 crystallized at 125°C for 120 minutes, amyl acetate etch for 20 seconds. Platinum shadowed at 30°.

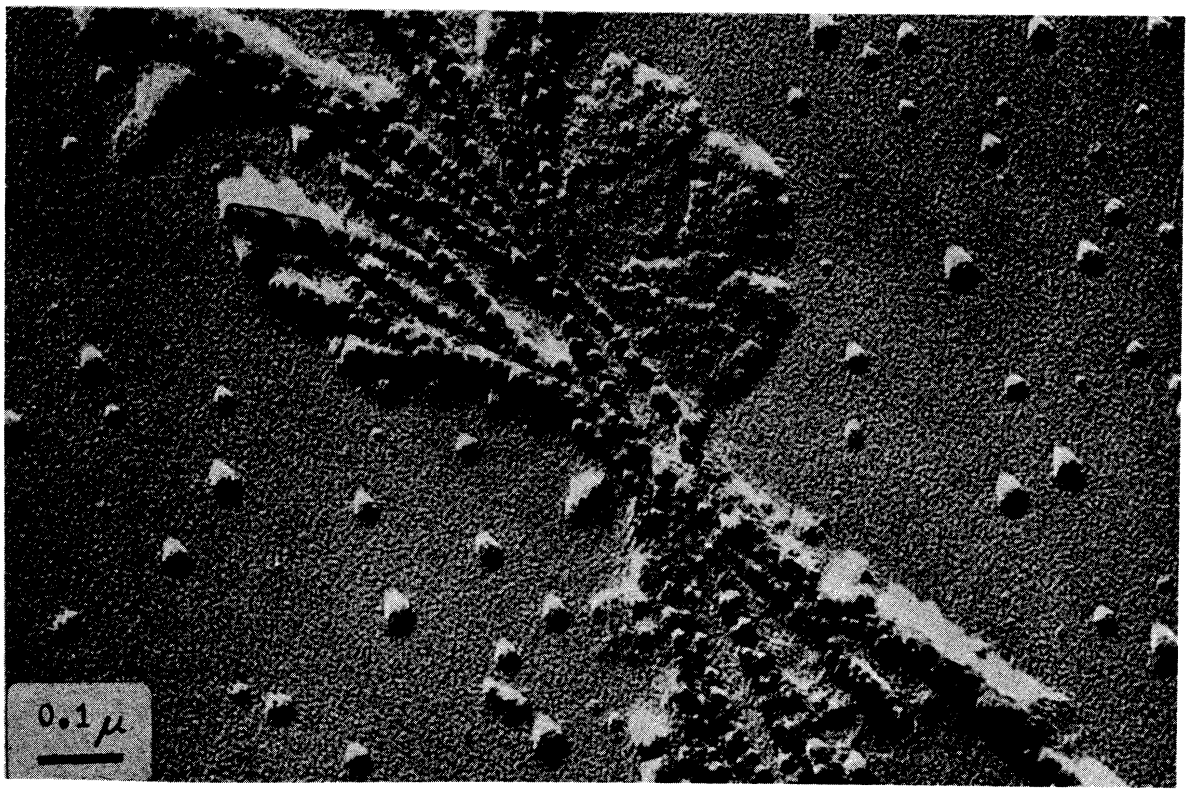

Figure 67: Isotactic polystyrene/atactic polystyrene 50/50 crystallized at 125°C for 60 minutes, amyl acetate etch for 20 seconds. Platinum shadowed at 30°.

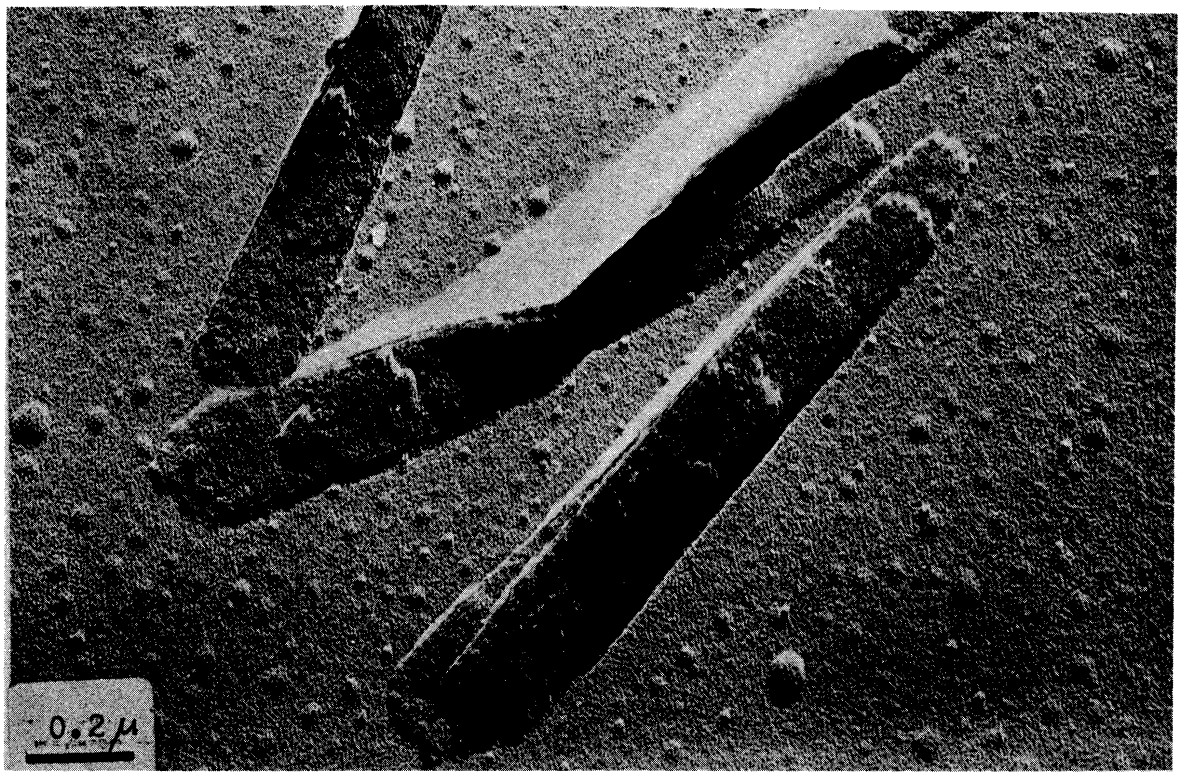

Figure 68: Isotactic polystyrene/atactic polystyrene 10/90 crystallized at 145°C for 60 minutes, amyl acetate etch for 20 seconds. Platinum shadowed at 30°.

appear to be made up of stacks of lamallar ribbon structures which have no surface nodules, Figure 68. The thickness of these ribbon lamallae measures 65-75Å, which is somewhat larger than the value of 60Å reported by Keith [29] for the thickness of single crystals of isotactic polystyrene grown from mixtures of isotactic/atactic polystyrene at 110°C.

It is uncertain at the present time why we find nodular structure in some etched films, but not in others. The nodules themselves might be caused either by preferential solvent attack in between primary structural units or perhaps by reprecipitation of partially dissolved polymer molecules.

D. Discussion

Amorphous thin films of atactic and isotactic polystyrene have a platinum shadowed microstructure on the order of 30Å, which appears to be essentially invariant with respect to the experimental conditions examined (molecular weight, solvent type, annealing temperature), Table XIII. In subsequent orientation studies on these thin films, it could not be clearly established whether these structures tend to preferentially align under tensile stress. In addition, these microstructures do not appear to align crystallographically in spherulitic fibers of crystallized isotactic polystyrene. These results suggest that the 30Å platinum shadowed microstructure observed in amorphous polystyrene might not be comparable to the 75Å paracrystalline ball-like structure observed by Yeh and Geil [62] in

poly(ethylene terephthalate) and the 125Å structures found by Carr and Geil [12] in polycarbonate A. Furthermore, there is no clear evidence linking this 30Å microstructure to the 60Å structure observed by Schoon and Teichman [50] in amorphous polystyrene and poly(methyl methacrylate). Therefore, the proper interpretation of this 30Å structure is still uncertain and is further complicated by the fact that the ultimate resolution of the platinum-carbon shadowing method, according to the results of Bradley [8], is also in the 20 to 30Å range.

Larger nodular structures, however, are observed in bulk samples of commercial atactic polystyrene annealed at 220°C and quenched in ice water. Similarly prepared samples quenched in ethanol-dry ice mixtures did not show this structure. Other samples of bulk atactic polystyrene annealed at 190°C and quenched in ice water likewise did not show this structure. At the present time, we have no reasonable explanation of why we should see this nodular structure in bulk samples annealed at higher temperatures (220°C) but not in samples annealed at lower temperatures (190°C). As mentioned earlier, these results suggest that successful isolation and examination of amorphous microstructure is highly dependent upon experimental conditions used.

In amorphous thin films of isotactic polystyrene crystallized from the glassy amorphous state, no surface aggregation of structural units is observed prior to the formation of spherulitic fibers. In fully crystallized

thin films, the only identifable structural units are the spherulitic fibers and the 30Å platinum shadowed microstructure. When these films are selectively etched, however, surface nodular structures on the order of 120-170Å are often observed. These nodules are quite irregular in shape and only occur on the surfaces of crystalline structures. The origin of these nodular structures is uncertain, but it might be related either to the presence of primary block units in crystalline fibers or the reprecipitation of partially dissolved molecules.

E. Conclusions

1. A platinum shadowed microstructure on the order of 30Å is found in all amorphous thin films of isotactic and atactic polystyrene examined. The size of this structure appears to be essentially unchanged with respect to the various conditions studied. In addition, these microstructures do not appear to align crystallographically in spherulitic fibers of crystallized isotactic polystyrene. Thus, the origin of these structures cannot be clearly established at the present time.

2. Spherulitic fibers of isotactic polystyrene have the same type of lamallar ribbon structure found in spherulitic fibers of other crystallizable polymers.

3. After annealing at 220°C for 30 minutes, nodular structures on the order of 150Å are observed on the surface of bulk samples of ice water quenched atactic polystyrene.

4. Irregularly shaped nodular structures, ranging from

120-170Å diameter, are often found in crystalline films of isotactic/atactic polystyrene which have been selectively etched with amyl acetate. Such nodules are thought to be either primarily structural units within the crystalline fibers or else the reprecipitation of partially dissolved molecules.

CHAPTER VII

GENERAL CONCLUSIONS AND MAJOR FINDINGS

The purpose of this study is to investigate the effect of a noncrystallizable diluent on the spherulitic crystallization kinetics and morphology of isotactic polystyrene and to examine strain induced crystallization from the glassy amorphous and rubbery states of similar blends. The significant findings and major conclusions are discussed in the following section.

In the kinetics study for mixtures of isotactic/atactic polystyrene, the measured spherulitic growth rates and morphology are generally quite similar to those reported by Keith and Padden [31]. However, for 40% and 60% dilutions with atactic polystyrene, the growth rate shows an unexpected, yet significant rise, as the diluent molecular weight increases from 19,800 to 51,000. This anomalous growth rate behavior cannot be explained on the basis of normal viscosity or diffusional effects, but can be reasonably explained in terms of the phenomenological theory of Keith and Padden [30] and the chain entanglement effect noted by Fox and Flory [15]. Since the critical molecular weight for chain entanglements in polystyrene is 36,000, we suggest that atactic impurity molecules having molecular weights

greater than 36,000, are substantially entrapped within the growing spherulite by means of these chain entanglements. As a result, the interfacial concentration of rejected impurity would be proportionally reduced, thus causing a noticible rise in the spherulitic growth rate.

In the kinetics study for the plasticized mixtures, a direct comparison of the spherulitic growth rate for mixtures of isotactic/atactic polystyrene and isotactic polystyrene/di-decyl phthalate over the same concentration and diluent molecular weight range indicates that there is a basic difference in the microstructure of these two systems. It is suggested that the former mixture behaves as a "homogeneous" phase since the growth rate is montonically depressed with increasing concentrations of atactic polystyrene. The latter mixture, however, appears to behave as a two phase system, both with regard to the measured spherulitic growth rate and the melting temperature depression. Thus, since the maximum spherulitic growth rate for the plasticized mixture is much higher than the comparable rate for the atactic mixture, the creation of a two phase system apparently affects either the viscous transport mechanism or the free energy of critical nucleus formation in the spherulitic growth process.

According to an analysis of the threshold crystallization temperatures for mixtures of isotactic/atactic polystyrene and isotactic polystyrene/benzophenone, the empirical constants C_1 and C_2 in the WLF form of the viscous transport term in the growth rate equation takes on different values

for these two mixtures. If we consider C_1 to be invariant for both systems, then C_2 is significantly lower for the benzophenone system, according to the methods of Boon and Azcue [5] and Suzuki and Kovacs [56]. The magnitude of this constant (C_2), however, is dependent upon which method is used. If the derived form of the spherulitic growth rate equation (equation 4) is correct, then the free energy of critical nucleus formation must also be lower for the benzophenone system in order to explain the higher maximum growth rates observed. Thus, it is suggested that the spherulitic growth mechanism for plasticized systems involves the addition of whole structural units (with a lower free energy of critical nucleus formation) to the growth front, while the mechanism for the atactic polystyrene system is a nonstructural nucleation process involving the addition of single molecules or small groups of loosely bound molecules to the growth front. This is the first time that an analysis of this type has ever been made on a polymer/diluent system.

In the study of strain induced crystallization of isotactic polystyrene, three different types of morphology were observed. Fibril type structures 130Å to 150Å wide and aligned parallel to the stretch direction were found in thin films of isotactic polystyrene/benzophenone 60/40 stretched 400% to 500% and annealed at 175°C from the rubbery amorphous state. The electron diffraction pattern corresponding to these fibrils indicates a high degree of molecular alignment parallel to the stretch direction, while dark field studies

using the (102) reflection indicate that the internal structure of these fibrils is segmented. This latter result suggests that the molecular conformation in the fibrils is predominately folded rather than extended chain. The segmented internal structure of these fibrils agrees with the experimental data of Yeh and Geil [61] and Wikjord and Manley [59] for different polymer systems strain crystallized under different conditions. These combined results suggest that the extended chain line nuclei model proposed by Keller [49] needs to be modified to account for a substantial number of chain folds in the proposed line nuclei. This is the first time that fibril type structures have been observed in strain induced crystallization from the rubbery amorphous state near Tg.

In thin films stretched to lower elongations (300%) prior to crystallization from the rubbery amorphous state, extended column type structures were often observed. These column structures are made up of rows of crystalline fibers 120Å to 160Å thick, oriented perpendicular to a common line type nucleus. A central filamentary backbone type structure (100 to 110Å diameter) has been found in mildly etched column type structures. This finding suggests that line type nuclei might be responsible for the generation of column type structures, a model proposed by Keller [49]. Filamentary backbone structures of this type have never been found before in column type structures produced by strain induced crystallization of a polymer from the rubbery amorphous state.

In thin films strain crystallized at very low elongations (100%), small groups or bundles of fibers aligned more or less perpendicular to the orientation direction appear to develop independently of any clearly distinguishable common line nucleus. This result suggests that there might be a mechanism for strain induced crystallization (oriented crystallization) other than the line nucleation model proposed by Keller [49].

CHAPTER VIII

RECOMMENDATIONS FOR FUTURE STUDY

1. The microscopic phase separation observed in plasticized mixtures can be independently verified by using small angle x-ray scatter to determine whether or not isotactic polystyrene and di-decyl phthalate form separate phases over concentrations ranging from 20% to 40% plasticizer. In addition, small angle x-ray techniques can be used to determine if phase separation is also present when other plasticizers are used. If this should be the case, then the proposed difference in the nucleation mechanism for crystallization also could be independently established, if it is verified by small angle x-ray that the isotactic/atactic polystyrene system is "homogeneous".

2. The proposed difference in the microstructure of the isotactic/atactic polystyrene and the isotactic polystyrene/plasticizer systems can be partially verified by using either an atactic polystyrene diluent in the 400 molecular weight range or a phthalic acid ester having a 900 molecular weight as diluents in the comparative spherulitic growth rate studies.

3. The differences in crystalline morphology caused by the addition of a noncrystallizable diluent to a crystallizable polymer could be studied by using crystalline thin

films which are selectively etched. The impurity should be much more sensitive to the etching solvent than is the crystalline polymer.

4. The effect of chain entanglements on the interfacial concentration of rejected impurity could be partially verified by using poly α-methyl styrene as the impurity diluent. The slower radial diffusion of poly α-methyl styrene should cause a greater depression of the radial growth rate over the critical molecular weight range than was noted for atactic polystyrene diluent.

5. Dark field microscopy using a beam tilting device might provide us with a better understanding of the internal structure of the fibrils observed in highly stressed thin films of isotactic polystyrene. In addition, comparable strain induced crystallization studies using amorphous polycarbonate A would help to show a) whether or not such fibril structures are found in other polymers, strain crystallized from the glassy amorphous state; and b) whether or not such fibril structures are formed by alignment of the nodules found in amorphous polycarbonate A, thus causing a segmented structure.

6. Measures of the spherulitic growth rate for mixtures of isotactic/atactic polystyrene of various molecular weights at temperatures other than 180°C would help to provide us with a better basis for suggesting modifications to the theoretical growth rate equation.

APPENDIX

Table IX

Spherulitic Growth Rate Data for Mixtures of Isotactic/Atactic Polystyrene

T_x, °C	M_w	R	G	Time, min./Size, μ						
180		100/0	0.383	48	38	121	145	164	198	
				18.2	32.3	47.7	56.0	62.9	76.2	
180		100/0	0.389	48	73	93	125			
				16.3	26.8	34.5	45.1			
190		100/0	0.284	59	95	133	160	194		
				16.7	26.2	37.3	45.9	54.7		
190		100/0	0.295	78	103	126	150	180		
				25.6	33.4	42.2	47.8	55.1		
200		100/0	0.157	214	249	281	315	357		
				9.3	14.6	19.5	24.1	32.0		
170		100/0	0.339	67	95	134	146	166	189	
				22.4	32.1	45.8	50.7	57.0	64.6	
160		100/0	0.291	103	130	148	176			
				30.5	38.2	43.7	52.9			
140		100/0	0.131	60	95	140	183	221		
				8.1	12.7	19.4	24.0	29.7		
180	4800	80/20	0.293	54	78	98	154			
				14.6	21.1	27.2	44.5			
180	4800	80/20	0.293	96	121	148	181	211	235	264
				12.9	19.7	29.3	38.4	46.7	53.3	61.9
190	4800	80/20	0.187	71	99	119	142	176	191	215
				13.2	19.7	22.4	25.1	32.4	35.8	41.1
200	4800	80/20	0.081	123	158	186	216	246		
				7.0	9.9	12.4	15.3	17.1		

T_x, °C	M_w	R	G	Time, min./size, μ					
170	4800	80/20	0.298	75	101	129	151	172	196
				7.8	15.7	24.2	28.9	47.6	46.4
160	4800	80/20	0.249	107	130	155	183	200	
				24.3	30.1	36.5	41.3	48.7	
140	4800	80/20	0.108	163	202	238	280		
				16.7	20.5	25.2	29.9		
180	4800	60/40	0.211	102	137	171	200	233	
				19.6	27.4	35.3	41.6	48.1	
190	4800	60/40	0.160	214	285	333	340	360	
				15.8	27.0	35.9	36.5	40.2	
170	4800	60/40	0.192	73	101	128	152	188	211
				14.1	18.5	23.4	29.7	38.2	43.9
160	4800	60/40	0.165	75	114	146	181	212	250
				6.2	14.9	20.2	25.1	30.9	35.7
140	4800	60/40	0.051	98	132	174	202		
				5.2	7.1	9.5	10.3		
180	4800	40/60	0.151	108	143	179	207	243	
				12.2	16.4	22.2	26.1	31.8	
180	4800	40/60	0.163	30	42	53	67	79	94
				5.1	7.3	8.6	11.3	13.2	16.8
190	4800	40/60	0.083	212	248	282	320	352	
				5.4	8.7	11.2	15.1	17.4	
190	4800	40/60	0.099	199	233	285	328		
				14.3	15.7	22.1	27.0		
170	4800	40/60	0.111	80	108	145	171	200	230
				9.2	12.1	15.7	19.2	22.0	26.8
160	4800	40/60	0.089	94	112	159	204	240	
				6.9	8.1	10.4	14.2	18.1	
190	4800	20/80	0.038	54	77	121	152		
				1.9	2.7	4.4	5.9		
180	4800	20/80	0.092	77	105	111	133	157	170
				7.2	9.9	10.7	12.2	14.9	16.3
170	4800	20/80	0.065	55	82	101	117		
				3.5	5.4	6.7	7.6		

T_x, °C	M_w	R	G	Time, min./size, μ					
160	4800	20/80	0.036	115	162	207	243		
				6.4	8.7	9.5	10.8		
180	411,000	60/40	0.213	33	58	85	112	127	136
				5.3	10.1	14.0	20.8	22.4	25.7
180	411,000	60/40	0.217	39	52	69	81	97	110
				6.3	9.6	13.4	15.9	18.7	21.2
180	411,000	40/60	0.148	47	65	87	116	129	
				6.1	8.4	12.8	16.1	18.3	
180	411,000	20/80	0.090	61	93	119	140	161	
				5.4	8.7	10.3	12.1	13.9	
180	51,000	80/20	0.293	25	41	57	71	91	101
				8.4	12.7	16.9	21.7	24.5	27.1
180	51,000	60/40	0.250	23	37	51	63	73	85
				6.3	9.7	12.9	16.7	19.4	20.2
180	51,000	60/40	0.248	18	30	40	50	60	70
				4.1	7.8	10.7	12.1	15.9	17.7
180	51,000	40/60	0.182	22	33	47	60	80	
				5.7	7.3	10.3	13.1	16.9	
180	51,000	40/60	0.180	25	38	48	58	70	80
				4.3	6.5	8.4	10.2	11.4	14.1
180	51,000	20/80	0.106	35	58	66	97	136	
				3.5	6.6	6.1	10.7	11.3	
180	51,000	20/80	0.098	56	78	100	136	174	
				6.4	8.7	11.0	14.3	15.6	
180	19,800	80/20	0.290	16	30	45	62	78	
				5.3	9.2	13.9	18.4	22.5	
180	19,800	60/40	0.180	17	30	42	52	62	72
				4.2	6.1	8.7	10.3	12.4	14.1
180	19,800	60/40	0.178	25	37	47	57	67	77
				6.2	8.1	10.9	12.4	13.3	15.4
180	19,800	40/60	0.143	26	39	49	59	69	80
				5.8	7.2	8.9	10.7	11.5	13.6
180	19,800	40/60	0.143	18	28	38	48	58	68
				3.6	4.2	6.9	7.4	9.5	10.6

T_x, °C	M_w	R	G	Time, min./size, μ					
180	19,800	20/80	0.075	40	59	64	76		
				3.7	4.3	4.3	4.4		
180	10,000	60/40	0.193	19	30	40	50	60	70
				4.2	6.7	9.8	11.2	12.9	14.7
180	10,000	40/60	0.148	27	36	46	56	66	
				3.8	5.4	6.7	8.1	9.5	
180	2,030	80/20	0.288	20	30	41	50	60	
				6.2	9.8	12.7	15.3	17.9	
180	2,030	60/40	0.195	20	30	40	50	60	70
				5.2	7.3	9.8	11.2	13.4	15.7
175	2,030	60/40	0.193	25	35	45	56		
				6.3	8.0	10.2	12.8		
180	2,030	40/60	0.118	40	50	61	70	80	
				5.7	6.1	8.7	9.5	9.5	
180	900	80/20	0.285	16	30	38	49	54	
				4.6	7.3	10.7	12.2	13.8	
170	900	80/20	0.290	26	36	46	60	76	
				8.2	11.9	14.3	18.8	23.6	
175	900	80/20	0.293	83	93	108	119	130	
				22.7	25.4	29.3	32.8	36.4	
175	900	60/40	0.150	19	29	48	60	70	80
				4.1	5.3	8.5	10.2	11.8	13.7
180	900	60/40	0.110	100	110	120			
				16.2	17.1	18.0			
175	900	40/60	0.097	71	82	95	106		
				5.0	6.3	7.5	7.7		
170	900	40/60	0.092	19	38	53	80		
				2.1	4.9	5.4	7.8		
175	900	20/80	0.021	62	86	121			
				1.3	1.8	2.5			
180	1,800,000	80/20	0.268	18	28	38	50	60	70
				6.1	8.7	11.3	15.4	17.3	19.8
190	1,800,000	60/40	0.160	24	34	46	69	69	
				4.1	6.4	7.7	9.8		

T_x, °C	M_w	R	G	Time, min./size, μ					
180	1,800,000	60/40	0.178	47	65	85	109	132	
				9.1	11.3	15.5	19.8	23.4	
190	1,800,000	40/60	0.092	26	42	59	70	85	
				3.1	3.8	6.2	7.5	7.8	
180	1,800,000	40/60	0.147	57	78	94	118	137	160
				9.1	12.7	14.8	17.9	20.3	24.5
180	1,800,000	20/80	0.075	36	53	72	89		
				2.2	3.8	5.1	6.2		

Nomenclature

T_x,°C = Crystallization temperature, °C
M^x = Molecular weight (number average)
R^w = Ratio of IPS/APS
G = Spherulitic growth rate, μ/minute
Time = Observed crystallization time, minutes
Size = Observed size of spherulites at any given time, μ

Table X

Spherulitic Growth Rate Data for Mixtures

of Isotactic Polystyrene and Di-methyl Phthalate

T_x, °C	R	G	Time, min./size, μ					
130	90/10	0.187	10	15	25	36		
			4.1	5.1	7.0	9.0		
140	90/10	0.417	9	14	21	26	32	
			5.9	8.1	10.9	12.9	15.5	
150	90/10	0.580	12	17	23	29	34	
			9.8	12.2	15.9	19.2	22.2	
160	90/10	0.595	6	13	18	23	28	33
			4.2	8.1	11.5	14.3	17.4	20.3
170	90/10	0.438	9	14	19	24	29	
			4.2	6.0	8.3	10.3	12.9	
120	80/20	0.270	5	10	15	20	31	40
			5.8	6.9	8.4	9.6	12.9	15.7
130	80/20	0.537	10	15	20	25	30	35
			8.8	11.5	14.5	16.9	19.3	22.1
140	80/20	0.725	10	15	20	25	30	36
			7.8	12.1	15.7	19.5	23.0	26.9
150	80/20	0.695	4	9	14	19	25	30
			4.6	8.5	11.9	15.2	18.7	21.9
160	80/20	0.560	6	11	16	21	26	
			4.1	7.0	9.5	12.5	15.4	
110	70/30	0.498	6	11	16	21	26	33
			7.8	9.4	11.0	14.6	17.1	20.4
120	70/30	0.725	7	12	17	22	28	
			8.4	12.4	15.8	19.7	24.1	
130	70/30	0.716	7	12	17	22	19	
			7.3	11.2	14.5	18.1	23.4	
140	70/30	0.604	7	12	18	23	28	37
			7.6	11.7	14.1	17.5	20.7	26.4
150	70/30	0.287	16	23	28	33	46	
			7.1	9.4	10.8	12.2	13.5	16.2

T_x, °C	R	G	Time, min./Size, μ					
103	60/40	0.635	3	8	13	18	24	
			6.6	9.6	12.9	16.0	19.6	
110	60/40	0.648	10	15	20	26	32	
			10.2	13.4	15.8	20.9	25.0	
120	60/40	0.560	4	9	14	19	24	29
			7.3	10.2	10.9	13.8	16.7	19.6

Nomenclature

T_x,C = Crystallization temperature, °C
R = Ratio IPS/DMP
G = Spherulitic growth rates,μ/minute
Time = Observed Crystallization Time, minutes
Size = Observed size of spherulites at any given time, μ

Table XI

Spherulitic Growth Rate Data for Mixtures of Isotactic Polystyrene and Di-decyl Phthalate

T_x, °C	R	G	Time, min./Size, μ						
140	90/10	0.459	5	11	17	29			
			5.2	7.9	10.4	16.3			
150	90/10	0.726	6	11	16	21	26	31	
			8.8	12.3	15.8	19.5	23.0	27.2	
160	90/10	0.847	4	9	14	19	24	29	
			4.8	9.2	12.9	17.4	21.8	26.1	
170	90/10	0.720	7	12	17	22			
			6.4	9.6	13.6	16.7			
170	90/10	0.720	5	10	15	20	25	30	
			4.6	8.4	11.6	15.4	18.6	21.5	
185	90/10	0.263	15	25	35	45			
			4.5	6.8	10.1	12.1			
120	80/20	0.780	3	8	13	18	23		
			9.1	12.2	16.4	20.6	24.6		
130	80/20	1.000	7	12	17	23	29	34	
			14.4	19.7	24.7	31.2	37.1	41.7	
140	80/20	1.100	5	10	15	20	26	32	
			9.7	14.7	19.8	26.4	33.0	38.8	
140	80/20	1.105	6	11	16	20	25	30	35
			7.8	10.9	14.6	24.5	29.9	35.4	40.2
150	80/20	1.092	8	13	19	24	30		
			9.5	15.6	21.4	26.9	33.5		
160	80/20	0.905	7	12	18	24	31	36	
			6.9	11.1	15.7	21.0	26.3	29.8	
175	80/20	0.400	14	20	25	31			
			9.5	10.7	12.5	15.3			
110	70/30	0.440	16	21	27	33	40	47	
			8.5	10.4	12.6	16.2	19.4	23.1	
120	70/30	0.710	5	10	15	20	25		
			8.3	12.2	15.7	19.1	22.5		

T_x, °C	R	G	Time, min./Size, μ					
130	70/30	0.855	4	9	14	19	25	
			6.0	10.6	14.4	17.7	21.4	
140	70/30	1.070	5	10	15	20	25	30
			7.6	14.2	20.0	24.9	30.9	36.3
140	70/30	1.050	6	11	16	22	29	35
			8.6	13.8	17.6	21.0	29.6	35.5
140	70/30	1.020	11	16	22	27	33	
			10.7	15.8	21.2	26.7	32.4	
150	70/30	1.100	4	9	14	19	24	
			8.4	13.7	19.0	26.1	30.7	
175	70/30	0.638	11	16	21	26		
			7.2	10.6	13.7	16.7		
110	60/40	0.430	2	7	12	17	22	27
			5.8	7.7	10.5	11.9	13.9	16.1
140	60/40	1.030	7	12	17	22	27	
			10.6	15.2	20.7	26.0	30.9	
150	60/40	1.100	5	10	15	20	25	30
			8.1	13.9	19.3	24.6	30.6	35.9
160	60/40	1.015	7	12	17	24	29	
			6.5	11.6	15.2	20.2	23.2	
175	60/40	0.640	11	16	22	27	32	
			6.4	9.7	13.4	16.6	20.2	
140	40/60	0.873	8	13	18	23		
			7.5	12.3	16.4	20.9		
150	40/60	0.870	27	32	37	42	47	
			18.4	22.4	26.9	30.2	33.5	
160	40/60	0.650	7	12	17	22		
			4.5	7.8	11.0	14.2		
130	20/80	0.417	16	21	27	32		
			12.4	14.8	17.8	--		
140	20/80	0.570	10	15	20	26		
			5.7	8.6	10.5	11.5		

T_x, °C	R	G	Time, min./Size, μ				
150	20/80	0.595	38 24.0	43 26.9	50 29.5		
160	20/80	0.487	11 9.8	16 13.0	21 14.6	26 17.2	31 19.7

Nomenclature

T_x, °C = Crystallization temperature, °C
R = Ratio of IPS/DDP
G = Spherulitic Growth Rate, μ/minute
Time = Observed Crystallization Time, minutes
Size = Observed Size of Spherulites at any given time, μ

Table XII

Unshadowed Microstructure

Material	M_W	Solvent	T	t	S	C
1-4 trans isoprene	-	benzene	26	-	18	25
syndiotactic PMMA	108,000	xylene	26	-	16	23
polystyrene	4,800	cyclohexanone	26	-	20	25
polystyrene	4,800	cyclohexanone	110	0	20	26
polystyrene	4,800	cyclohexanone	110	60	19	26
polystyrene	4,800	dichlorobenzene	26	-	19	24
polystyrene	1,800,000	cyclohexanone	26	-	21	25
polystyrene	1,800,000	cyclohexanone	110	60	20	26
polystyrene	1,800,000	dichlorobenzene	110	0	18	24
polystyrene	1,800,000	dichlorobenzene	110	60	19	24
polystyrene	1,800,000	dichlorobenzene	10	120	20	25
1-4 cis isoprene	-	benzene	26	-	18	22
isotactic polystyrene	550,000	dichlorobenzene	26	-	18	24
isotactic polystyrene	550,000	dichlorobenzene	140	60	21	22
poly(vinyl chloride)	-	methyl ethyl ketone	26	-	19	26

Nomenclature

M_W = molecular weight
T_W = casting temperature, °C
t = annealing time, minutes
S = diameter of particle, Å
C = center to center distance between particles, Å

Table XIII

Platinum Shadowed Microstructure

Material	M_w	Solvent	T	t	S	C
1-4 trans isoprene	-	benzene	26	-	25	30
polystyrene	4,800	cyclohexanone	26	-	24	32
polystyrene	1,800,000	cyclohexanone	26	-	25	32
1-4 cis isoprene	-	benzene	26	-	26	33
isotactic polystyrene	550,000	dichlorobenzene	140	0	24	30
isotactic polystyrene	550,000	dichlorobenzene	140	60	28	33
polystyrene thin section	-	-	26	-	25	32

Nomenclature

M_w = molecular weight
T^w = casting temperature, °C
t = annealing time, minutes
S = diameter of particle, Å
C = center to center distance between particles, Å

BIBLIOGRAPHY

1. Andrews, E.H., "Crystalline Morphology in Thin Films of Natural Rubber, II Crystallization under Strain," *Proceeding of the Royal Society*, A Vol. 277, pp. 562-570 (1964).

2. Banks, W.; Gordon, M.; Sharples, A., "The Crystallization of Polyethylene after Partial Melting," *Polymer*, 4(3), pp. 289-302, (1963).

3. Bassette, G.A.; Blundell, D.J.; Keller, A., "Surface Structure of Polyethylene Crystals as Revealed by Surface Decoration, I. Preliminary Survey," *J. of Macromolecular Science* (Physics), B1(1), pp. 161-184, (1967).

4. Blais, P.; Manley, R. St. John, "Crystallization of Isotactic Polystyrene from Solution," Technical Report No. 460, Pulp and Paper Research Institute of Canada, Montreal, Canada.

5. Boon, J.; Azcue, J.M., "Crystallization Kinetics of Polymer-Diluent Mixtures. Influence of Benzophenone on the Spherulitic Growth Rate of Isotactic Polystyrene," *J. of Polymer Science*, Part A-2, Vol. 6, pp. 885-894 (1968).

6. Boon, J.; Challa, G.; Van Krevelen, D.W., "Crystallization Kinetics of Isotactic Polystyrene. II. Influence of Thermal History on Number of Nuclei," *J. of Polymer Science*, Part A-2, Vol. 6, pp. 1835-1851 (1968).

7. Boon, J.; Challa, G.: Van Krevelen, D.W., "Crystallization Kinetics of Isotactic Polystyrene. I. Spherulitic Growth Rate," *J. of Polymer Science*, Part A-2, Vol. 6, pp. 1791-1801 (1968).

8. Bradley, D.E., "Study of Background Structure in Platinum/Carbon Shadowing Deposits," *British J. of Applied Physics*, Vol. 11, p. 506 (1960).

9. Buchanan, D.R.; Miller, R.L., "X-ray Line Broadening in Isotactic Polystyrene," *J. of Applied Physics*, Vol. 37, No. 11, pp. 4003-4012 (1966).

10. Bueche, F., *Physical Properties of Polymers*, Interscience Publishers, New York (1962).

11. Busse, W.F., "Mechanical Structure in Polymer Melts. II. Roles of Entanglements in Viscosity and Elastic Turbulence," *J. of Polymer Science*, A-2, Vol. 5, pp. 1261-1281 (1967).

12. Carr, S.H.; Geil, P.H.; Baer, E., "The Development of Spherulites from Structural Units in Glassy Poly(bisphenol-A-carbonate)," *J. of Macromolecular Science* (Physics), B2(1), 13, (1968).

13. Clark, E.S.; Garber, C.A., "The Effect of Industrial Processing on the Morphology of Crystalline Polymers," A.I.Ch.E. Meeting, Atlanta, Georgia, February (1970).

14. Dedeurwaerder, J.F.; Oth, M., "Properties of Mixtures of Polystyrene and Benzophenone," *J. of Chim. Physics*, Vol. 56, p. 940 (1959).

15. Fox, T.G.; Flory, P.J., "Second-Order Transition Temperatures and Related Properties of Polystyrene. I. Influence of Molecular Weight," *J. of Applied Physics*, Vol. 21, pp. 581-591 (1950).

16. Frank, W.; Goddar, H.; Stuart, H.A., "Electron Microscopic Investigations on Amorphous Polycarbonate," *J. of Polymer Science*, Vol. B, pp. 711-713 (1967).

17. Geil, P.H., *Polymer Single Crystals*, Interscience Publishers, New York, (1963).

18. Gezovich, D.M.; Geil, P.H., "Morphology of Plasticized Polyvinylchloride," Division of Macromolecular Science, Case Western Reserve University, Cleveland, Ohio.

19. Gornick, K.; Mandelkern, L., "Effect of Noncrystallizing Component on the Crystallization Kinetics of Polymers," *J. of Applied Physics*, Vol. 33, No. 3, p. 907 (1962).

20. Haller, M.H.; Magill, J.H., "Morphology of Polysiloxane Crystallized from the Melt," *J. of Applied Physics*, Vol. 40, No. 11, p. 4261 (1969).

21. Hay, J.N., "Crystallization Kinetics of Isotactic Polystyrene," *J. of Polymer Science*, Vol. A, No. 3, p. 433 (1965).

22. Hay, J.N.; Sabir, M., "Crystallization Kinetics of High Polymers. Polyethylene Oxide-Part I," *Polymer*, Vol. 10, pp. 187 (1969).

23. Hoffman, J.D.; Weeks, J.J., "Rate Spherulitic Crystallization with Chain Folds in Polychlorotrifluorethylene," *J. of Applied Physics*, Vol. 37, p. 1723 (1962).

24. Holland, V.; Lindenmeyer, P., "The Morphology and Crystal Growth Rate of Polyethylene Complexes," *J. of Polymer Science*, Vol. 57, p. 589 (1962).

25. Jenckel, E.; Teege, E.; Hinrichs, W., "Transkristallisation in hockmolekularen Stoffen," *Kolloid*, Vol. 129, p. 19 (1952).

26. Kargin, V.A.; Koretskaya, T.A.; Bogayevskaya, T.A., "Crystallization of Isotactic Polystyrene," *Polymer Science USSR*, Vol. 6, No. 3, pp. 489-494 (1964).

27. Kargin, V.A.; Sogolava, T.I.; Talipor, G., "Supermolecular Structures of Plasticized and Nonplasticized Crystalline Polystyrene," *Polymer Science USSR*, Vol. 5, pp. 937-945 (1964).

28. Kargin, V.A.; Koretskaya, T.A.; Markova, G.S.; Ovchinnikov, Yu. K., "Electron Microscopy and Electron Diffraction Studies of the Spherulites of Isotactic Polystyrene," *Polymer Science USSR*, Vol. 8, No. 7, pp. 1410-1417 (1966).

29. Keith, H.D., "On the Relation between Different Morphological Forms in High Polymers," *J. of Polymer Science*, A, Vol. 2, pp. 4339-4360 (1964).

30. Keith, H.D.; Padden, F.J. Jr., "Spherulitic Crystallization from the Melt. I. Fractionation and Impurity Segregation and their Influence on Crystalline Morphology," *J. of Applied Physics*, Vol. 35, No. 4, pp. 1270-1285 (1964).

31. Keith, H.D.; Padden, F.J. Jr., "Spherulitic Crystallization from the Melt. II. Influence of Fractionation and Impurity Segregation on the Kinetics of Crystallization," *J. of Applied Physics*, Vol. 35, No. 4, pp. 1286-1296 (1964).

32. Keller, A., "The Spherulitic Structure of Crystalline Polymers. Part I. Investigations with the Polarizing Microscope," *J. of Polymer Science*, Vol. 17, pp. 291-307 (1955).

33. Keller, A.; Machin, M.J., "Oriented Crystallization in Polymers," *J. of Macromolecular Science* (Physics), B1(1), pp. 41-61 (1967).

34. Luch, D., "Strain Induced Crystallization of Rubber," Private Communications.

35. Lunak, S.; Bohdanecky, M., "Crystallization Kinetics of Polycarbonate in Solution," *J. of Polymer Science*, C, No. 16, p. 103 (1965).

36. Magill, J.H., "Crystallization Kinetics of Polytetramethyl-P-Silphenylene Siloxane (TMPS) Fractions," *J. of Polymer Science, Polymer Letters*, Vol. 6, pp. 853-857 (1968).

37. Magill, J.H., "Spherulitic Crystallization Studies of Poly (tetramethyl-p-silphenylene)-siloxane (TMPS). Part III," *J. of Polymer Science*, Part A-2, Vol. 7, pp. 1187-1195 (1969).

38. Magill, J.H., "Spherulitic Crystallization. Part I. 'Odd Even' Polyamides: Nylon 56 and Nylon 96," *J. of Polymer Science*, Part A, Vol. 3, pp. 1195-1219 (1965).

39. Magill, J.H., "Crystallization of Polyamides. Part II: Nylon 6 and Nylon 66," *Polymer*, Vol. 6, pp. 367-371 (1965).

40. Magill, J.H., "Formation of Spherulites in Polyamide Melts: Part III. Even-Even Polyamides," *J. of Polymer Science*, Part A-2, Vol. 4, pp. 243-265 (1966).

41. Mandelkern, L., *Crystallization of Polymers*, McGraw-Hill, New York, (1964).

42. Mandelkern, L., "The Crystallization Kinetics of Polymer-Diluent Mixtures: The Temperature Coefficient of the Process," *Polymer*, Vol. 5, No. 12, pp. 637-648 (1964).

43. Manley, R. St . John; Blais, J.J., "X-ray Long Periods in Bulk Crystallization Polymers," *J. of Macromolecular Science* (Physics), B1(3), pp. 525-566 (1967).

44. Natta, G.; Corradini, R.; Bassi, I.W., "Crystal Structure of Isotactic Polystyrene," *Nuovo Cimento Supplement*, Vol. 15, p. 68, (1960).

45. Nielsen, L.E., *Mechanical Properties of Polymers*, Reinhold Publishing Corp., New York, p. 55 (1962).

46. Padden, F.J.; Keith, H.D., "Crystallization in Thin Films of Isotactic Polypropylene," *J. of Applied Physics*, Vol. 37, No. 11, pp. 4013-4020 (1964).

47. Pennings, A.J.; Kiel, A.M., "Fractionation of Polymers by Crystallization from Solution. III. On the Morphology of Fibrillar Polyethylene Crystals Grown in Solution," *Kolloid Z.*, Vol. 205, p. 160 (1966).

48. Price, F.P., "Nucleation in Polymer Crystallization," Report No. 67-C-411, General Electric Research and Development Center, Schenectady, New York.

49. Price, F.P., "Polymer Crystallization During Flow," Report No. 67-C-097, General Electric Research and Development Center, Schenectady, New York.

50. Schoon, G.F.; Teichman, O., "Elektronenmikroskoposche Untersuchung des Quellungsvorgangs bei Makromolekulen," *Kolloid Z.*, Vol. 157, pp. 35-45 (1964).

51. Schoon, G.F.; Kretschmer, R., "Elektronmikroskopische Untersuchungen des Quellungsvorgangs bei Makromolekulen II Teil: Des System Polymethyl-methancrylat," *Kolloid Z.*, Vol. 197, pp. 45-50 (1964).

52. Schoon, T.F.; Kretschmer, R., "Interpretation of Micromorphological Structure," *Kolloid Z*, Polymer Z, Vol. 211, Nos. 1 & 2, pp. 53-62 (1966).

53. Siegman, A.; Geil, P.H., "Crystallization of Polycarbonate from the Glassy State, Part I. Thin Films Cast from Solution," T.R. 127, T.R. 128, Division of Macromolecular Science, Case Western Reserve University.

54. Sjostrand, F.S., *Electron Microscopy of Cells and Tissues*, Vol. 1, Instrumentation and Techniques, p. 232, Academic Press, New York (1967).

55. Spit, B.J., "Gold Decoration Applied to Polymers," *J. of Macromolecular Science* (Physics), B2(1), pp. 45-54 (1968).

56. Suzuki, T.; Kovacs, A.J., "Temperature Dependence of Spherulitic Growth Rate of Isotactic Polystyrene," *Polymer Journal*, Vol. 1, No. 1, pp. 82-100 (1970).

57. Taeger, A.A.; Suvorova, A.I.; Dreval, V. Ye.; Gakova, N.P.; Lutskaya, S.P., "Newtonian Viscosity and Glass Temperature of Polystyrene Plasticized with Aromatic Acid Esters," *Polymer Science USSR*, Vol. 10, No. 10, p. 2649 (1968).

58. Turnbull, D.; Fisher, J.C., "The Rate of Nucleation in Condensed Systems," *J. of Chemical Physics*, Vol. 17, p. 71 (1949).

59. Wikjord, A.G.; Manley, R. St. John, "The Morphology of Fibrillar Polyethylene Crystals," *J. of Macromolecular Science* (Physics), B2(3), pp. 501-537 (1968).

60. Williams, M.L.; Landel, R.F.; Ferry, J.D., "The Temperature Dependence of the Relaxation Mechanism in Amorphous Polymers and Other Glass Forming Liquids," *J. of American Chemical Society*, Vol. 77, p. 3701 (1955).

61. Yen, G.S.Y.; Geil, P.H., "Strain Induced Crystallization of Polyethylene Terephthalate," *J. of Macromolecular Science*, (Physics), B1(2), pp. 251-277 (1967).

62. Yeh, G.S.Y.; Geil, P.H., "Crystallization of Polyethylene Terephthalate from the Glassy Amorphous State," *J. of Macromolecular Science* (Physics), B1(2), pp. 235-249 (1967).